POLITECNICO DI MILANO
DEPARTMENT OF ELECTRONIC, INFORMATION AND BIOENGEERING
DOCTORAL PROGRAMME IN BIOENGINEERING

TITLE **STUDY OF THE BIOMECHANICS OF SURGICAL AORTIC VALVES - A MERGED MEDICAL AND BIOENGEENIRING VIEW**

Doctoral Dissertation of:
GIORDANO TASCA

Supervisors:
Prof. Redaelli Alberto
Prof. Vismara Riccardo

Tutor:
Prof. Rodriguez Matas Jose Felix

The Chair of the Doctoral Program:
Prof. Andrea Aliverti

XXX Cycle

".....Cosicché, se gli uomini hanno filosofato per liberarsi dell'ignoranza, è evidente che ricercarono il conoscere solo al fine di sapere e non per conseguire qualche utilità pratica".....

(Aristotele. Metaph. A 2, 982 b 11-21)

DEDICA: .....*a chi dedicare questo mio faticoso lavoro se non a coloro che non hanno rispetto delle visioni altrui delle cose, e quindi anche delle mie, specialmente quando queste visioni non hanno risvolti pratici*.....

Abstract

CHAPTER 1

CHAPTER 2

BIOMECHANICS OF PERICARDIAL PROSTHESES SURGICALLY IMPLANTED

CHAPTER 3

STUDY OF THE EFFECT OF THE VALVE DESIGN ON PRESSURE RECOVERY AND SPATIAL POSITION OF VENA CONTRACTA

CHAPTER 4

IMPACT OF AORTIC VALVES PROSTHESIS ON CORONARY FLUID DYNAMIC

CHAPTER 5

IMPACT OF SURGICAL PROCEDURE ON HYDRODYANAMIC PERFORMANCE OF PERICARDIAL BIOPROSTHESES.

CHAPTER 6

Abstract

Background

New devices and therapeutic approaches, for the treatment of cardiac valve diseases, have been put forward in the last decade. These technological advancements have completely changed the landscape of the cardiovascular discipline providing new therapeutic opportunities to patients. Regrettably, many functional aspects of the devices used in patients are still neglected by the physicians that use them. Indeed, there is a tendency to privilege the technical aspects directly related to the surgical implant, neglecting the specific structural and functional characteristics of the devices themselves. This attitude has generated a knowledge gap between the technological content of the materials used and physicians, while a better knowledge would allow to exploit the devices at best with positive consequences for patients. To bridge this gap, a research project with the bioengineering approach is a starting point. By setting up experimental studies, on the base of the formulated hypotheses, indeed it is possible to comprehend the main factors which govern the biomechanical behaviours of implanted valves as well as their impact on the local aortic root fluid dynamics. Once this gap is bridged, physicians may adopt the new available therapeutic strategies with more discernment.

Materials and methods

This research project, which was made up by four phases, has been planned and conducted through a series of experimental tests, by devising new experimental as well as by employing existing systems.

In the first phase of the project, two experimental tests were carried out on surgically implanted bioprostheses, with the aim to acquire information on their biomechanical

behavior, using a mock loop pulsatile system (ForCardioLab Mock Loop), with a test section designed to house a whole real aortic root unit (Fig.1).

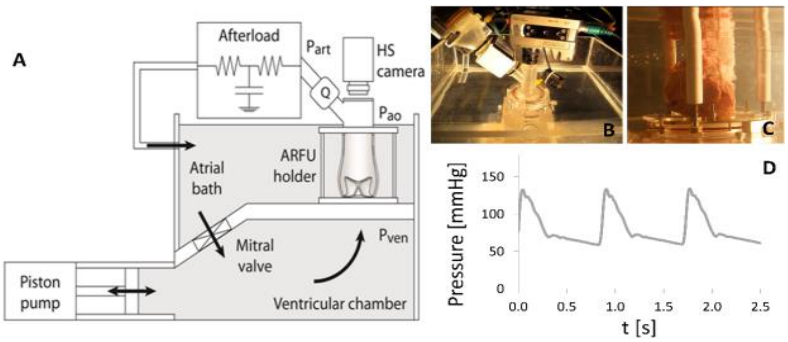

Figure 1. Panel A, schematic of the mock loop. The black arrows indicate flow directions. P_{ven}: port for ventricular pressure measurement; P_{ao}: port for pressure measurement downstream of the aortic root; P_{art}: port for measurement of simulated arterial pressure; Q: flow meter probe; HS camera: High speed camera. Overall encumbrance of the device was about 600x400x500 mm. Panel B, photograph of the test section of the experimental apparatus; Panel C: a detail of the housing section, with an aortic root mounted. Panel D: a representative course of the systemic pressure simulated with the mock loop.

The devices tested were stented pericardial bioprostheses which differ in term of design and size. The valve size, for each type of bioprosthesis, was selected according to the dimension that fitted the porcine aortic root of a specific annulus size.

In the first experimental test 4 different bioprostheses were selected, which fitted a native porcine aortic annulus size of 21 mm. Two of the 4 valves had the pericardial sheet placed outside the stent posts (Trifecta, St-Jude. St. Paul MN with a labelled of 21 and Mitroflow. Sorin Group. Saluggia. Italy with a labelled size of 23), while the other two shared the same strategy design by having the pericardial sheet placed inside the stent posts (Magna Ease. Edwards Lifescience. Irvine. CA with a labelled size of 20 and Soprano-Armonia. Sorin Group. Saluggia. Italy with a labelled size of 20 (Fig. 2).

T Trifecta **Magna-Ease** **Soprano-Armonia** **Mitroflow**

Fig. 2 Type of bioprostheses used for the experimental campaigns.

All the bioprostheses were surgically implanted in 8 porcine aortic roots according to a randomized sequence. The valves were then studied in terms of fluid dynamics (mean pressure drop, effective orifice area and energy loss) and in geometrical terms (by measuring 2 different geometric areas at peak flow aside from the internal geometric orifice area calculated from the internal diameter provided by the manufacture) at set flow levels. In addition, a leaflets kinematics study was undertaken to describe the dynamic response to the flow of the stent-leaflet compound of each prosthesis.

In the second test, two bioprostheses, with macroscopic similar structural features (i.e. with the pericardial sheet outside the stent posts), were tested to detect any subtle differences in the biomechanical behaviour. For this test, Trifecta with a labelled size of 19 and a Mitroflow with a labelled size of 21 were randomly surgically implanted in 10 porcine aortic roots with annulus size of 19 mm. The valves were studied in terms of fluid dynamics and geometrical characteristics.

In the second phase of the project, the experimental campaigns were dedicated to the study of the impact of the bioprosthesis geometry, in particular the form assumed at peak flow, on pressure recovery and spatial position of the "*vena contracta"*. The tests were set up by devising a stationary flow circuit in which the prostheses were housed in a modular model of aorta made in polymethyl methacrylate (PMMA). This modular model,

which included the Valsalva sinuses and a straight ascending aorta, as outflow, was created by a 3-D printer from real aortic root dimensions taken from patients by ultrasound studies. The pressure distribution downstream from the valve, was measured directly by a port, and the velocity of the flow, at *vena contracta*, was measured by doppler. (Fig. 3).

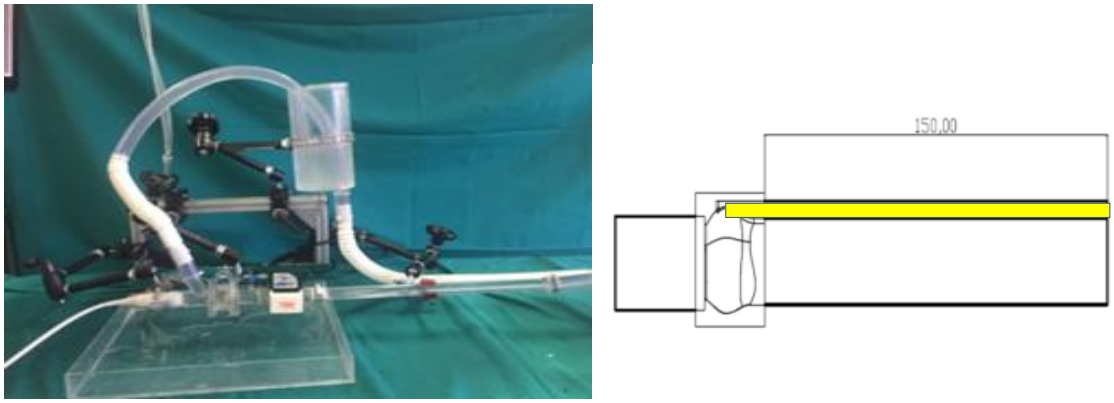

Fig.3 Left. Circuit set-up with the doppler probe. Right. Cylindrical section of 25 mm of diameter and 150 mm long with related port (in yellow) to measure the pressure.

In this experiment, 2 labelled sizes of the Trifecta (19 and 21), 2 of Magna-Ease (19 and 21) and 2 of Crown (21 and 23) were tested.

In a second test on the same prostheses and with the same experimental protocol was performed to confirm the correctness of the results obtained by the previous test by the direct measurements of the pressures and fluid velocities. For this experiment, an equal MRI compatible prototype of the modular model was created and the analysis of the flow through the bioprostheses, was performed by the MRI 4D flow technique,

The third phase of the project, consisted in the development of a coronary flow simulator to analyse the impact of a bioprosthesis implanted in a real aortic root on the local fluid dynamics and coronary flow. The system was conceived to reproduce the characteristic impedance of each coronary artery (Fig. 4), to be adaptable to an existing pulsatile mock

loop and to be connected to each coronary inflow of a real aortic root to exploit its natural anatomy. The tests were conducted comparing the coronary flows of both coronaries of a natural and normal with that of a natural valve after causing a regurgitation. Besides, the coronary flows were tested after the implant of different bioprostheses. For the last test, an aortic root with an annulus of 19 mm was selected in which a Trifecta labelled 19 and 21 as well as a Magna-Ease labelled 19 were implanted.

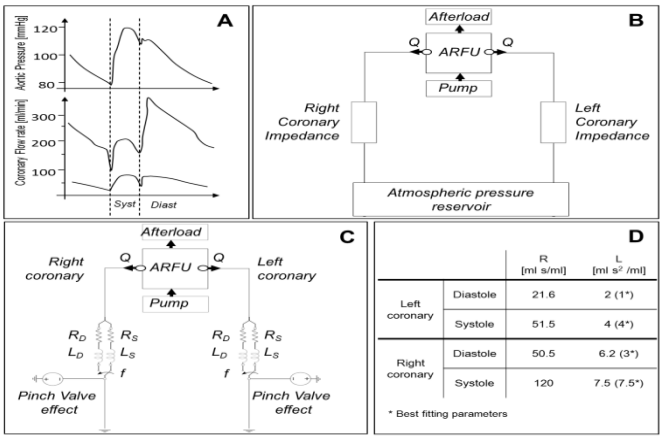

Fig. 4 A) Representative aortic pressure and left and right coronary flow rate tracings. B) Schematic of the coronary impedance simulator. C) Lumped parameter model of the coronary impedance simulator. D) Values of the lumped parmater element adopted in the model. AV: aortic root functional unit; Q: flow rate; R_D, R_S: diastolic and systolic hydraulic resistances respectively; L_D, L_S: diastolic and systolic inertance;

In the fourth phase of the project, in which two experimental tests were carried out, dealt with the impact of the surgical strategy adopted to implant bioprostheses on valve fluid dynamic. In this regard, in the first test two different types of suture techniques were tested comparing a simple suture technique (Fig. 5 A) with a non-everting mattress suture with pledgets (Fig. 5 B). The second test was set up to compare the fluid dynamics of standard surgical bioprostheses, implanted by a standard surgical suture, with a new type of bioprostheses called “sutureless” valve which can be implanted without a surgical suture (Fig.6)

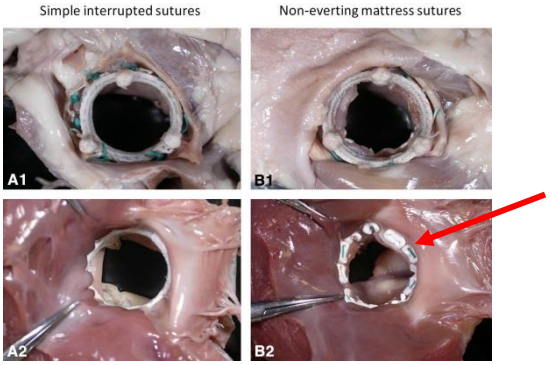

Fig. 5 A 21-mm Carpentier-Edwards Perimount Magna (Edwards Lifesciences, Irvine, Calif) aortic heart valve was implanted in the porcine heart with simple interrupted sutures (A) and noneverting mattress sutures (B). Prosthetic leaflets and aortic sinuses were removed after implantation. A_1, Aortic view of simple interrupted sutures. A_2, Ventricular view of simple interrupted sutures. B_1, Aortic view of noneverting mattress sutures. B_2, Ventricular view of noneverting mattress sutures. The red arrow points at the pledegets.

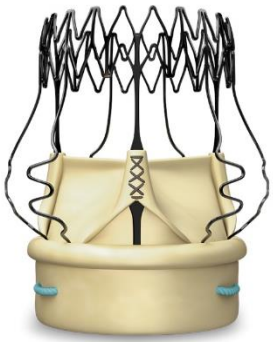

Fig. 6 Sutureless pericardial aortic bioprosthesis

Results

Results of the first phase tests.

The prostheses tested showed to possess a reserve of area (Fig. 7) with the geometric orifice area which increased parallel to the flow increment. In addition, those valves with pericardium housed outside the stent (such Trifecta and Mitroflow), were fluid dynamically more efficient as reported in Table 1 and Fig. 8. The fluid dynamic parameters appeared to be related to the form assumed by the valve at peak flow which was peculiar to the design of the prosthesis (Table 1).

The study of the valve geometric orifice areas revealed that, the Trifecta valve assumed at peak flow a “divergent” form, the Mitroflow assumed a “cylindrical” form, while both Magna-Ease and Soprano-Armonia assumed an “hourglass” form.

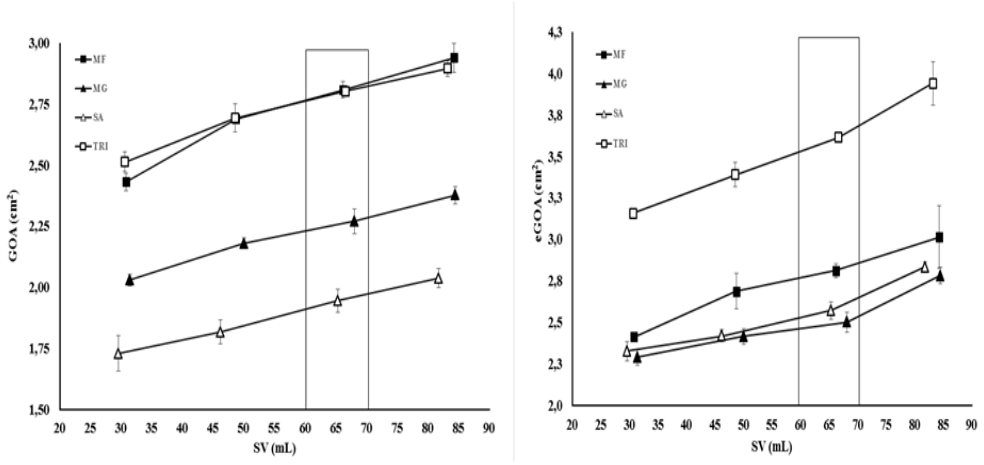

Fig. 7 Relationship between Geometric Orifice Areas (a) and edge Geometric Orifice Area (b) with stroke volumes (SV). Bars represent 95% confidence intervals. The rectangle represents the physiologic SV interval at rest in patients whose body size matches these sizes of prostheses.

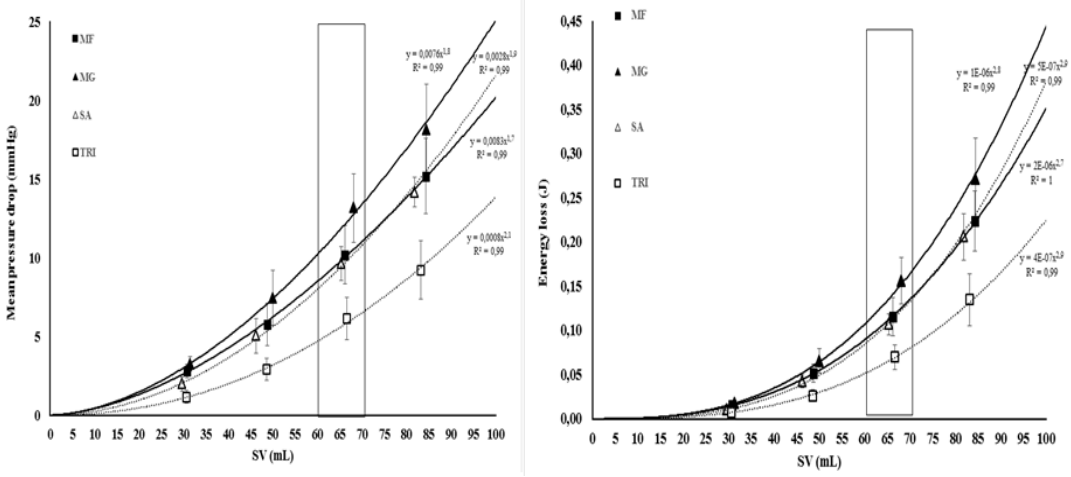

Fig. 8 Relationship between Mean Pressure Drops (left) and Energy Loss (right) with stroke volumes (SV). Bars represent 95% confidence intervals. The rectangle represents the physiologic SV interval at rest in patients whose body size matches these sizes of prostheses.

Table 1. Fluid dynamics and geometrical valve study results

Variables	30 ml	50 ml	65 ml	85 ml	Effect	p-value
Mean Gradient (mmHg)						
MF	2.8±0.64	5.8±1.93	10.2±2.67	15.2±3.46	Valve	<0.001
MG	3.2±0.65	7.4±2.51	13.2±3.15	18.1±4.16	Time (SV)	<0.001
SA	2.0±0.67	5.0±1.57	9.6±1.57	14.1±1.34	Interaction	<0.001
TRI	1.1±0.58	2.9±1.02	6.1±1.93	9.2±2.68		
Energy Loss (%)						
MF	6.5±1.42	8.7±2.45	10.7±2.51	13.3±1.89	Valve	<0.001
MG	7.3±1.41	10.8±3.78	13.5±3.25	15.7±2.81	Time (SV)	<0.001
SA	4.6±1.19	8.3±2.72	10.9±1.79	13.1±1.38	Interaction	<0.001
TRI	2.7±1.23	4.3±1.59	6.6±1.63	8.4±1.79		
EOA (cm^2)						
MF	1.6±0.22	1.8±0.26	1.8±0.21	1.8±0.23	Valve	<0.001
MG	1.5±0.17	1.6±0.26	1.6±0.18	1.6±0.20	Time (SV)	0.57
SA	1.9±0.33	1.80.42	1.7±0.21	1.8±9.20	Interaction	0.13
TRI	2.7±0.48	2.6±0.56	2.3±0.34	2.4±0.42		
GOA (cm^2)						
MF	2.4±0.05	2.7±0.03	2.8±0.05	2.9±0.09	Valve	<0.001
MG	2.0±0.03	2.2±0.03	2.3±0.07	2.4±0.05	Time (SV)	<0.001
SA	1.7±0.10	1.8±0.07	1.9±0.07	2.0±0.05	Interaction	<0.001
TRI	2.5±0.06	2.7±0.08	2.8±0.02	2.9±0.04		
edge GOA (cm^2)						
MF	2.42±0.05	2.69±0.03	2.81±0.05	3.01±0.05	Valve	<0.001
MG	2.29±0.07	2.42±0.07	2.50±0.09	2.78±0.07	Time (SV)	<0.001
SA	2.33±0.08	2.42±0.05	2.57±70.1	2.83±0.04	Interaction	<0.001
TRI	3.16±0.11	3.39±0.11	3.62±0.04	3.95±0.19		
Cc						
MF	0.67±0.10	0.62±0.08	0.62±0.10	0.58±0.08	Valve	<0.001
MG	0.75±0.12	0.67±0.10	0.65±0.04	0.64±0.07	Time (SV)	<0.001
SA	1.07±0.12	0.90±0.18	0.85±0.10	0.85±0.10	Interaction	0.203
TRI	1.05±0.22	0.92±0.14	0.77±0.11	0.76±0.10		
Performance Index						
MF	0.56±0.08	0.62±0.09	0.62±0.08	0.63±0.08	Valve	<0.001
MG	0.49±0.05	0.51±0.08	0.50±0.06	0.52±0.06	Time (SV)	0.56
SA	0.61±0.11	0.59±0.14	0.57±0.07	0.58±0.07	Interaction	0.12
TRI	1.03±0.18	0.98±0.21	0.88±0.13	0.90±0.16		
Geometric Area Ratio						
MF	0.86±0.02	0.95±0.01	0.99±0.02	1.04±0.03	Valve	<0.001
MG	0.65±0.01	0.69±0.01	0.72±0.02	0.76±0.02	Time (SV)	<0.001
SA	0.56±0.03	0.59±0.02	0.63±0.02	0.66±0.02	Interaction	<0.001
TRI	0.96±0.02	1.02±0.03	1.07±0.01	1.10±0.02		

EOA: effective orifice area, GOA: geometric orifice area, Cc= coefficient of discharge.

The study of the leaflets kinematics (fig. 9), did not show any effect of the valve design on leaflets kinematic behaviour, but the latter, appeared to be depending more on other, not apparent, intrinsic structural characteristics related to the material used for the stent and leaflets. In addition, the valve kinematics did not appear to affect the fluid dynamic valve performance (Table 2).

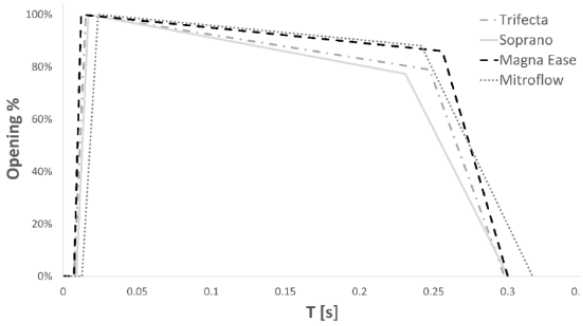

Fig.9 Opening patterns of all the valves tested. T=time.

Table 2. Kinematics and hydrodynamic study results

	TRI	**SA**	**MG**	**MF**	**Anova p-value**	**TRI vs SA** p-value	**TRI vs MG** p-value	**TRI vs MF** p-value	**SA vs MG** p-value	**SA vs MF** p-value	**MG vs MF** p-value
ET (ms)	299±12	300±17	300±12	315±13	0.760	1.0	1.0	1.0	1.0	1.0	1.0
RVOT (ms)	15±3	17±2	12±2	23±3	**<0.01**	1.0	0.286	**<0.01**	**0.03**	**<0.01**	**<0.01**
SVCT (ms)	247±14	231±15	256±26	241±11	0.170	0.463	0.853	0.931	0.213	1.0	1.0
RVCT (ms)	35±19	52±13	32±17	52±4	0.07	0.474	1.0	0.494	0.236	1.0	0.247
TVCT (ms)	283±10	283±19	289±10	293±11	0.584	1.00	1.0	1.0	1.0	1.0	1.0
RVOVI (ms^{-1})	132±25	126±19	209±17	94±8	**<0.01**	0.959	**<0.01**	**0.02**	**<0.01**	0.07	**<0.01**
SVCVI (ms^{-1})	-0.9±0.3	-1.1±0.4	-0.6±0.1	-0.5±0.1	**<0.01**	1.0	0.353	0.292	**0.045**	**0.04**	1.0
RVCVI (ms^{-1})	-16±4	-10±2	-18±6	-10±1	**<0.01**	0.396	1.0	0.513	**0.025**	1.0	**0.03**
Δp (mmHg)	6.7±3.6	10.6±5.5	15.2±7.9	10.7±6.1	**<0.01**	**0.01**	**<0.01**	**0.01**	**0.04**	1.0	**<0.01**
EOA (cm^2)	2.2±1.2	1.7±0.9	1.5±0.8	1.7±0.9	**<0.01**	**0.03**	**<0.01**	**0.01**	0.261	0.617	0.11
El %	7.3±1	11.9±1	15.4±2	11.8±3	**<0.01**	**<0.01**	**<0.01**	**<0.01**	**0.04**	1.00	**0.03**
CO (L/min)	3.1±0.4	2.8±0.5	3.1±0.3	3.0±0.5	0.534	0.282	0.792	0.702	0.106	0.552	0.559

ET= Ejection Time, RVOT= Rapid Valve-Opening Time, SVCT= Slow Valve-Closing Time, RVCT= Rapid Valve-Closing Time, TVCT= Total Valve-Closing Time, RVOVI= Rapid Valve-Opening Velocity Index, SVCVI= Slow Valve-Closing Velocity Index, RVCVI= Rapid Valve-Closing Velocity Index, Δp= Mean Pressure Drop, EOA= Effective Orifice Area, El%= Energy Loss, CO= cardiac output.

Results of the second phase tests

The tests conducted in this phase showed that the spatial pressure distribution downstream the bioprostheses, and thus the pressure drop, differed according to the design of the prostheses (which is related to the form assumed a peak flow) and the level of flow. The Trifecta showed a complete different spatial pressure distribution compared with the Crown and the Magna. The main differences among the valves, were in terms of spatial position of the "vena contracta" as well as on the extent and on the pattern of the pressure

recovery (Fig. 10). Yet, these results may be explained by the specific form assumed by each prosthesis.

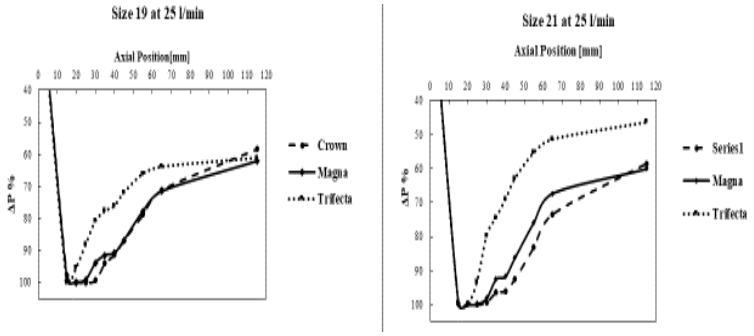

Fig. 10 Pattern of pressure recovery at 25 l/m for each prosthesis. ΔP% is the percentage of the maximal gradient reached by each prosthesis.

The MRI 4D Flow analysis confirmed that the profile velocity was peculiar to each type of valve and consistent with the direct measurements (Fig. 11).

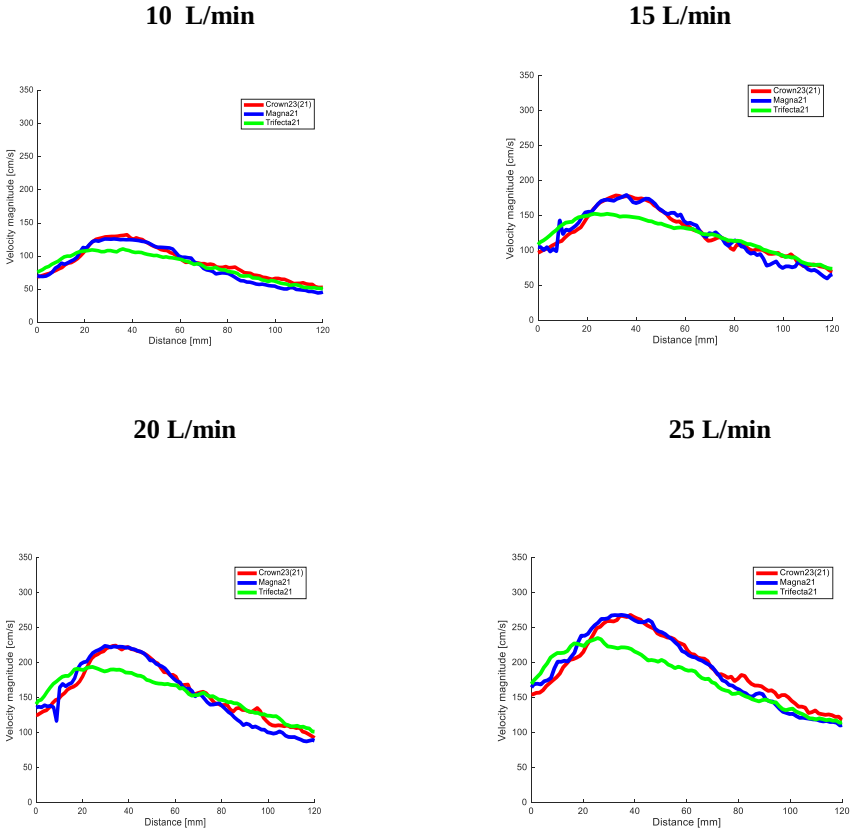

Fig. 11. Velocity profiles at different flow levels for Trifecta 21, Magna 21 and Mitroflow 23.

Results of the third phase tests

The coronary flow simulation system devised can be integrated with the existing left-circulation simulator and appeared to be a simple and well-suited system capable to replicate a physiologic coronary flow behavior (Fig. 12).

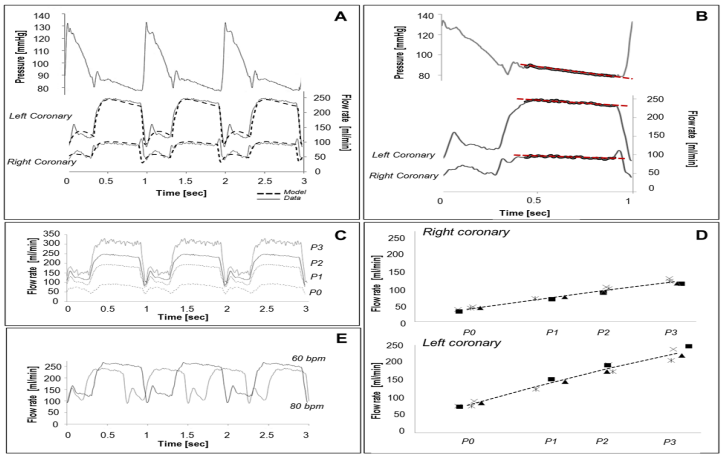

Fig. 12 (A) Representative systemic pressure and left and right coronary flow rate tracings obtained under physiological basal condition (P2). (B) Relation between diastolic pressure slope and coronary flow slope during the diastolic phase (C and E) Right and left coronary flow rate tracings obtained by changing the mean aortic pressure at a fixed beat rate (60 bpm). D Systemic pressure/coronary flow rate relation. Different symbols refer to four distinct experimental sessions.

The coronary simulator was also able to detect a systolic flow perturbation in the right coronary artery when bioprostheses, of different size, were surgically implanted in the aortic root (Table 3 a Fig. 13).

	Left coronary flow mean values			**Right coronary flow mean values**		
	mean systo/diastolic (mL/min)	**mean diastolic (mL/min)**	**mean systolic (mL/min)**	**mean Systo/diastolic (mL/min)**	**mean diastolic (mL/min)**	**mean systolic (mL/min)**
Native Valve	**117±2**	**141±2**	**84±2**	**43±1**	**53±2**	**30±1**
Magna 19	**117±2**	**141±2**	**85±2**	**37±1**	**55±1**	**12±1**
Trifecta 19	**118±1**	**144±2**	**84±1**	**42±0,5**	**55±1**	**26±1**
Trifecta 21	**117±5**	**143±6**	**83±3**	**34±1**	**54±2**	**7±1**

Table 3. Mean coronary flow results for both coronaries

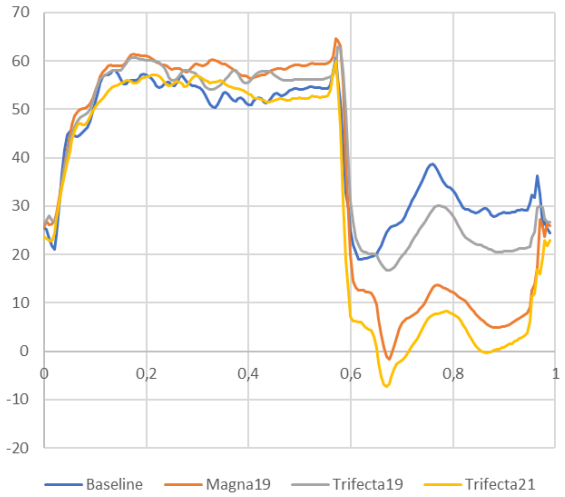

Fig. 13. Right coronary flow comparison, at a stroke volume of 80 mL, between the native valve (baseline) and the group of prostheses implanted.

Results of the fourth phase tests

The results of these tests showed that the type of surgical suture adopted for bioprostheses implantation, especially in small annuli ≤ 21 mm, impacts on prosthesis fluid dynamics. Using a technique such the non-everting suture with pledgets, which may gather tissue underneath the prosthesis (Fig. 14), may be compromised the fluid dynamic performance of a bioprosthesis (fig.15). On the contrary, the adoption a strategy in which a sutureless bioprosthesis is implanted, it is possible to achieve excellent fluid dynamic performances with very low pressure drops and somewhat close to the performance of the native aortic valve (Fig. 16).

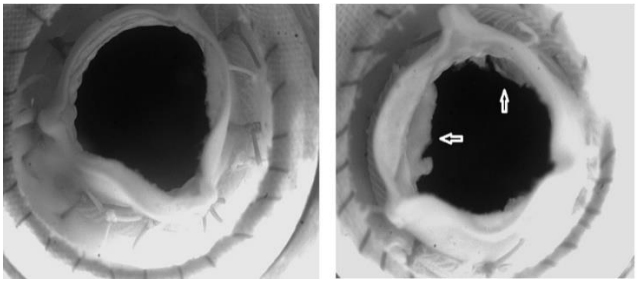

Fig. 14 Left: a 21-size prosthesis implanted with a simple suture. Right: the same prosthesis implanted with non-everting mattress suture with pledgets suture. Arrows point to the tissue gathered underneath the valve.

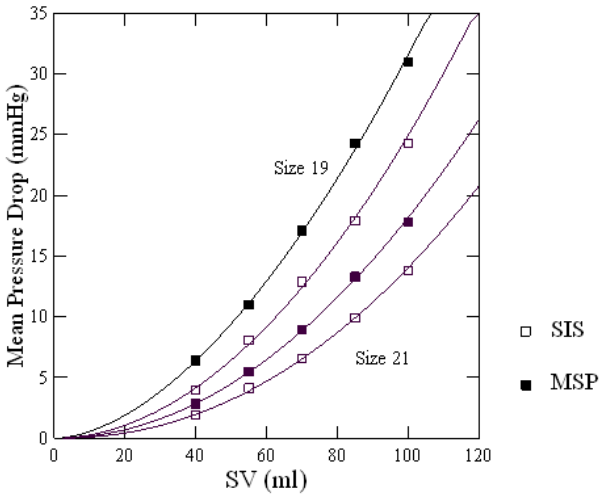

Fig. 15 Mean pressure drops according to prosthesis size (19 and 21) and type of suture adopted. (SIS=Simple Interrupted Suture, MSP= non-everting Mattress Suture with pledgets)

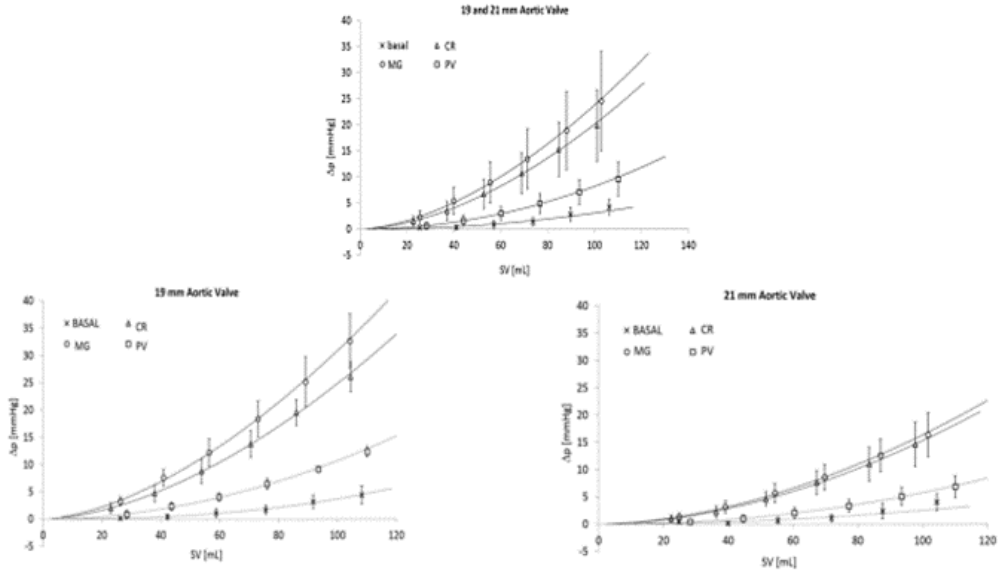

Fig. 16 Mean pressure drops for (A) 19 mm and (B) for 21 mm aortic valves. CR=Crown valve; MG=Magna valve; PV=Perceval valve.

Conclusion

With the present research project, by means of the bioengineering approach, it was possible to describe which were the main biomechanical variables that influenced the fluid dynamic performance of bioprostheses when are implanted inside a native aortic root. It is clear that, aside from the structural characteristics of a device, other aspects must be considered when evaluating the clinical impact of its performance on patients. Indeed, the performance of a bioprothesis depends upon the context in which is implanted, i.e. the patient, with the related the specific anatomical and physiological characteristics. With the new platform devised for reproducing the coronary flow, which proved to be reliable in the assessing the coronary perfusion after a conventional aortic valve implantation. Thus, it will be possible to assess devices such TAVI or "sutureless" valves which use is in rapid expansion.

The acquisition of a widen perspective and knowledge by the physicians', makes the clinical practice more articulated and comprehensive with possibly a more effective decision-making process. The integration of both medical and bioengineer background can prompt a novel "hybrid" vision in physicians. Indeed, merging medical knowledge with the bioengineering analytical approach, increase the ability of the surgeons to analyze and understand the complex physiologic phenomena which are affected by the surgical procedure of a valve implantation.

CHAPTER 1

Introduction

Cardiac surgery is a medical discipline which, by now, is out of its pioneering phase. Indeed, in the last decade the operative mortality has declined to such an extent that the attention has now turned to how to improve the long-term survival of the patients. Meanwhile, new therapeutic approaches for the treatment of aortic valve disease, have been put forward, gaining solid ground. One of these is the technique of implanting valves without the need of a surgical suture by using "sutureless" bioprostheses (1). This technical solution has captured the attention of many physicians and has been implemented at a rapid rate, offering new therapeutic opportunities.

Although these new procedures still must provide the same solid results as the traditional ones, a fact is apparent namely the overwhelming irruption of technology in the medical field and in particular in the cardiovascular discipline. But, one of the "side effect" of this relentless development brought by the technology, is the widening of the knowledge gap between the technological content of the device and the physician that use it.

Biological cardiac prostheses have been developed to be an alternative to mechanical ones, which require anticoagulant therapy that carries morbidity with it. The first bioprostheses were made available in the 60s and were natural heart valves (from human and animals) but due to the rapid structural deterioration, for a certain period, their use has been substantially abandoned.

In the 70s biological prostheses, made up using a rigid support structure and porcine or

bovine pericardium valvular leaflets, have become available. These valves had the advantage of being implanted by means of a simple, reproducible and standardized technique. In addition, thanks to the improvement in their resistance of fatigue, this type of prostheses has become widespread since.

With further improvements, the bioprostheses in the last 2 decades have proven to be devices with good fluid dynamic and durability characteristics.

Following the increase of the life expectancy of the western population and the appearance of the degenerative native valve disease age-related (2), the demands of biologic valves have risen sharply.

Notwithstanding the substantial technological improvement of the last two decades, the bioprostheses currently on the market yet offer a certain degree of flow obstruction and, therefore, still far from the performance of a native aortic valve.

Fluid dynamics of a bioprosthesis is of paramount importance because its residual flow obstruction demands the heart to provide an extra energy, at every beat, to maintain the adequate flow to the body needs. This cardiac extra-load increases short and long-term probability of death in addition to the increase of the patients' morbidity (3,4). Besides, a prosthesis with a high gradient degenerates more rapidly (5), which in turn, influences the patient's likelihood of survival and increases the risk of reoperation. Thus, an efficient bioprosthesis, i.e. with low pressure drop, might improve patient's survival.

Design and the materials used to make a prosthesis are the unique structural properties of each prosthesis which affect their biomechanical behavior.

To know which prostheses are the most efficient is a critical information for surgeons. Unfortunately, clinical studies, even when randomized do not provide solid answers on

the difference in fluid dynamic characteristics among bioprostheses because it is difficult to make a fair comparison among the different prostheses.

Complexity of the clinical scenario

Surgical valve implantation is a very intricate process because is affected by the specific patient's anatomic and physiologic characteristics, the technique adopted for the valve implantation, the manufacturer's sizing strategy and surgeon experience. All these variables affect the size of prosthesis to be implanted and thus the fluid dynamics. The left ventricular outflow tract (LVOT) characteristics (shape and size) and annulus-prosthesis interaction may affect how smoothly/abruptly the flow lines approach and enter the prosthesis. In addition, the size of sinotubular junction (STJ) and the ascending aorta w affect the extent of pressure recovery and the velocity of the fluid at the "*vena contracta*" (6). The manufacturer's sizing strategy is specific to each valve brand and implies that, prostheses with different labeled sizes but made by different manufacturers, may fit the same aortic root (7). While the impact of the surgical procedure depends on the surgeon's aptitude and experience, as well as the suture technique adopted. Clearly, a prosthesis which has an efficient design and thus an excellent intrinsic fluid-dynamic performance tends to blunt the effects of a suboptimal-size valve implantation. Hence, it is important for the surgeons to know, in dept, the peculiarity of each valve to exploit it at best. For this reason, it is indeed crucial to provide the surgeons with reliable, complete and realistic information on the valves biomechanical features. The information are reliable, complete and realistic when the bioprostheses are compared in the same anatomical (i.e. aortic root geometry) and physiological (i.e. pulsatile flow) conditions.

Besides, to enhance the reliability of the information acquired, the first step is to replicate as faithfully as possible the real scenario. This can be obtained by implanting the bioprostheses, by a surgical procedure, in real aortic roots. Indeed, standard pulsatile in vitro systems have the limitations to not realistically reproduce the local conditions which impact on the fluid dynamics. All these conditions at the same time, can be obtained only in an in vitro setting with real aortic root. In traditional in-vitro studies, the prostheses are not implanted by a suture, eliminating a variable necessary for a realistic fluid dynamics evaluation of a prosthesis. Thus, the experimental setting should be a natural aortic root in which the prostheses are implanted with a surgical suture and evaluated with a pulsatile flow.

Aim of the project

The objective of the work of this PhD course, was to study the biomechanics of bioprostheses surgically implanted in a real aortic functional root unit to acquire realistic information to be put into clinical context. Indeed, the integration of both medical and bioengineering background should prompt a novel “hybrid” vision merging medical knowledge with the bioengineering mechanistic approach. This approach should allow to identify most of the challenging aspects of the complex surgical scenario that surgeons face in his/her everyday activity improving the decision-making process.

Bibliography

1-Zannis K., Folliguet T., Laborde F. New sutureless aortic valve prosthesis: another tool in less invasive aortic valve replacement. Curr. Opin. Cardiol. 2012;27(2):125–129.

2-Thaden JJ1, Nkomo VT2, Enriquez-Sarano M. The global burden of aortic stenosis. Prog Cardiovasc Dis. 2014;56(6):565-71

3-Tasca G, Brunelli F, Cirillo M, et al. Impact of valve prosthesis-patient mismatch on left ventricular mass regression following aortic valve replacement. *Ann Thorac Surg*. 2005;79(2).

4-Tasca G, Mhagna Z, Perotti S, et al. Impact of prosthesis-patient mismatch on cardiac events and midterm mortality after aortic valve replacement in patients with pure aortic stenosis. *Circulation*. 2006;113(4).

5-Flameng W, Herregods MC, Vercalsteren M, Herijgers P, Bogaerts K, Meuris B. Prosthesis-patient mismatch predicts structural valve degeneration in bioprosthetic heart valves. Circulation. 2010; 18;121(19):2123-9

6-Toninato R, Salmon J, Susin FM, Ducci A, Burriesci G. Physiological vortices in the sinuses of Valsalva: An in vitro approach for bio-prosthetic valves. J Biomech. 2016;49(13):2635-2643.

7-Doenst T, Amorim PA, Al-Alam N, Lehmann S, Mukherjee C, Faerber G. Where is the common sense in aortic valve replacement? A review of hemodynamics and sizing of stented tissue valves. J Thorac Cardiovasc Surg 2011;142:1180-7.

CHAPTER 2

BIOMECHANICS OF PERICARDIAL PROSTHESES SURGICALLY IMPLANTED

These studies have been undertaken in collaboration with the following Institutions:

-Cardiovascular Surgery Depatment, "L. Sacco" Hospital, Università degli Studi di Milano, Milan, Italy.

-ForCardio.lab, Fondazione per la Ricerca in Cardiochirurgia ONLUS, Milan, Italy

-Cardiovascular Department, Cardiac Surgery Unit, Ospedale "A. Manzoni" ASST-Lecco. Lecco, Italy.

This Chapter is based upon the following papers:

-Tasca G, R. Vismara, GB Fiore, et. Al. "Fluidodynamic results of "in-vitro" comparison of 4 pericardial bioprostheses implanted in small porcine aortic roots. *Eur J Cardiothorac Surg*. 2015;47:e62-7.

-Tasca G, Fiore GB, Redaelli P, et. Al. Hydrodynamic and Geometric Behavior of Two Pericardial Prostheses Implanted in Small Aortic Roots. *ASAIO J*. 2017; 64(1):86-90.

-Tasca G, Vismara R, Fiore GB, et. Al. A comprehensive fluid dynamic and geometric study from an "in-vitro" comparison of 4 pericardial stented valves surgically implanted. The complex scenario of an implanted bioprosthesis. *J Heart Valve Dis* 2015 ;24(5):596-603.

-Tasca G, Fiore GB, Mangini A, et. Al. Opening-closing pattern of four pericardial prostheses: results from an in vitro study of leaflet kinematics. *J Artif Organs*. 2016;19(4):350-356.

Introduction and aim

After aortic valve replacement (AVR), patients with native small aortic valve annuli, are at risk of residual high pressure drops across the prosthesis (1,2). In this unphysiological condition the left ventricle must transfer to the blood an extra-energy, at every beat, to maintain the body blood flow requirements. Patient-prosthesis mismatch, which is an estimation of this extra workload, has demonstrated to affect patients' clinical outcomes after aortic AVR (3-6).

Stented bioprostheses are still quite inherently obstructive, and their hydrodynamic performances are far from being close to that of native aortic valves (7).

Apart from intrinsic structural features (i.e. materials used and design), the fluid dynamical performance of a prosthesis is affected by the context in which is being implanted. In actual fact, the patient's heart possesses its specific anatomical and physiological peculiarities that may differ considerably from one patient to another. Besides, prostheses from different manufactures, apart from design, are different in their true dimensions, such as internal diameter (ID), tissue annulus diameter (TAD) and external diameter (ED) (8-10) although the equal labelling.

The combination of this valve heterogeneity in geometrical terms with the variability in patients' aortic root physiology and anatomy, hinders a proper comparison among prostheses even with randomized *in-vivo* studies.

The geometry of the aortic root is of particular importance because it cannot be modified. Indeed, left ventricular outflow tract (LVOT) features (in term of shape and size) and the annulus-prosthesis interaction may affect how smoothly/abruptly the upstream lines

approach and enter the prosthesis affecting the size of the *vena contracta*. Additionally, the size of sino-tubular junction (STJ) and the ascending aorta affect the downstream lines reattachment and the vortex formation with an impact on the extent of the size of the *vena contracta* and the pressure recovery (11-12).

In the real case scenario, i.e. in patients, one other tile of the mosaic plays an important role, that is the need to surgically suture the prosthesis inside the aortic root. This is a process which hides several pitfalls that influences the size of prosthesis to be implanted, which is the main factor affecting the fluid dynamics performance. In the implantation process, the size of the prosthesis implanted depend upon manufacturer's sizing strategy (8), surgical procedure adopted and the patient's aortic root anatomical characteristics (9,10).

The manufacturer's sizing strategy is specific to each valve brand and implies that prostheses with different labelled sizes, but made by different manufacturers, may fit the same aortic root size (9,10). Besides, in this process, the surgeon's aptitude and experience, as well as the suture technique adopted (13) may influences the prosthesis size implanted.

Some authors (14) have also suggested that leaflets kinematics behavior may influence the pressure drop with the assumption that the faster the valve opens the lower the pressure drop.

This extremely complex scenario makes very difficult to differentiate the fluid dynamic characteristics in the comparison of different prosthesis types. In this regard, in evaluating the fluid dynamics of a prosthesis, the *in vitro* setting is the "gold standard" on account

of the high accuracy of measurements and its experimental reproducibility.

To obtain a realistic prostheses comparison, it is required to limit the bias related to the anatomic and physiologic variabilities linked to the aortic roots, as well as those related to the surgical techniques. That means that, different prostheses should be implanted in the same aortic root with the same suture technique and exposed to the same levels of flow.

The following experimental campaigns were aimed at evaluating any differences in the biomechanical characteristics (in term of fluid dynamics, geometry and leaflets kinematics) of the most widely available pericardial bioprostheses for clinical use. To obtain a fair comparison, in all the experiments, the valves were selected among those that fitted equal real porcine aortic roots and tested at equal physiologic conditions. Besides, to render the experiments more realistic the valves were surgically implanted. In the first experiment, bioprostheses such Mitroflow, Soprano-Armonia (Sorin Group. Saluggia. Italy), Magna Ease (Edwards Lifescience. Irvine. CA) and Trifecta (St-Jude Medical. St Paul. MN) (See Fig. 2 from the abstract) were tested with the aim to understand the impact of the valve design on the biomechanical behaviour, in term of fluid dynamics, valve geometry and leaflets kinematics.

In the second experimental campaign, two prostheses from different manufactures but with similar design (Fig. 1), were tested to find out any subtle differences in their biomechanical behaviour. That because, usually, being similar in design these two prostheses are regarded as equal in terms of fluid dynamics. The two pericardial

bioprosthesis tested were Mitroflow (Sorin Group. Saluggia, Italy), and Trifecta, (St-Jude Medical, St Paul, MN).

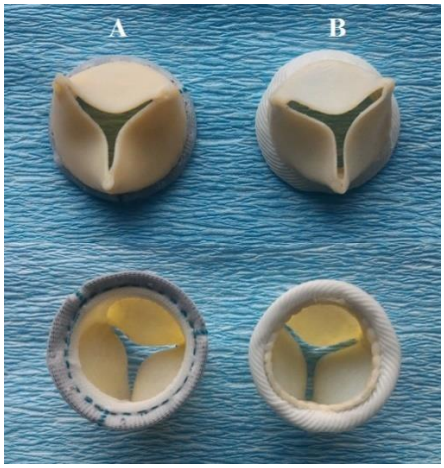

Figure 1. Panel A**:** the Mitroflow bioprosthesis from aortic view and from ventricular view. Panel B: Trifecta bioprosthesis from aortic view and from ventricular view.

Materials and Methods

FoRcardioLab pulsatile mock loop

The FoRcardioLab mock loop (15-18) is a computer-controlled volumetric pump able to replicate left ventricular flow waveforms (Fig. 2); its test section is designed to house a whole aortic root unit (ARU) and it is equipped with an adjustable hydraulic afterload mimicking the hydraulic input impedance of the systemic circulation.

For these experimental campaigns, the mock loop was equipped with a transit-time flow-meter (HT100R, Transonic System Inc., Ithaca, NY), the 1” probe of which was placed downstream of the ARU sample, and with three pressure transducers (PC140 series, Honeywell Inc, Morristown, NJ): one immediately upstream and one immediately downstream of the sample, and the third placed at the inlet section of the hydraulic

afterload part. A high-speed digital camera set at 1000 frames per second (Phantom Miro2, Vision Research, Morristown, NJ) was placed downstream of the sample so as to acquire an aortic view of the working prostheses. Hydrodynamic data were acquired via an A/D board (USB 6210, National Instrument, Austin, TX).

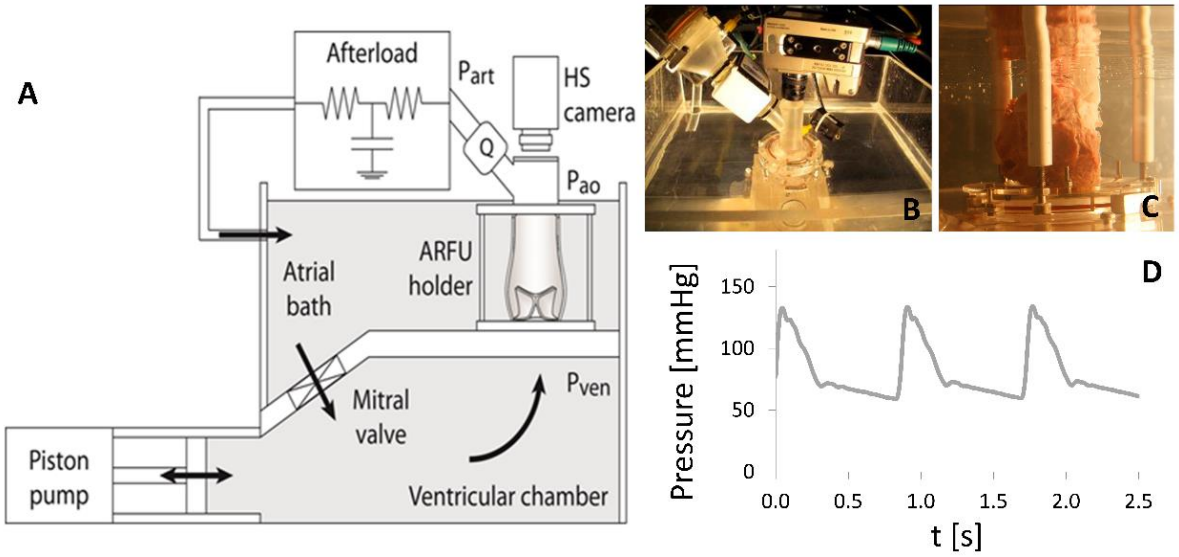

Figure 2. Panel A, schematic of the mock loop. The black arrows indicate flow directions. P_{ven}: port for ventricular pressure measurement; P_{ao}: port for pressure measurement downstream of the aortic root; P_{art}: port for measurement of simulated arterial pressure; Q: flow meter probe; HS camera: High speed camera. Overall encumbrance of the device was about 600x400x500 mm. Panel B, photograph of the test section of the experimental apparatus; Panel C: a detail of the housing section, with an aortic root mounted. Panel D: a representative course of the systemic pressure simulated with the mock loop.

Sample preparation and prosthesis sizing for the First test

Eight fresh whole swine hearts, with a native aortic valve annulus of 2.1 cm, were selected. Prosthesis sizing procedure, was performed by using the probes and the valve replica, provided by the manufacturers for each prosthesis, on the 8 whole porcine hearts to select the prosthesis that fitted the annulus size.

The Trifecta (TRI) and the Magna Ease (MG) probes, that fitted the annulus, had the label size of 21. For Mitroflow (MF), the sizing procedure was undertaken exclusively with the valve replica, because it was the only tool provided by the manufacturer, and the labeled size 23 was chosen. These 3 valves – i.e. TRI, MG and MF – have the same ED, which is 2.6 cm.

Concerning the Soprano-Armonia (SA), even though the probe for the size labeled 22 was able to get through the native valve annulus, the valve replica appeared too bulky; thus, the size 20 was chosen.

The ARU samples were then harvested by including 1.5 cm of the left ventricular outflow tract, which was rendered cylindrical by suturing the anterior mitral valve leaflet to the adjacent muscular septum.

The ascending aorta was transected 0.5 cm above the sino-tubular junction and the coronary ostia were ligated. Circular Dacron meshes were sutured to the inflow and outflow to hold the aortic root samples into the housing section of the mock loop (15-18).

The implantation valve sequence was conducted by following a randomization protocol.

Sample preparation and prosthesis sizing for the second test

For this experimental campaign, we selected 10 fresh swine hearts with native aortic valve annuli of 19 mm, as measured by a metric probe. The matching of the prosthesis size to the aortic valve annulus size was performed using the valve replica provided by each manufacturer. The probes that fitted in the ARU for the TRI had the label size of 19, while for the MF the size was 21.

Albeit the labelled size was higher for the MF, compared to the TRI, both had the same sewing cuff diameter, i.e. 24 mm. Thus, the only macroscopic difference between the two prostheses was in their internal diameter (ID), which were 15.7±0.3 mm for TRI and 17.5±0.3 mm for MF. These values, which lead to 24,3% difference in cross-sectional area, were in accordance with both that reported in literature (19).

The samples were prepared to be tested as detailed in the above paragraph (15-18) and, in each aortic root, the two prostheses were implanted following a randomization

protocol.

Experimental protocols

Protocol for the first experimental test

Tests were conducted at stroke volumes (SV) of 30 ml, 50 ml, 65 ml and 85 ml. The systolic ejection time was set at ⅓ of the entire cardiac cycle, the heart rate at 70 bpm, and the mean simulated arterial pressure was maintained between a range of 80–104 mmHg.

After housing each aortic root unit (ARU) sample in the test-section holder, the 4 bioprostheses were implanted in a randomized sequence. For each experimental point, data were evaluated over 5 consecutive simulated heart cycles.

The prostheses were implanted, in each ARU, by an experienced surgeon and by means of a simple interrupted suture technique with ethylene terephthalate sutures (Ethibond 2/0).

The flow rate, the pressures upstream and downstream of the aortic root, and the pressure in the afterload were acquired at a sampling rate of 200 Hz via an A/D acquisition board.

Post-processing of the raw data was performed to calculate the following quantities:

- The mean systolic pressure drop (Δp_m, mmHg) across the aortic root unit: i.e. the difference between pressures measured immediately upstream and downstream of the ARU was averaged over the systolic interval.
- The effective orifice area (EOA) cm^2, was calculated from the following formula: $EOA(cm^2) = \frac{Q_{rms}}{k\sqrt{\Delta p_m}}$

where Q_{rms} (L/min) is the square root of the mean systolic flow rate, Δp_m (mmHg) the mean systolic pressure drop across the sample and k is a conversion factor (k = 3.1 to yield the EOA in cm^2).

- Geometric Orifice Area (GOA) (cm^2) was semi-quantitatively evaluated by means of high-speed as the largest cross-section opening area recorded during systole.
- Edge Geometric Orifice Area (eGOA) (cm^2) was semi-quantitatively evaluated from the high-speed videos by tracking the free edges of the prostheses' leaflets at the systolic peak, and by integrating the resulting area.
- Space efficiency = was defined as the ratio between GOA and the area calculated from the external diameter of the prosthesis (or the diameter of the sewing cuff).
- Performance index (Pi) = was defined as the ratio between EOA/inner GOA. Inner GOA was calculated directly from the ID values provided by the manufacturers: TRI=1.83 cm, MF=1.9 cm, SA=1.98 cm and MG=2.0 cm.
- Systolic Energy loss: as the energy provided by the pump that is lost when the fluid passes through the prosthesis and was expressed in Joules (J).
- Systolic Energy loss (%): as percentage of the energy provided by the pump that is lost when the fluid passes through the prosthesis.
- Coefficient of Contraction (Cc)= was defined as the ratio between EOA/GOA

- Geometric Area Ratio= was defined as the ratio between GOA/inner GOA, where the Inner GOA was directly calculated from the ID of the prosthesis.

The GOAs and eGOAs were evaluated from high-speed videos by mean of a semi-automated tracking algorithm developed in Matlab (MathWorks Inc, MA, USA) (18). The data on leaflet kinematics were obtained from the high-speed movies by extracting the time-course of the two-dimensional geometric orifice area. For this purpose, an in-house developed code was implemented in MATLAB (The Math Works, Natick, MA, USA) to automatically identify and segment the valvular orifice in each frame of three consecutive cardiac cycles. The time-course of the area in these three cycles was subsequently averaged and normalized to obtain a single curve ranging from 1 (maximum valve opening) to 0 (closed valve) for each valve tested. By adapting the approach described by Leyh et Al. (20) for echocardiography data, three distinct phases of the ejection time (ET) leaflets valve motion were identified and quantified as:

• Rapid valve-opening time (RVOT), ms

• Slow valve-closing time (SVCT), ms

• Rapid valve-closing time (RVCT), ms

Time-intervals were estimated from experimental data through a least mean square approach, which enables the interpolating segments a, b and c to be identified for each phase (Fig. 3), where GOAn in the ordinate is the GOA normalized to the maximum value of GOA. A more detailed description of this procedure has been published elsewhere (18). The slope of each segment provides the velocity indexes:

• Rapid valve-opening velocity index (RVOVI), ms^{-1}

• Slow valve-closing velocity index (SVCVI), ms^{-1}

• Rapid valve-closing velocity index (RVCVI), ms^{-1}

In only 5 of the 8 samples in each prosthesis group was the prosthesis well aligned to the root axis, thereby ensuring a correct geometric area measurement.

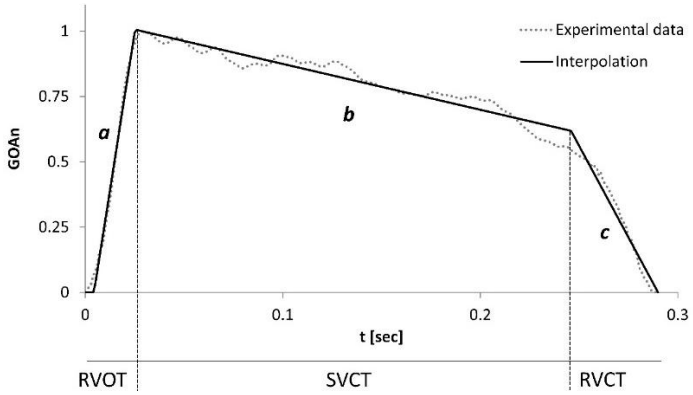

Figure 3. Example of experimental course of the GOAn (geometric orifice area normalized to its maximum value, grey dotted line) interpolated with segments a, b, c (black line). RVOT: rapid valve-opening time; SVCT: slow valve-closing time; RVCT: rapid valve-closing time. Slopes of a, b, c provide the velocity indexes RVOVI, SVCVI, RVCVI, respectively. T= time. Adapted from Vismara et al. 2014, IJAO.

Protocol for the Second experimental test

In this experiment, the tests were run at different physiologic stroke volumes (SVs) imposed by the pump (30 mL, 45 mL, 60 ml, 75 mL, 90 mL and 105 mL).

The systolic ejection time was set at ⅓ of the entire cardiac cycle, and the heart rate at 70 bpm, with a mean simulated arterial pressure of 80–104 mmHg. For a fair assessment and realistic comparison, the cardiac output (CO) and the simulated arterial pressure, at each SV, were acquired and compared.

The prostheses were implanted, in each ARU, by an experienced surgeon by means of a simple interrupted suture technique with ethylene terephthalate sutures (Ethibond 2/0). Raw data from five consecutive heart cycles were post-processed to calculate the following quantities:

- The mean systolic pressure drop (ΔP_m, mmHg) across the ARU, as the difference between the pressures measured upstream from and downstream of the prosthesis,

averaged over the systolic interval.

- Valve Resistance (VR, dyne s/cm^5) was calculated by the following formula:

$$VR = h\,\frac{\Delta P_m}{SV}$$

Where h was a conversion factor to yield the VR in dyne s/cm^5 (h = 1333), ΔP_m was the mean systolic pressure drop (mmHg), and SV was the stroke volume (mL).

- The EOA (cm^2), calculated by means of the following formula [11]:

$$EOA = \frac{Q_{rms}}{k\sqrt{\Delta p_m}}$$

where Q_{rms} (L/min) was the root-mean-square of the systolic flow rate, ΔP_m (mmHg) the mean systolic pressure drop across the sample, and k a conversion factor (k = 3.1 to yield the EOA in cm^2).

- Percent Energy loss ($E_{l\%}$): was the ratio, expressed as a percentage, of the energy dissipation (E_l) through the prosthesis to the energy (E_p) provided by the pump to the fluid.

E_p was calculated by the following equation:

$$E_p = \int_T P_V(t)Q(t)\,dt$$

where T was the cycle pulse period, P_v(t) was the pressure in the ventricle, and Q(t) was the measured flow rate;

E_l in turn was evaluated with the following equation:

$$E_l = \int_{T_s} \Delta P(t) Q(t)\, dt$$

where T_s was the systolic duration in time, and Δp(t) was the pressure drop across the valve. The design of the experimental apparatus ensured that pressure downstream from the valve was acquired where the pressure-recovery was complete.

Energy loss evaluation based on pressure drop hence represented the whole hydrodynamic energy dissipation across the valve.

From the geometrical standpoint, the internal geometrical orifice areas (iGOA) of the two prostheses were calculated directly from the IDs.

In each cycle analyzed, the following areas were semi-quantitatively measured from the high-speed videos at the systolic peak following the same protocols of the first experiment:

- The edge geometrical orifice area (eGOA), defined as the cross-sectional area evaluated at the free margin of the cusps of the prostheses, where the images from the high-speed recordings were dimensionally calibrated.
- The percent geometrical orifice area (%GOA), defined as the limiting cross-sectional area available for the fluid at peak systole for each SV, normalized over the maximum value recorded with the same prosthesis across all the tested SVs.

Statistical analysis

Continuous variables were expressed as mean values ± standard deviation (SD) and compared by means of ANOVA for repeated measures with Bonferroni's test used in

post-hoc analysis; in the graph, the values are reported with 95% confidence intervals; p values < 0.05 were considered significant. The data were analyzed by means of Statsoft 8.2 software.

Results from the first test

No valves displayed any significant structural problems in any of the test sessions. Table 1 reports the results of the study. The Energy loss and the mean pressure gradients (Fig. 4) increased with SV in all the valves tested, with TRI displaying the lowest extent of both terms which were statistically significant compared with those of the other prostheses tested.

The EOA values were rather stable across the SV intervals (p=0.57) and consistent with the pressure drops and Energy loss results; Once more the TRI showed the largest EOAs values (Table 1 and Figure 5) which were statistically significant compared with that of the other 3 prostheses. Same considerations apply for the Pi, being the ratio between EOA and Inner GOA.

The eGOA increased significantly as SV increased, with TRI providing the largest values as shown in Table 1 and Figure 6. In TRI (and MG with a lesser extent), the most distal cross-section area was systematically greater than in the other prostheses, which suggests a divergent configuration at systolic peak. The GOA also increased significantly on increasing SV, with TRI and MF providing the largest area (Table 1 and Figure 6).

Results from the study of Leaflet Kinematics

During the opening phase, the MG showed the shortest interval time, with an RVOT of 12±2 ms, and thus, the fastest opening velocity with an RVOVI of 209±17 ms^{-1}.

The MG RVOT was significantly shorter than that of MF (P<0.01) and SA (P=0.03)

respectively while the MG RVOVI was significantly higher than those of all the other prostheses (Table 2). Conversely, MF showed the slowest profile, with an RVOT of 23±3 ms and an RVOVI of 94±8 ms^{-1} (Table 1 and Figure 3). The TRI and the SA showed similar opening patterns, with an RVOT of 15±3 ms and an RVOVI of 132±25 mm^2/sec for TRI and 17±2 ms and 126±19 mm^2/sec for SA, respectively, without statistically significant differences.

Regarding the closing phase, no significant differences among the bioprostheses were found in the two components of the closing time, namely the SVCT and RVCT. Conversely, the TRI and the SA showed the highest SVCVI, but only the SA SVCVI was significantly higher than those of MG and MF (p=0.045 and p=0.04, respectively). The RVCVI of MG and TRI (-18±6 ms^{-1} and -16±4 ms^{-1}, respectively) were higher than those of MF (-10±1 ms^{-1}, p=0.03) and SA (-10±2 ms^{-1}, p=0.025). MG and MF displayed similar SVCVI values: -0.57±0.1 ms^{-1} and -0.55±0.1 ms^{-1}, respectively (p=1.0).

From the fluid-dynamic standpoint, the CO ranged from 2.8±0.5 L/min (SA) to 3.1±0.4 (TRI), differences being not statistically relevant (P=0.534). The TRI showed the lowest mean pressure drop (6.7±3.6 mmHg), which was statistically significant when compared with MF (p=0.01), SA (p=0.01) and MG (p<0.01) respectively. Accordingly, the EOA of TRI (2.2±1.2 cm^2) was the largest and statistically significant when compared with MF (p=0.01), SA (p=0.03) and MG (p<0.01) respectively (Table 2). MF and SA displayed similar pressure drops and EOAs, while MG showed the greatest pressure drop with 15.2±7.9 mmHg, (p≤0.04) and an EOA that was lower than those of MF and SA, though not significantly. Energy loss displayed a trend consistent with pressure drops across the valve, ranging from 7.3% (TRI) to 15.4% (MG).

Results from the second test

Depending on the imposed SV, the CO and the mean arterial pressure ranged from 1.4±0.2 to 6.2±0.9 L/min and from 63±9 to 102±11 mmHg, respectively (for TRI), and from 1.3±0.5 to 6.1±0.9 L/min and from 60±12 to 105±6 mmHg, respectively (for MF), with no statistical differences between the two prostheses when compared at the same SV (p=0.164). Table 3 reports the experimental data obtained in all the configurations tested. The panels in Figure 8 report the courses of the data as a function of the SV. Figure 8A reports the ΔP_m as a function of SVs. In both prostheses, the ΔP_m varied significantly with the SV. TRI performed slightly better than MF at SVs <60 ml (p<0.01) while providing the same ΔP_m at physiologic SV, i.e. 60 ml. At higher SVs, the performance of MF was slightly better than that of TRI (p=0.09). The $E_{I\%}$ and the VR (Figures 8B and 8C, respectively) were consistent with the trends of the ΔP_m. Notably, for the TRI, VR increased linearly over the whole range of SVs tested, while in MF it was stable at the lower SVs. The EOA (Figure 3D) of TRI was stable over the whole range of SVs (from 1.5±0.12 cm^2 at 30 mL to 1.5±0.13 cm^2 at 105 mL, p=0.45). Conversely, the MF better exploited its geometric characteristics at higher SVs, with EOA increasing with SV (from 1.0±0.06 cm^2 at 30 mL to 1.6±0.06 cm^2 at 110 mL, p<0.01).

From the geometrical standpoint, in both prostheses the eGOA increased with SV (Figure 8E), with TRI showing significantly larger distal areas than MF (p=0.01). The iGOA of the two prostheses, as evaluated from manufacturers' data, were 2.0 cm^2 for TRI and 2.4 cm^2 for MF. TRI provided a larger eGOA than the iGOA at all the SVs tested; this suggested a divergent-shaped fully opened configuration. In the MF, the eGOA was smaller than the iGOA at lower SVs, thus suggesting a convergent configuration at these

values of SV, while at SVs ≥ 60 ml, eGOA exceeded iGOA; this suggests that MF also displays a divergent configuration at higher SVs. Concerning the %GOA (Figure 8F) TRI opened to its maximum extent in a stable fashion over all the SVs tested. Conversely, MF showed an area-recruitment behavior, reaching 100% of its available geometrical area at the highest SVs.

Discussion

Theoretical aspects

Prostheses are totally passive structures; thus, the biomechanical characteristics are affected by the interaction between the hydrodynamic determinants and the inertial mass of the cusps-stent complex. Interaction between prosthesis and flow is mainly subjected to the concentrated loss of head laws.

The magnitude of the mechanical energy dissipated correlates well, after pressure recovery has taken place, with the pressure drop across the orifice (21) with a quadratic relationship with flow.

Pressure drop, for a certain flow, depends upon prosthesis structural characteristics (which are peculiar of stent design and material used), geometric property (ID and the GOA projected by the leaflets) and both inflow (left ventricular outflow tract (LVOT)/prosthesis) and outflow (prosthesis/sino-tubular junction and ascending aorta) characteristics (11-12).

The orifice provided to the flow by the bioprosthesis is the result of the interaction between the inner GOA, calculated from the ID and theoretically the largest orifice available for the flow, and the projected GOA of the leaflets when the valve is fully opened. The flow, passing through these two orifices contracts with its minimum at the

level of "*vena contracta*" and where the fluid reaches its maximal velocity.

The EOA represents the actual geometric area used by the flow and is the term from which the pressure drop mainly depends. Contrary to the Doppler, the EOA calculated with invasive procedure or "*in vitro*" setting, is usually larger than the real "*vena contracta*" because the calculation is made by the Gorlin formula in which the term pressure drop, is actually the net gradient, which magnitude depends upon the extent of the pressure recovery (12).

Interpretation of the results

Fluid-dynamic terms (Energy loss, Mean pressure drop and EOA)

Mean pressure drops and Energy losses increased on increasing SV (Table 1); these terms displayed strongly non-linear trends, with different patterns according to the bioprosthesis model (Fig. 4).

The TRI showed the best fluid-dynamic behavior in energetic terms and, accordingly, in terms of the EOA (Fig. 5) than MF, SA and MG respectively. Moreover, at physiologic SVs, i.e >50 ml, the EOA values were stable for all valve models, despite a statistically significant increase in GOA.

The trends of the mean pressure drop for MF, MG and SA are consistent with those obtained by Gerosa et al. (22) in a standard "*in vitro*" experimental setup. In addition, at the physiologic SVs, i.e >50 ml, the EOA values were stable for all valve models which suggests that, for these prostheses, the interaction between the flow and the valve structure is well exploited in this SV range. In fact, as the EOA is the result of hydrodynamic measurements, it should be considered an index of hydrodynamic performance, although at a first glance it might be assimilated to a geometrical parameter.

The EOA of the SA was stable across the entire range of SV, while the EOA values, yielded by TRI, were higher at SV < 50 ml than at SV >50 ml. This can be explained by the pliability of the leaflets, which are almost completely opened at low flow regimens (Fig. 8E).

In order to obtain an EOA that is peculiar of a specific prosthesis size and brand, the anatomy upstream and downstream the prosthesis must be equal; this is easily achieved "*in vitro"*. Accordingly, the fact that we found larger standard deviations of EOA than Gerosa et al. (22) can be explained by the use of 8 different ARUs, the LVOTs and aortic roots of which, had different geometrical shapes and sizes. As the EOA value is influenced by the specific anatomic features, "*in vivo",* either the application of the Gorlin's formula or the continuity equation, can provide only a partial view of the performance of a specific type and size of prosthesis. This makes the EOA value relevant only for that patient in which the prosthesis is being implanted and much less relevant for the type and size at which the prosthesis belongs.

Geometric Terms (GOA, Edge GOA, Geometric area Ratio and Space Efficiency)

In all the bioprostheses, both GOA and eGOA increased as the SV increased, confirming that pericardial stented valves possess a reserve opening area (23, 24). At each value of SV, the prostheses with pericardial leaflets housed inside the stent posts (i.e. MG and SA) showed smaller GOAs and eGOAs than both TRI and MF, in which the pericardium is placed outside (Table 1 and Fig. 6).

Interestingly, while the GOAs of both TRI and MF were similar, the Cc proved to be lower for MF (confirmed by a larger pressure drop and energy loss), indicating a higher flow velocity due to some not immediately apparent structural characteristics.

The shape assumed by the prostheses, at peak of the ejection period, played a role in the fluid dynamic results. Indeed, at 65 ml, the TRI provided an eGOA consistently larger than inner-GOA, suggesting a "divergent" aperture, thus achieving the lowest gradients and energy losses, despite the smallest inner-GOA. This valve shape allowed a better exploit of the inner-GOA aside from have probably caused a larger flow deceleration downstream the "*vena contracta*" than the other prostheses. Besides, this shape might have allowed a more gradual flow expansion (due to the lower ratio between eGOA and STJ ratio) prompting a less flow separation in the flow deceleration zone, than the other bioprostheses, and resulting in a greater energy recovery

Regarding the MF it opened like a "cylinder" while the SA and MG, showed a convergent-divergent shape (or "hourglass") having the eGOA smaller than the inner-GOA but larger than GOA. This morphology should be peculiar to the internal position of the pericardium.

The space efficiency (SE) was not related to the valve performance. This was clear on comparing MF and TRI, which showed similar SE, and SA with MG where SA performed better than MG although a smaller SE.

It is worth noting that the size of the ID, when prostheses that fit the same aortic root are considered, is a parameter that does not affect fluid-dynamic and/or geometric terms such eGOA and GOA. Thus, a larger ID does not guarantee neither a larger GOA nor a lower pressure drop but, what is most important, is how much of this area is used by the flow (26).

Geometry and hydrodynamics of prostheses with small sizes valve with pericardial sheet outside the stent posts.

The results confirmed that the TRI opened like a "divergent" with the eGOA consistently larger than its iGOA (Table 3) and showed that the prosthesis ID, at high SVs became a fluid dynamic limiting factor. Indeed, its valve resistance (Table 3 and Figure 8C) increased proportionally with the SV as a fixed orifice (25 19). That was also possible thanks to its large aperture, close to its maximum, already at the smaller SVs (i.e. ≤ 60 mL), with both EOA and %GOA remaining stable across the entire range of SVs (Table 3). On the contrary, the MF prosthesis, reached its maximal cross-sectional areas at supra-physiological values of SVs ≥ 75 mL displaying a more complex opening pattern than TRI. Indeed, the convergent shape of the prosthesis at lower SVs (eGOA < iGOA), changed to a cylindrical/divergent shape at higher SVs (eGOA ≥ iGOA). The geometric orifice area was about 70% of its maximum value at the lowest SV, then gradually increased, reaching its maximum at the highest SVs (Figure 8F).

The trend in the EOA was consistent with the %GOA, and the valve resistance confirmed the valve's behavior was that of a variable-area orifice.

With regard to the fluid dynamics, at supra-physiologic SVs for these prostheses size, i.e. ≥ 75 mL, the TRI showed a slightly, non-significantly higher pressure drop than the MF. The smaller ID of the TRI than the MF did not seem to be, *per se*, a limiting factor in its fluid-dynamic performance at the sub-physiologic and physiologic range of SVs. Nevertheless, at the higher SVs a quadratic trend in the pressure drop became more apparent and the impact of ID size of fluid dynamics became clear resulting in a performance slightly worsened in comparison with MF.

The advantage of having a larger ID began to be apparent at a supra-physiologic flow rate for this prosthesis, i.e. for SVs over 90 mL, when the %GOA reached its maximum, and the eGOA was substantially greater than the iGOA. At these SVs, the MF prosthesis showed a change in the trend of its hydrodynamic parameters with ΔP_m, $E_{l\%}$ and VR increasing less steeply than the TRI. The larger ID of the MF seemed to be optimally exploited at higher level of SVs than the TRI, when the increased eGOA allowed the flow to take advantage of a larger available cross-sectional passage.

Hybrid Indexes (Cc and Performance index)

In normally functioning bioprostheses, the Cc is expected to be >0.9 (27). We found this value only in the TRI and SA at SV values of 30 and 50 ml; then as the SV increased, the Cc decreased. This can be explained by the presence of the real LVOT that influences how sharply/smoothly the flow lines approach and enter the prosthesis due to the LVOT characteristics and aortic annulus-prosthesis interaction. By contrast, Pi, which describes a sort of "dynamic" efficiency, seems to be rather well related to the Energy loss %. Performance appears to be specific to each valve because they differ in terms of the material used, stent design and dimensions. The Pi showed that the TRI made the best use of the small area available. The second prosthesis with a better Pi was the MF that share with the TRI the position of the pericardium outside the stent.

Leaflets Kinematic Study

The study of the leaflet kinematics of both opening and closing phases may unveil some important structural valve features. The time needed for the leaflets to open might influence the amount of area available throughout the systolic cycle, but above all, the

amount of backflow during valve closure is related to the length of the closure phase.

The mechanical behavior of a prosthesis depends upon the amount of SV, the size, material and the design of the prosthesis.

As the hydrodynamic conditions were similar for each type of prosthesis, our findings suggest that there were no apparent specific structural characteristics that influenced leaflet kinematics. This means that specific features in term of material used for the stent and leaflets played a greater role than macroscopic features such the design of the valves. Indeed, the two valves with the pericardial sheet housed outside the posts stent (i.e. the MF and TRI) behaved differently from each other. The same was for the valves in which the pericardial sheet was housed inside the stent (i.e. MG and SA). In addition, the kinematic variables reported in Table 2 were not related to the classical fluid dynamic terms. As expected, the role of the opening profile of a normal valve has a very limited effect on valve performance in terms of mean gradient and EOA attained (19).

Opening phase

MG showed the shortest opening time (12±2 ms) and accordingly, the highest leaflet-opening velocity (209±17 ms^{-1}). TRI and SA showed similar opening patterns (15±3 ms and 132±25 ms^{-1} for TRI and 17±2 ms and 126±19 ms^{-1} for SA), while MF displayed the slowest opening profile with opening time of 23±3 ms and velocity of 94±8 ms^{-1} respectively. The differences were small but statistically significant (Table 2). We found slightly shorter opening times than those reported for pericardial valves *in vitro* by Bakhtiary et. al. (14,29) and Kuhehuel et al. (24). These discrepancies might be explained by the different *in vitro* setting.

The slowest opening profile of the MF may be interpreted as due to a higher inertia of the

leaflets/stent complex than that of the other bioprostheses, especially the MG. The Fig. 8F shows the percentage of maximal opening area according to the SV confirming this assumption. Hence, it may be assumed that, with the need to overcome a higher prosthesis inertia, that might translate into a higher stress applied on the leaflets and stent, with possible consequences for valve durability. Nevertheless, the differences were small, perhaps because some mechanical characteristics of the prostheses might have been masked, during the systolic phase, owing to the high momentum possessed by the flow. In other words, the sudden temporal changes in the local hemodynamic quantities, that occur in the early systolic phase, play a significant role in determining the opening kinematics, which may, to a certain extent, mask the effects of increased tissue inertia.

Closing phase

The closing profile has a key role because, once the forward flow decreases its momentum and inverts its direction, prolonging the closing time causes a higher backflow volume. However, the differences among the prostheses were still small and probably clinically negligible. This consideration was supported also by the fact that no statistically relevant differences in the cardiac output was recorded among the tested prostheses.

The closing phase is usually divided into 2 parts; the first is the slow closing phase, which is influenced by the local fluid dynamics in the fluid region, delimited by the aortic side of the cusps and the sinuses of Valsalva. This phase could be affected by some aspects of the design of the prostheses (e.g. the position of the pericardium with respect to the stent, and the stiffness of the cusps). The second part is the rapid closing phase, in which the leaflets reach the fully-closed configuration. No statistically significant differences among the prostheses were found regarding the times of the two phases.

Data concerning rapid valve closure were quite spread indicating that the kinematics of the prostheses, in this highly dynamic phase, was driven by a complex interplay between different determinants, such the compliance of the native structures and that of each prosthesis, leaflet stiffness, leaflet inertia and fluid inertia.

Despite our data suggest that there are no relevant differences in RVCT among the tested prostheses, a deeper investigation could be of interest about possible relations between prostheses design factors, closing kinematics, and flow regurgitation that occur during fast valve closure.

Some difference emerged in terms of how fast these two phases took place. The MG and MF displayed similar SVCVI values (-0.57±0.1 ms^{-1} and 0.55±0.1 ms^{-1} (p=1.0) respectively), which were lower than those of the other two valves, i.e. the TRI and SA; however, the differences were statistically significant only in comparison with SA (p=0.045 and p=0.04, respectively). It might be hypothesized that the leaflets of the SA prosthesis react promptly to the eddy currents formed in the Valsalva sinus, owing to the less stiffness of the leaflet-stent complex; it might therefore take least to overcome leaflet inertia. The RVCVI was higher in MG (-18±6 ms^{-1}) than in MF (-10±1 ms^{-1}, p=0.03) and SA (-10±2 ms^{-1}, p=0.025).

It has been claimed (29) that maximizing the aperture during systole, in order to obtain a better fluid-dynamic performance, can be achieved only at the expense of a longer closing time and higher regurgitant volume. This was not the case in our study, as the valve with the best fluid-dynamic characteristics displayed similar kinematics to the valve that performed worst. Indeed, TRI and MG showed similar opening and closing times and velocities.

Conclusions

These studies confirmed that pericardial stented prostheses have a reserve of geometric area which depend upon the structural characteristics and flow regimen, and those with the pericardium housed outside the stent are more efficient in biomechanical term. The fluid dynamic parameters are related to the shape assumed by the valve at peak flow. Albeit some of the bioprostheses tested, in this series of studies, shared similar design strategies, they showed different biomechanical behaviors.

At physiologic flows the geometric characteristic such ID is not a parameter that can reliably predict which prosthesis perform better than others. Indeed, the TRI displayed the best fluid-dynamic behavior despite having the smallest ID. It appears that, the shape assumed by the TRI, i.e. like a "divergent", allowed to exploit at best its internal geometric area and might have induced a substantial fluid slow down, in the space adjacent of the valve, enhancing the pressure recovery and reducing the local flow separation.

Regarding the opening/closing profile, it is not influenced by the position of the pericardial leaflets but depends more on other intrinsic structural characteristics related to the material used for the stent and leaflets than on the stent design of the valve. Moreover, kinematics does not affect the fluid dynamic valve performance.

Study limitations

Even though all the conditions to which the prostheses were exposed in this study were equal, the "implantability" characteristics of each bioprosthesis, along with the surgeon's level of experience in implanting a specific type of prosthesis, might have influenced the

results. However, such biases are difficult to avoid, as they are specific to the surgical procedure. The GOA and eGOA were evaluated from a 2D video. This implies that their values are planar projections of a 3D area, and could be affected by experimental errors due to misalignment between the evaluation plane and the CCD.

Bibliography

1-Suri RM, Michelena HI, Burkhart HM, Greason KL, Daly RC, Dearani JA, Park SJ, Joyce LD, Stulak JM, Sundt III TM, Li Z, Schaff HV. A prospective, randomized comparison of 3 contemporary bioprosthetic aortic valves: Should hemodynamic performance influence device selection? J Thorac Cardiovasc Surg 2012;144:1387-98.

2- Tasca G, Brunelli F, Cirillo M, Dalla Tomba M, Magna Z, Troise G, Quaini E. Mass regression in aortic stenosis after valve replacement with small size pericardial bioprosthesis. Ann of Thorac Surg 2003;76,4:1107-1113

3-Blais C, Dumesnil JG, Baillot R, Simard S, Doyle D, Pibarot P. Impact of prosthesis-patient mismatch on short-term mortality after aortic valve replacement. Circulation. 2003;108:983–988.

4-Tasca G, Mhagna Z, Perotti S, Berra Centurini P, Sabatini T, Amaducci A, Brunelli F, Cirillo M, Dalla Tomba M, Quiani E, Troise G, Pibarot P. Impact of Prosthesis-Patient Mismatch on Cardiac Events and Midterm Mortality After Aortic Valve Replacement in Patients With Pure Aortic Stenosis. Circulation. 2006;113:570-576.

5-Tasca G, Brunelli F, Cirillo M, DallaTomba M, Magna Z, Troise G, Quaini E. Impact of valve Prosthesis-Patient Mismatch on left ventricular mass regression following aortic valve replacement. Ann Thorac Surg 2005;79:505–10.

6-Ruel M, Rubens FD, Masters RG, Pipe AL, Bedard P, Hendry PJ, Lam BK, Burwash IG, Goldstein WG, Brais MP, Keon WJ, Mesana TG. Late incidence and predictors of

persistent or recurrent heart failure in patients with aortic prosthetic valves. J Thorac Cardiovasc Surg. 2004;127: 149–159.

7-Tasca G, Vismara R, Fiore GB, Mangini A, Romagnoni C, Pelenghi S, Antona C, Redaelli A, Gamba A. Fluidodynamic results of “in-vitro” comparison of 4 pericardial bioprostheses implanted in small porcine aortic roots. Eur J Cardiothorac Surg. 2015;47:e62-7.

8-Doenst T, Amorim PA, Al-Alam N, Lehmann S, Mukherjee C, Faerber G. Where is the common sense in aortic valve replacement? A review of hemodynamics and sizing of stented tissue valves. J Thorac Cardiovasc Surg 2011;142:1180-7.

9-Von Oppel UO, Segadal L, Busund R, Johnston GG, Dimitrakakis G, Masani N, Lung TH. Aortic annulus diameter and valve design each determine the valve size implanted. J Heart Valve Dis. 2012;21:591-598.

10-Ruzicka DJ, Hettich I, Hutter A, Bleiziffer S, Badiu C, Bauernschmitt R, Langhe R, Eichinger WB. The complete supraannular concept. In vivo hemodynamics of bovine and porcine aortic bioprostheses. Circulation 2009; 120 [suppl 1]:S139-S145.

11- Toninato R, Salmon J, Susin FM, Ducci A, Burriesci G. Physiological vortices in the sinuses of Valsalva: An in vitro approach for bio-prosthetic valves. J Biomech. 2016;49(13):2635-2643.

12- Garcia D, Pibarot P, Dumesnil JG, Sakr F. Durand LG. Assessment of Aortic Valve Stenosis Severity. A New Index Based on the Energy Loss Concept. Circulation. 2000;101:765-771.

13- Tabata M, Shibayama K, Watanabe H, Sato Y, Fukui T, Takanashi S. Simple interrupted suturing increases valve performance after aortic valve replacement with a small supra-annular bioprosthesis. J Thorac Cardiovasc Surg. 2014;147:321-5

14-Bakhtiary F, Dzemali O, Steinseiffer U, Schmitz C, Glasmacher B, Moritz A, Kleine P. Opening and closing kinematics of fresh and calcified aortic valve prostheses: An in vitro study. J Thorac Cardiovasc Surg 2007;134:657-62.

15-Vismara R, Fiore GB, Mangini A, Contino M, Lemma M, Redaelli A, Antona C. A Novel Approach to the In Vitro Hydrodynamic Study of the Aortic Valve: Mock Loop Development and Test. ASAIO J. 2010;56(4):279–284.

16-Vismara R, Leopaldi AM, Mangini A, Romagnoni C, Contino M, Antona C, Fiore GB. In vitro study of the aortic interleaflet triangle reshaping. J Biomech. 2014;47(2):329–333.

17-Vismara R, Mangini A, Romagnoni C, Contino M, Redaelli A, Fiore GB, Antona C. In vitro study of a quadricuspid aortic valve J Heart Valve Dis. 2014;23(1):122-6.

18-Vismara R, Leopaldi AM, Romagnoni C, et al. In vitro study of a standardized approach to aortic cusp extension. Int J Artif Organs. 2014;37(4):315–24.

19- Bapat VN, Attia A, Thomas M. Effect of Valve Design on the Stent Internal Diameter of a Bioprosthetic Valve A Concept of True Internal Diameter and Its Implications for the Valve-in-Valve Procedure. J Am Coll Cardiol Intv 2014;7:115–27

20-Leyh RG, Schmidtke C, Sievers HH, Yacoub MH. Opening and Closing Characteristics of the Aortic Valve After Different Types of Valve-Preserving Surgery. Circulation. 1999;100:2153-2160.

21-Heinrich RS, Fontaine AA, Grimes RY, Sidhaye A, Yang S, Moore KE, Levine RA, Yoganathan AP. Experimental analysis of mechanical energyl loss in aortic valve stenosis: importance of pressure recovery. Annals of Biomedical Eng.1996; 24.685-694.

22-Gerosa G, Tarzia V, Rizzoli G, Bottio T. Small aortic annulus: The hydrodynamic performance of 5 commercially available tissue valves. J Thorac Cardiovasc Surg 2006; 131:1058-64.

23-Kuehnel RU, Puchner R, Pohl A, Wendt MO, Hartrumpf M, Pohl M, Albes JM. Characteristics resistance curves of aortic substitutes facilitate individualized decision for particular type. Eur J Cardiothorac Surg. 27 (2005) 450-455.

24-Kuehnel RU, Pohl A, Puchner R, Wendt MO, Hartrumpf M, Pohl M, Albes JM. Opening and closure characteristics of different type of stented biologic valve. Thorac Cardiovasc Surg. 2006 Mar;54(2):85-90

25-Voelker W, Reul H, Nienhaus G, Stelzer T, Schmitz B, Steegers A, Karsch. Comparison of valvular resistance, stroke volume loss, and Gorlin valve area for quantification of aortic stenosis: an in Vitro study in a pulsatile aortic flow model. Circulation. 1995;91:1196-1204.

26- Cristakis GT, Buth KJ, Goldman BS, Fremes SE, Rao V, Cohen G, Borger MA, Weisel RD. Innacurate and misliding valve sizing: A proposed standard for valve size nomenclature. Ann Thorac Surg 1998;66:1198-1203.

27- Garcia D, Pibarot P, Landry C, Allard A, Chayer B, Dumesnil JG, Durand LG. Estimation of aortic valve effective orifice area by Doppler echocardiography: effects of valve inflow shape and flow rate. J Am Soc Echocardiogr. 2004 Jul;17(7):756-65.

28- Dellimore K, Kemp I, Scheffer C, Weich H, Doubell A. The influence of leaflet skin friction and stiffness on the performance of bioprosthetic aortic valves. Australas Phys Eng Sci Med (2013) 36:473–486.

29- Bakhtiary F, Dzemali O, Steinseiffer U, Schmitz C, Glasmacher B, Moritz A, Kleine P. Hydrodynamic comparison of biological prostheses during progressive valve calcification in a simulated exercise situation. An in vitro study. Eur J Cardiothorac Surg. 2008 Nov;34(5):960-3.

Table 1. Fluid-dynamic and geometric results

Variables	30 ml	50 ml	65 ml	85 ml	Effect	p-value
Mean Gradient (mmHg)						
MF	2.8±0.64	5.8±1.93	10.2±2.67	15.2±3.46	Valve	<0.001
MG	3.2±0.65	7.4±2.51	13.2±3.15	18.1±4.16	Time (SV)	<0.001
SA	2.0±0.67	5.0±1.57	9.6±1.57	14.1±1.34	Interaction	<0.001
TRI	1.1±0.58	2.9±1.02	6.1±1.93	9.2±2.68		
Energy Loss (J)						
MF	0.015±0.01	0.05±0.01	0.11±0.03	0.22±0.05	Valve	<0.001
MG	0.018±0.01	0.07±0.02	016±0.04	0.27±0.07	Time (SV)	<0.001
SA	0010±0.01	0.04±0.01	0.11±0.02	0.21±0.04	Interaction	<0.001
TRI	0.008±0.01	0.03±0.01	0.07±0.02	0.14±0.04		
Energy Loss (%)						
MF	6.5±1.42	8.7±2.45	10.7±2.51	13.3±1.89	Valve	<0.001
MG	7.3±1.41	10.8±3.78	13.5±3.25	15.7±2.81	Time (SV)	<0.001
SA	4.6±1.19	8.3±2.72	10.9±1.79	13.1±1.38	Interaction	<0.001
TRI	2.7±1.23	4.3±1.59	6.6±1.63	8.4±1.79		
EOA (cm^2)						
MF	1.6±0.22	1.8±0.26	1.8±0.21	1.8±0.23	Valve	<0.001
MG	1.5±0.17	1.6±0.26	1.6±0.18	1.6±0.20	Time (SV)	0.57
SA	1.9±0.33	1.80.42	1.7±0.21	1.8±9.20	Interaction	0.13
TRI	2.7±0.48	2.6±0.56	2.3±0.34	2.4±0.42		
GOA (cm^2)						
MF	2.4±0.05	2.7±0.03	2.8±0.05	2.9±0.09	Valve	<0.001
MG	2.0±0.03	2.2±0.03	2.3±0.07	2.4±0.05	Time (SV)	<0.001
SA	1.7±0.10	1.8±0.07	1.9±0.07	2.0±0.05	Interaction	<0.001
TRI	2.5±0.06	2.7±0.08	2.8±0.02	2.9±0.04		
edge GOA (cm^2)						
MF	2.42±0.05	2.69±0.03	2.81±0.05	3.01±0.05	Valve	<0.001
MG	2.29±0.07	2.42±0.07	2.50±0.09	2.78±0.07	Time (SV)	<0.001
SA	2.33±0.08	2.42±0.05	2.57±70.1	2.83±0.04	Interaction	<0.001
TRI	3.16±0.11	3.39±0.11	3.62±0.04	3.95±0.19		
Cc						
MF	0.67±0.10	0.62±0.08	0.62±0.10	0.58±0.08	Valve	<0.001
MG	0.75±0.12	0.67±0.10	0.65±0.04	0.64±0.07	Time (SV)	<0.001
SA	1.07±0.12	0.90±0.18	0.85±0.10	0.85±0.10	Interaction	0.203
TRI	1.05±0.22	0.92±0.14	0.77±0.11	0.76±0.10		
Performance Index						
MF	0.56±0.08	0.62±0.09	0.62±0.08	0.63±0.08	Valve	<0.001
MG	0.49±0.05	0.51±0.08	0.50±0.06	0.52±0.06	Time (SV)	0.56
SA	0.61±0.11	0.59±0.14	0.57±0.07	0.58±0.07	Interaction	0.12
TRI	1.03±0.18	0.98±0.21	0.88±0.13	0.90±0.16		
Space Efficiency						
MF	0.46±0.01	0.51±0.01	0.53±0.01	0.55±0.02	Valve	<0.001
MG	0.38±0.01	0.41±0.01	0.43±0.01	0.45±0.01	Time (SV)	<0.001
SA	0.30±0.02	0.32±0.01	0.34±0.01	0.36±0.01	Interaction	<0.001
TRI	0.47±0.01	0.51±0.02	0.52±0.01	0.55±0.01		
Geometric Area Ratio						
MF	0.86±0.02	0.95±0.01	0.99±0.02	1.04±0.03	Valve	<0.001
MG	0.65±0.01	0.69±0.01	0.72±0.02	0.76±0.02	Time (SV)	<0.001
SA	0.56±0.03	0.59±0.02	0.63±0.02	0.66±0.02	Interaction	<0.001
TRI	0.96±0.02	1.02±0.03	1.07±0.01	1.10±0.02		

EOA= Effective Orifice Area, GOA= Geometric Orifice Area, Cc= Coefficient of Contraction.

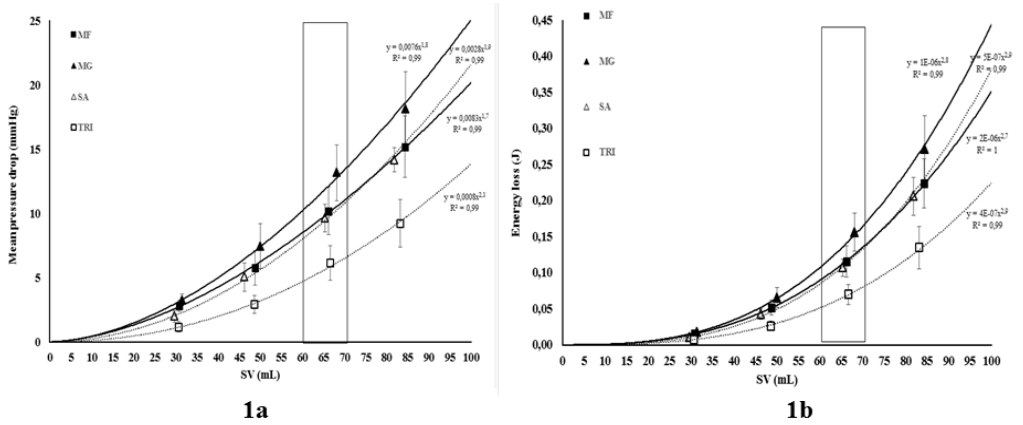

1a 1b

Fig. 4 Relationship between Mean Pressure Drops (1a) and Energy Loss (1b) with Stroke volumes. Bars represent 95% confidence intervals. The rectangle represents the physiologic SV interval at rest in patients whose body size matches these sizes of prostheses.

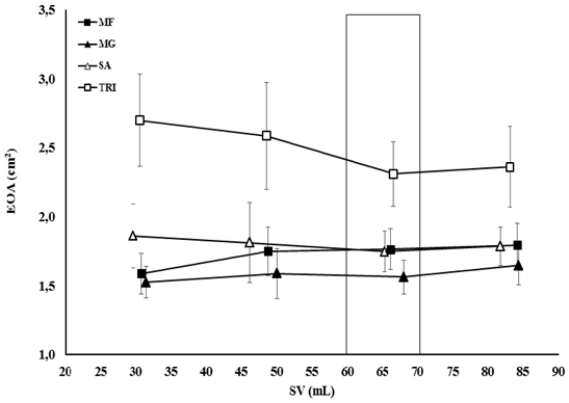

Fig. 5 Relationship between Effective Orifice Areas with Stroke volumes. Bars represent 95% confidence intervals. The rectangle represents the physiologic SV interval at rest in patients whose body size matches these sizes of prostheses.

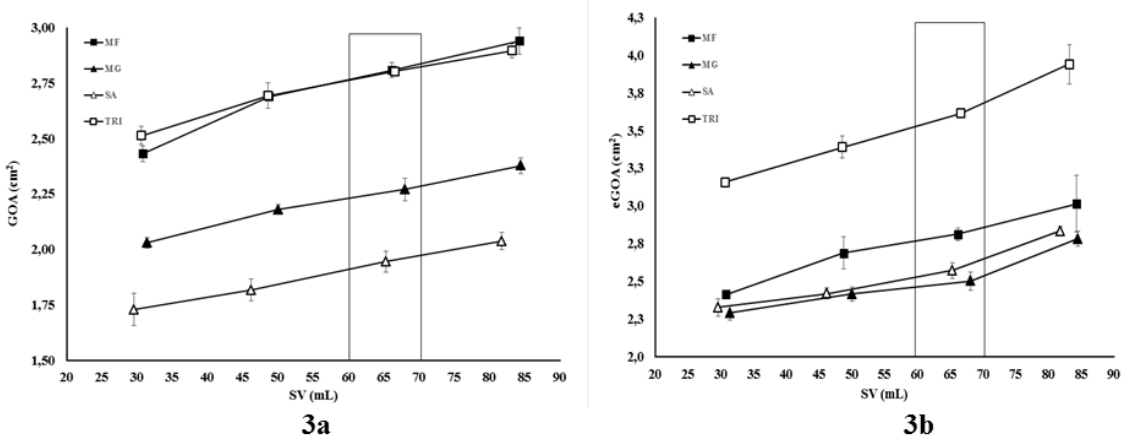

3a 3b

Fig. 6 Relationship between Geometric Orifice Areas (3a) and edge Geometric Orifice Area (3b) with Stroke volumes. Bars represent 95% confidence intervals. The rectangle represents the physiologic SV interval at rest in patients whose body size matches these sizes of prostheses**.**

Table 2. Kinematics and hydrodynamic results

	TRI	**SA**	**MG**	**MF**	**Anova p-value**	**TRI** vs **SA** p-value	**TRI** vs **MG** p-value	**TRI** vs **MF** p-value	**SA** vs **MG** p-value	**SA** vs **MF** p-value	**MG** vs **MF** p-value
ET (ms)	299±12	300±17	300±12	315±13	0.760	1.0	1.0	1.0	1.0	1.0	1.0
RVOT (ms)	15±3	17±2	12±2	23±3	**<0.01**	1.0	0.286	**<0.01**	**0.03**	**<0.01**	**<0.01**
SVCT (ms)	247±14	231±15	256±26	241±11	0.170	0.463	0.853	0.931	0.213	1.0	1.0
RVCT (ms)	35±19	52±13	32±17	52±4	0.07	0.474	1.0	0.494	0.236	1.0	0.247
TVCT (ms)	283±10	283±19	289±10	293±11	0.584	1.00	1.0	1.0	1.0	1.0	1.0
RVOVI (ms^{-1})	132±25	126±19	209±17	94±8	**<0.01**	0.959	**<0.01**	**0.02**	**<0.01**	0.07	**<0.01**
SVCVI (ms^{-1})	-0.9±0.3	-1.1±0.4	-0.57±0.1	-0.55±0.1	**<0.01**	1.0	0.353	0.292	**0.045**	**0.04**	1.0
RVCVI (ms^{-1})	-16±4	-10±2	-18±6	-10±1	**<0.01**	0.396	1.0	0.513	**0.025**	1.0	**0.03**
Δp (mmHg)	6.7±3.6	10.6±5.5	15.2±7.9	10.7±6.1	**<0.01**	**0.01**	**<0.01**	**0.01**	**0.04**	1.0	**<0.01**
EOA (cm^2)	2.2±1.2	1.7±0.9	1.5±0.8	1.7±0.9	**<0.01**	**0.03**	**<0.01**	**0.01**	0.261	0.617	0.11
El %	7.3±1	11.9±1	15.4±2	11.8±3	**<0.01**	**<0.01**	**<0.01**	**<0.01**	**0.04**	1.00	**0.03**
CO (L/min)	3.1±0.4	2.8±0.5	3.1±0.3	3.0±0.5	0.534	0.282	0.792	0.702	0.106	0.552	0.559

Data are reported as means and standard deviations, evaluated over the tested heart samples. ET= Ejection Time, RVOT= Rapid Valve-Opening Time, SVCT= Slow Valve-Closing Time, RVCT= Rapid Valve-Closing Time, TVCT= Total Valve-Closing Time, RVOVI= Rapid Valve-Opening Velocity Index, SVCVI= Slow Valve-Closing Velocity Index, RVCVI= Rapid Valve-Closing Velocity Index, Δp= Mean Pressure Drop, EOA= Effective Orifice Area, El%= Energy Loss, CO= cardiac output.

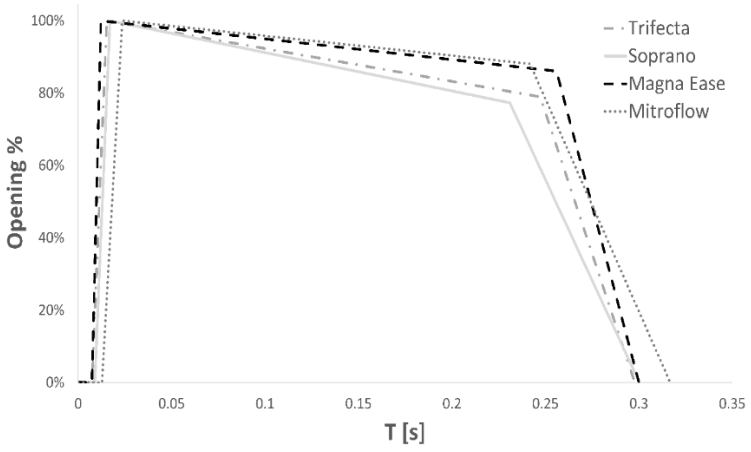

Figure 7. Opening patterns of all the valves tested. T=time.

Table 3. Hydrodynamic results obtained in all the configurations tested.

	SV (mL)						
Variables	**30**	**45**	**60**	**75**	**90**	**105**	***p-value***
ΔP_m (mmHg)							
MF	4.4±0.4	7.3±0.6	10.9±0.9	15.6±1.3	21.1±2.0	27.1±2.6	*<0.01*
TRI	2.4±0.4	5.9±0.7	10.6±0.6	16.6±1.0	23.8±1.7	30.4±3.3	*<0.01*
p-value	*<0.01*	*<0.01*	*0.42*	*0.27*	*0.10*	*0.22*	
EOA (cm^2)							
MF	1.0±0.06	1.3±0.05	1.4±0.04	1.5±0.03	1.5±0.04	1.6±0.06	*<0.01*
TRI	1.5±0.12	1.4±0.07	1.4±0.04	1.5±0.06	1.5±0.07	1.5±0.13	*0.45*
p-value	*<0.01*	*<0.01*	*0.10*	*0.38*	*0.15*	*0.46*	
VR (dyne*s/cm^5)							
MF	31.9±8.6	50.0±7.1	65.6±5.3	80.8±8.5	96.4±12.7	106.0±22.3	<0.01
TRI	61.4±9.5	62.5±6.6	68.6±5.6	76.4±6.4	85.7±9.5	94.1±11.0	<0.01
p-value	*<0.01*	*<0.01*	0.16	0.25	0.10	0.23	
$E_{l\%}$, (%)							
MF	7.9±1.7	9.4±1.8	11.8±1.7	14.4±1.7	16.6±2.2	19.0±3.0	<0.01
TRI	4.3±1.0	7.5±1.4	11.1±1.1	15.2±1.4	19.0±2.2	21.5±3.0	<0.01
p-value	*<0.01*	*<0.01*	*0.10*	*0.28*	*0.02*	*0.10*	
eGOA (cm^2)							
MF	2.0±0.06	2.4±0.04	2.6±0.04	2.8±0.06	2.9±0.06	2.9±0.03	*<0.01*
TRI	2.5±0.02	2.8±0.03	2.9±0.04	3.1±0.05	3.2±0.08	3.3±0.11	*<0.01*
p-value	*<0.01*	*<0.01*	*<0.01*	*<0.01*	*<0.01*	*0.01*	

ΔP_m: mean systolic pressure drop across the prosthesis; EOA: Effective Orifice Area; VR: valve resistance; El%: percentage of the mechanical energy lost by the fluid crossing the prosthesis; eGOA: edge Geometric Orifice Area, the cross-sectional area evaluated at the free edges of the prosthesis cusps.

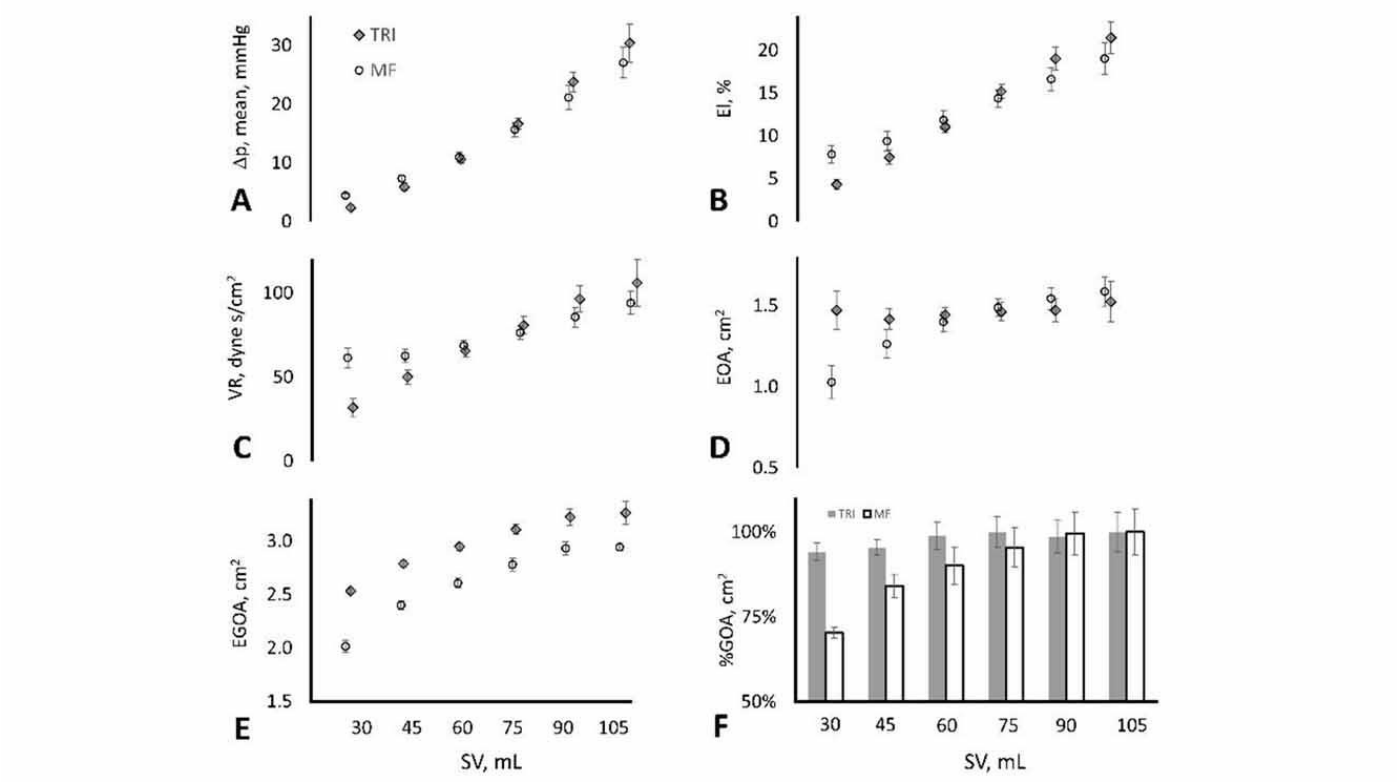

Figure 8**.** Data trends plotted as a function of stroke volume (SV). **Panel A**: Mean systolic pressure drop (ΔP_m); **Panel B**: percent energy los of the fluid crossing the prostheses ($E_{l\%}$). **Panel C**: Valve resistance (VR); **Panel D**: Effective Orifice Area (EOA); **Panel E**: Edge geometrical orifice area evaluated at the free margins of the cusps of the prostheses (eGOA); **Panel F**: Geometrical Orifice Area expressed as a percentage of the maximum value reached by each prosthesis, as a function of the stroke volumes tested (%GOA). Bars represent 95% confidence interval.

CHAPTER 3

STUDY OF THE EFFECT OF THE VALVE DESIGN ON PRESSURE RECOVERY AND SPATIAL POSITIONING OF THE VENA CONTRACTA

These studies have been undertaken in collaboration with the following Institutions:

-Cardiovascular Surgery Depatment, "L. Sacco" Hospital, Università degli Studi di Milano, Milan, Italy.

-ForCardio.lab, Fondazione per la Ricerca in Cardiochirurgia ONLUS, Milan, Italy

-Cardiovascular Department, Cardiac Surgery Unit, Ospedale "A. Manzoni" ASST-Lecco. Lecco, Italy.

-Radiology Department, Ospedale San Donato, San Donato, Milano, Italy

Introduction and Aims

At the base of the patient-prosthesis mismatch (PPM) concept and its unfavorable clinical impact (1-4) stands the obstructive nature of the prosthetic heart valves. Therefore, the use of valves fluid dynamically very efficient contribute to meet a low level of incidence of PPM.

The actual work-load sustained by the left ventricle, at each beat, can be assessed by measuring the pressure drop across the aortic prosthesis. However, the actual work-load is more related to the net gradient, which is the pressure drop ottained after pressure recovery has taken place dowstream, than the pressure drop measured at "*vena contracta"* (VC). Hence, anything that could improve the extent of the pressure recovery may decrease the burden on the left ventricle. Pressure recovery occurs during the systolic phase (5) and substantially in the first half of the ascending aorta while, from mid-ascending aorta to the brachiocephalic trunk, it appears to be negligible (6). One of the reasons might be that, at the mid-ascending aorta onward, the flow is no longer axi-symmetrical to the vessel axis due to the curved nature of the aorta, disrupting the pressure recovery process.

Bioprostheses are complex structures and tend to function more like nozzles than simple orifices (7), yielding a very complex fluid dynamics. In fact, the interaction between the fluid and the inertial mass of the cusps-stent compound, determines the specific shape, and size (8,9) assumed by the prosthesis at peak flow, which may affect its hydrodynamic behaviour. Hence, it can be hypothesized that the pattern of opening of a bioprostheses may affect the position of the VC and, consequently, influence the pattern and the extent of pressure recovery downstream the VC.

The 2 steps *in-vitro* studies were undertaken to quantify the fluid dynamic terms (pressure drop and effective orifice area), verify the position of the VC as well as the pattern and the extent of the pressure recovery in 3 bioprostheses (Crown, Sorin. Saluggia. Italy. Magna Ease, Edwards Lifescience. Irvine. CA and Trifecta, St-Jude Medical. St Paul. MN).

In a previous study each of the above 3 bioprostheses showed to assume, at peak flow, a peculiar shape with the CR assuming a "cylindrical" shape, the Magna Ease a "hourglass" shape and the Trifecta a "divergent" shape .

The first step of the experiment, consisted of a direct pressure and velocity meausements obtained at different stationary flow regimens.

The second step consisted of measuring the flow velocity, following the same protocol adopted for the above test, with a similar but MRI compatible *"in vitro"* steady flow loop.

In addition, a retrospective CT scan analysis was performed on patients who underwent transcathether aortic valve replacement to measure the distance between the aortic annulus and the point where the aorta start curving. That, as above hypotesized, might have implication on the extent of pressure recovery.

Materials and Methods for the first step experiment

Experimental set-up

The fluid dynamic study was performed on 3 pericardial aortic valve prostheses of 2 different sizes each (Crown 21and 23, Trifecta 19 and 21, and Magna 19 and 21) in a "ad hoc" devised steady flow loop circuit filled with a 35% aqueous glycerine fluid to replicate blood viscosity and density (3.7 cP and 1.07 g/ml measured at 22°C).

Each bioprosthesis was tested at 4 different flow rates (10, 15, 20 and 25 l/min) imposed

by a centrifugal pump and measured by a transit-time flowmeter (HT110R, Transonic System, Inc., Ithaca, NY, USA), equipped with a 1" probe. The 25 l/min flow corresponds to the peak systolic flow at rest condition in a patient with an aortic annulus of 20 mm in which either sizes of 19 (or 21 in case of CR) and 21 (or 23 in case of CR) can be implanted.

The prostheses were housed in a modular model of aorta made in polymethyl methacrylate (PMMA), which included Valsalva sinuses and a straight ascending aorta as outflow Fig.1. The Valsalva sinuses size and form were machined into PMMA to have a total height of 19 mm and maximum diameter of 30 mm. Inflow tube had a 22 mm internal diameter while sino-tubular junction diameter was 25 mm and the overall model length was 140 mm. The values of the sinus of Valsalva diameter and height as well as the diameter of the sino-tubular junction were taken from a previous clinical study.

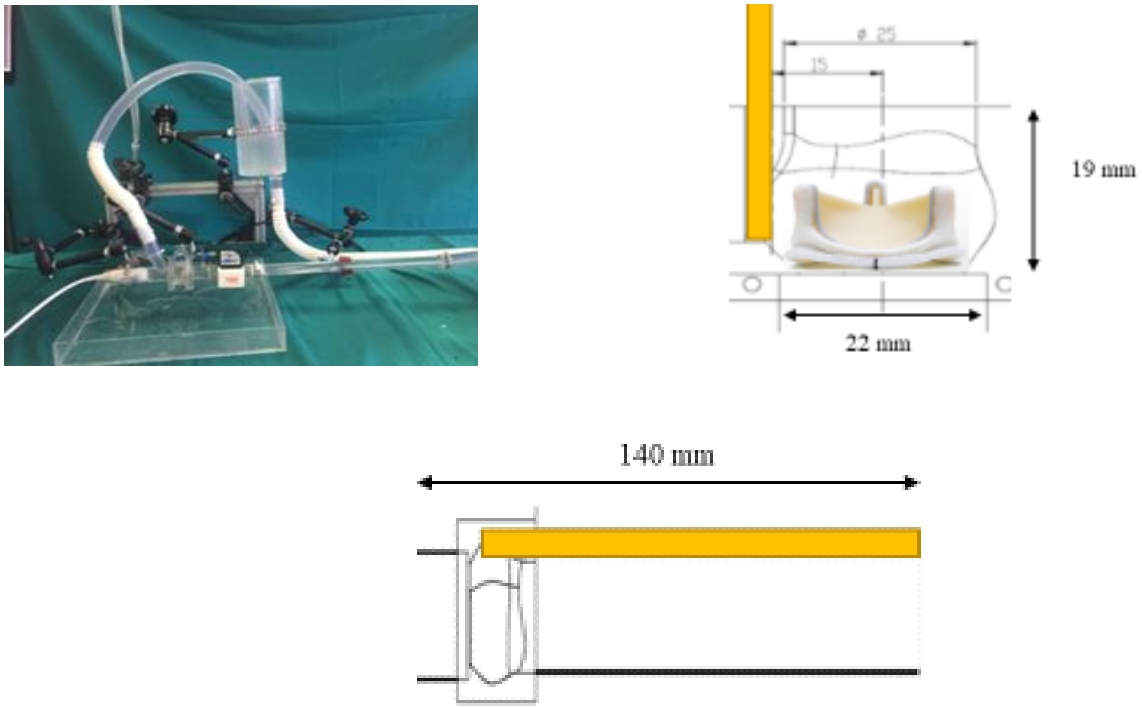

Fig.1 Left. The experimental set-up with the doppler probe. Right. Dimensions of the part that houses the valves. Below. The overall modular model. In yellow is the side port

A 3 mm wide cut was made through the wall of the model starting at the halfway of the Valsalva sinus height and all along the outflow cylindric surface. On this cut, a guide rail was fixed obtained from a PMMA tube of 10 mm external and 7 mm internal diameter. The guide was used to house a rigid catheter with a side port on the tip facing the fluid stream across the through cut. This catheter, once connected to piezoresistive pressure transducer (140PC series, Honeywell Inc., Morristown, NJ) allowed to (i) measure pressure inside the aortic model without altering fluid dynamic, since it was not directly immersed in the flow, (ii) take into account only static pressure, excluding kinematic contribution thanks to its port placed perpendicular to flow direction and (iii), chose the distance downstream from the prosthesis where to measure pressure.

Parameters measurement

Spatial pressure distribution was evaluated by direct static pressure measurements obtained by sliding the catheter in several standardized positions. In order to have an adequate spatial resolution of the pressure profile downstream form the valve, measurements were taken with a step of 5 mm from 5 and 50 mm downstream the annulus. Pressure was then evaluated at a distance of 60, 70 and 110 mm downstream form the annulus.

Pressure upstream the valve was measured through a fixed port placed 25 mm before the annulus. Average of 3 measurements at each point was performed.

Doppler velocity was measured by the continuous doppler interrogation probe averaging 3 samples. These acquisitions were performed by iE33 echocardiographic device (Philips. Netherland) using a 2.5 MHz probe.

Internal diameter (ID) of each prosthesis was measured by a calliper, averaging 3 measurements.

Parameters calculation

Effective orifice area (EOA) was calculated for each prosthesis at each flow level. The principle of mass conservation was applied for doppler calculation with the following equation:

$EOA = Area * V_1/V_2$

where Area was the inflow area (for whole protheses group equal to 3,8 cm2), V_1 was the inflow velocity (calculated from the flowmeter measurement) and V_2 was the maximal velocity obtained by the continuous doppler interrogation.

The Gorlin's equation was applied for calculating the EOA from the direct measurement of the pressure drop using the following equation:

$-EOA = Q\_rms/(k\sqrt{(\Delta p\_m)})$

where Qrms (L/min) was the root-mean-square of the systolic flow rate, ΔPm (mmHg) the mean systolic pressure drop across the sample, and k a conversion factor (k = 3.1 to yield the EOA in cm2).

Doppler pressure drop calculation was performed by applying the modified Bernoulli equation:

$\Delta P = 4(V_1 - V_2)^2$

where V_1 was the inflow velocity (calculated from the flowmeter measurement) and V_2 was the maximal velocity obtained by the continuous doppler interrogation. The latter

correspond to the peak velocity in a pulsatile flow regimen.

Percentage of pressure drop (%ΔP) was calculated according to the following formula (〖ΔP〗max-〖ΔP〗i)/〖ΔP〗max

where ΔP_{max} was the highest measured pressure drop which was regarded as the point in which VC was located, while ΔPi is pressure drop evaluated at each pressure measurement point. The space development of the VC was considered the space in which, the values of the pressure measured remained unchanged

Internal Geometric orifice area (iGOA) was calculated from the direct measurement of the internal diameter as iGOA=πr2 where r is the ID/2.

Coefficient of Contraction (Cc) was calculated with the following equation

Cc= EOA/iGOA

Methods for the second step experiment

4D-flow MRI Experimental set-up

A dedicated MRI compatible in vitro system was designed to test the bioprostheses under controlled conditions of continuous flow (Q =10, 15, 20, 25 L/min). An ad-hoc 3-D printed model of a paradigmatic aortic root (AR) with sinuses of Valsalva housed the valvular apparatus. The dimensions of the model were equal to that of used for the above experiment (Fig.1).

Prototype 4D-flow sequences were performed on a Magnetom Aera 1.5 T (Siemens Healthcare, Erlangen, Germany) encompassing the whole AR model, with a field of view size 270 x 184 x 93 mm, spatial resolution 1.3 x 1.3 x 1.3mm, echo-time 3.70÷2.77 ms, repetition time 125.4÷107.2 ms, flip angle 8°, and with a simulated ECG signal with a

700 ms period to trigger the temporal signal (140 ms time resolution). VENC was adjusted starting from previous eco-doppler measurements so to avoid velocity aliasing.

In-house software was exploited to post-process 4D-flow data, so as to quantify velocity distributions. The prostheses tested were the Trifecta and Magna 21 and the Crown 23.

CT scan study of human aorta

Ten patients who underwent a CT scan performed before transcatheter aortic valve implantation procedure were analysed. The patient selection was on account of the size of the true aortic annuli which has to be $\leq$ 21mm, i.e. the size in which all the bioprostheses tested could be accommodated.

The measurements were the length of the aorta from the sinotubular junction to the brachiochephalic artery and the distance from the annulus to the point where the axis, perpendicular to the valve annulus, diverged from the axis of the aorta (Fig. 2).

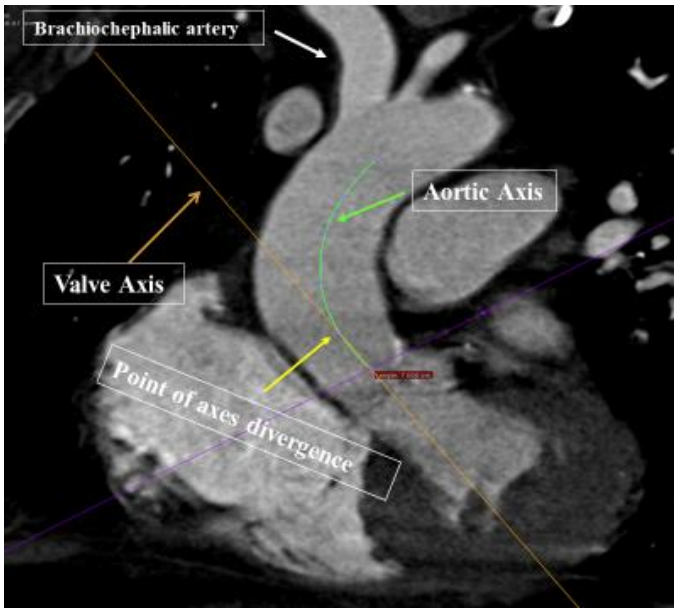

Fig. 2. CT scan. Yellow-brown line represents the axis perpendicular to the annulus plane. Green line represents the axis of the aorta. Yellow is the point at which the two axes diverge.

Statistical analysis

Continuous variables were expressed as mean±ds. OneWay ANOVA was used to test the difference among the ID. A Two-Way ANOVA for independent sample was used to test all the fluid dynamic parameters for each type and size of prosthesis and the level of flow.

Results

Direct fluid pressure and velocity measurements

The direct measurement of the ID for each prosthesis provided a similar value in case of CR 21 (17.1±0.03 mm) and the MG 19 (17.3±0.01 mm) ($p=0.25$) while the ID of TRI 19 (15.8 ±0.01 mm) was smaller ($p<0.01$). As for the larger valve sizes tested, the internal diameter of MG 21, with 19.3±0.01 mm, resulted larger than both CR 23 (1.88±0.006 mm, $p<0.01$) and TRI 21 (1.81±0.02 mm $p=0.01$). In turn, the ID of CR 23 resulted larger than TRI 21 ($p<0.01$).

The spatial pressure distribution downstream the bioprostheses, differed according to the type of prostheses and the level of flow. The TRI showed the most favorable spatial pressure distribution compared with CR and MG (Table 1). The CR, in turn, showed a slighly better performance than MG when bigger sized prostheses were compared.

Fluid dynamics in the region from valve entry to the vena contracta

In this region, the TRI bioprosthesis showed a different fluid dynamic behaviour than both MG and CR (Table.1). In particular, at 25 l/min, the doppler interrogation showed that the velocities for TRI were 2.55±0.06 m/s and 2.13±0.06 m/s for 19 and 21 respectively, for MG were 3.01±0.03 m/s and 2.59±0.03 m/s for 19 and 21 respectively

and for CR 21 and 23 it was 2.94±0.01 m/s and 2.49±0.09 m/s respectively ($p<0.01$). The direct measurement of the pressure drops for TRI were 26.5±0.3 mmHg and 14.9±0.1 mmHg for size 19 and 21 respectively; MG featured 37.1±1.0 mmHg and 27.3±0.4 mmHg (19 and 21 respectively), and for CR the pressure drops were 36.6±1.0 mmHg and 22.7±0.1 mmHg for size 21 and 23 respectively ($p<0.01$). The pressure drop of CR 23 proved to be lower compared with MG 21. The pressure drops obtained by the direct mesurement were consistent with those obtained by the doppler interrogation (Tables 2 and 3).

As for the EOAs, the results were consistent with the that of the pressure drops and between the two methods adopted for the calculation, i.e. by doppler and direct measurement of the pressure drop (Tables 2 and 3).

The extent of internal geometric orifice area used by the flow, was larger for TRI than CR and MG for both sizes. The calculation of Cc provided values of 0.80±0.01 and 0.80±0.003 ($p=0.54$) for TRI 19 and 21 respectively. In case of the CR bioprosthesis, the Cc resulted superior (0.58 and 0.62 for 21 and 23 respectively) than that for MG in both sizes compared with 0.53 and 0.53 for the size 19 and 21 of MG $p<0.01$ (Table 2). As for the VC location the Fig. 3 and 4 shows how in case of the TRI was closer to the valve than CR and MG respectively.

Fluid dynamics in the region from the vena contracta to the distal "aorta".

As regards the pressure recovery, started in the first 40 mm from the annulus for all prostheses (Fig. 3). Nevertheless, a difference was found according to the type of prosthesis. Indded, in the TRI the pressure recovery started within at 15 mm and 25 mm downstream from the annulus for the 19 and 21 size respectively, while for MG and CR

it was at 35 mm and 40 mm respectively (Fig. 3). Besides, the TRI displayed the largest extent of pressure recovery compared with both MG and CR (Table 2). In particular, at 25 l/min, the percentages of pressure recovery were 39±2% and 54±1% for TRI 19 and 21, respectively compared with 37±1% and 39±1% for MG 19 and 21 respectively and 40±2% and 41±2% for CR 21 and 23 respectively. However, the results were statistically significant only when the comparison was made among the size 21 for the TRI and MG and 23 for the CR. In Fig. 3 and 4 are shown the different patterns of the pressure recovery among the bioprostheses. In case of TRI these accounted for the lowest net pressure drop of 16.2±0.2 mmHg and 7.3±0.6 mmHg at 25 l/min for the size 19 and 21 respectively, compared with 23.1±.7 mmHg and 16.4±0.5 mmHg for the MG 19 and 21 respectively and for 21.8±0.2 mmHg and 13.1±0.6 mmHg for CR 21 and 23 respectively.

Results from the CT scan study

The results from the analysis of the CT scan of 10 patients revealed that, the point at which the axis perpendicular to the annulus plane (axis which is supposed to be that of the jet issued, and the axis of the aorta, starts to diverge on average at 30±6 mm from the annulus as reported in the Table 5.

Table 5. Parameters obtaine from the CT Scan study

Parameters	Mean±SD
Annulus Diameter (mm)	21±0,5
Divergence point (mm)	30±6
Aorta Lenght (mm)	65±5

MRI 4-D flow measurements

4D-flow sequences were successfully completed for all testing conditions, with an average time demand of 5’23”, allowing for extracting the velocities along the 3D model. At the different testing conditions, the valve opening was stable. Velocity distribution computed on the aortic root longitudinal axis (Fig.6) appeared consistent with the velocities measurements by doppler (Figure 4) for the sizes valve considered. These results confirmed that the peak of flow velocity, which is physically located at the “*vena contracta*”, differed according to the type of prosthesis and were consistent with the results obtained from the direct measurements.

Discussion

The results of the tests performed, confirmed the hypothesis that the design of a bioprosthesis impacts on the spatial position of the VC and on the pattern of pressure recovery. That, *in vivo*, might affect the left ventricle work-load with possible ripercution on patient's outcome.

At peak systolic flow, the interaction between the fluid and the cusps-stent compound of the prosthesis determines the size, shape and form (8,9). These geometric characteristics differ according to the valve design which, in turn, affect the hydraulic behaviour (9).

Analysis of the fluid dynamics in the region from valve entry to the vena contracta

In this region the fluid, in its approaching the inflow orifice of the bioprosthesis, accelerates reaching its maximal velocity at VC. The TRI bioprosthesis proved to be more fluid dynamically efficient than MG and CR despite its smaller internal geometric area. The doppler assessment yielded, for both sizes of the TRI, the lowest velocities and largest EOA across the whole range of flows (Tables 2 and 3). These results were confirmed by the direct measurement of the pressure drops with the TRI outperforming the other bioprosthesis.

The whole range of the pressure drops and EOAs obtained, were consistent with those previously published from "*in vitro*" (9-11) and "*in vivo*" studies (12-13). The clinical implications of these results are that, with the equal anatomical contex, to obtain the same fluid dynamic performance of a TRI 19, it would requires either a 21 MG or a 23 CR size to be implanted and, plausibly, with a native aortic annulus enlargement. This assumption is confirmed by the results of some studies in which the TRI has been associated with a

very low prevalence of PPM after aortic valve replacement (14).

The different valve shape and size at peak flow, may explain the whole results. Indeed, bioprosthesis such the TRI and CR, with the pericardium outside the stent, potentially exploit at best their fixed internal geometic orifice area. That assumption was strongly supported by the results of the coefficient of contraction that, at 25 l/min of flow, resulted larger for both sizes of the TRI compared with that of the MG (Table 2). This consideration, was valid for the CR as well, which share a similar design with the TRI, event though the results were less evident. This difference accounted for a lower pressure drop, up to -5 mmHg at 25 L/min, for CR 23 notwithstanding a smaller internal geometric area compared with MG.

The substantial difference in fluid dynamics between TRI and CR may be explained by the geometric "divergent" shape assumed by the TRI despite a similar valve design.

The spatial position and of the VC was also affected by the valve design. In fact, with TRI the VC was located closer to the bioprosthesis than that of MG and CR (Fig. 3 and 4) which was more apparent for the TRI size 19 where, the VC, appeared possibly to be located inside the bioprosthesis.

On the contrary, in both MG and CR, the VC location was more downstream and as far as 1 cm from the valve leaflets fringe, passing the sino-tubular junction, moving the site of the onset of the pressure recovery further downstream (Fig. 3 and 4).

The MRI study provided consisted results with those obtained from the test above mentioned. In this regards, in Fig. 5, it is showed the velocity profile along the whole aortic model showing that the peack velocity, where the VC is located, for the TRI, it is

positioned spatially more closely to the valve without any plateau when compared with MG and CR.

Fluid dynamics in the region from the vena contracta to the distal "aorta".

This region of the flow is neglected by doppler interrogation and a direct measurement of pressure is required. Downstream from the VC the flow decelerates and expands resulting in a loss of mechanical energy by its dissipation into heat. However, at the same time, some extent of kinetic energy is converted into static pressure. This is called pressure recovery and it has been related to the level of flow, size of the orifice and the diameter of the receiving chambers (i.e. the aorta) (15).

Albeit we focused our analysis on the pressure recovery that took place along the all model aorta, one interesting result, with a potential clinical impact was the different pattern of pressure recovery of the TRI when compared with both the CR and the MG. Indeed, as shown in figure 3 and 4, a substantial part of the pressure recovery take place in the first 30 mm for the TRI while for the other two the pressure recovery starts further downstream. It is reasonable to assume that when the flow is no longer axisymmetric with the vessel axis, due to the curvature of the vessel, the recovery process may be disrupted becoming less efficient. In support of this consideration, it has been reported that, from mid-aorta to the brachiocephalic artery, a negligible extent of pressure recovery of 1 mmHg has been measured (6). The CT scan study showed that at 30±6 mm from the annulus, the axis of the vessel and that of the axis perpendicular to the valve plane, which may represent a surrogate of the flow axis, started to diverge. Thus, further to this point, in a curve vessel, the pressure recovery might drastically decrease leaving the value of

the net pressure gradient, very close to that of the maximal gradient. The net gradient represents the extra-energy that the heart has to provide to the flow, at every beat, to overcome the obstruction caused by the prosthesis. The characteristic shape assumed at peak flow by each prosthesis, seemed have affected the extent of pressure recovery on for the largest valve sizes, while for the smallest the role of the shape appeared nonexistent.

Conclusion

Trifecta bioprostheses provided a better fluid dynamic performance compared to Magna and Crown valve and not only in the form of the pressure drop across the valve (as measured at the VC) but on the pressure recovery as well. It appears that not only the size but also the design and thus the shape assumed matters.

Bibliography

1- M. Ruel, F. D. Rubens, R. G. Masters, A. L. Pipe, P. Bédard, and T. G. Mesana, 'Late incidence and predictors of persistent or recurrent heart failure in patients with mitral prosthetic valves', J. Thorac. Cardiovasc. Surg., vol. 128, no. 2, pp. 278–283, Aug. 2004.

2- G. Tasca et al., 'Impact of valve prosthesis-patient mismatch on left ventricular mass regression following aortic valve replacement', Ann. Thorac. Surg., vol. 79, no. 2, 2005.

3- G. Tasca et al., 'Impact of prosthesis-patient mismatch on cardiac events and midterm mortality after aortic valve replacement in patients with pure aortic stenosis', Circulation, vol. 113, no. 4, 2006.

4- C. Bassano et al., 'An Unexpected Risk Factor for Early Structural Deterioration of Biological Aortic Valve Prostheses', Ann. Thorac. Surg., vol. 105, no. 2, pp. 521–527, Feb. 2018.

5- Clark C. The fluid mechanics of aortic stenosis - II. Unsteady flow experiments. J Biomech. 1976;9(9):567-73.

6- K. Isaaz et al., 'How important is the impact of pressure recovery on routine evaluation of aortic stenosis? A clinical study in 91 patients.', J. Heart Valve Dis. 2004;13(3) 347–56.

7- Garcia D, Pibarot P, Landry C, Allard A, Chayer B, Dumesnil JG, Durand LG. Estimation of aortic valve effective orifice area by Doppler echocardiography: effects of valve inflow shape and flow rate. J Am Soc Echocardiogr. 2004;17(7):756-65.

8-G. Tasca, R.Vismara, B. Fiore et Al. 'Hydrodynamic and Geometric Behavior of Two Pericardial Prostheses Implanted in Small Aortic Roots'. ASAIO J. 2017; 64(1):86-90.

9- G. Tasca, R. Vismara, B. Fiore et Al, 'A Comprehensive Fluid Dynamic and Geometric Study for an "In-Vitro" Comparison of Four Surgically Implanted Pericardial Stented Valves. J. Heart Valve Dis. 2015;24(5) 596–603.

10-J. D. Cleveland et al., 'Evaluation of Hemodynamic Performance of Aortic Valve Bioprostheses in a Model of Oversizing.', Ann. Thorac. Surg., vol. 103, no. 6, pp. 1866–1876, Jun. 2017

11- G. Tasca et al., ‘Comparison of the Performance of a Sutureless Bioprosthesis With Two Pericardial Stented Valves on Small Annuli: An In Vitro Study’, Ann. Thorac. Surg., vol. 103, no. 1, pp. 139–144, Jan. 2017.

13- M. Ugur et al., ‘Comparison of early hemodynamic performance of 3 aortic valve bioprostheses’, in J of Thoracic and Cardiovasc Surg, 2014, vol. 148, no. 5, pp. 1940–1946.

14- D. Hernandez-Vaquero et al., ‘The Prevalence of Patient-Prosthesis Mismatch Can Be Reduced Using the Trifecta Aortic Prosthesis.’, Ann. Thorac. Surg., vol. 105, no. 1, pp. 144–151, Jan. 2018.

15- DS. Bach, C. Schmitz, G. Dohmen, KD. Aaronson, U. Steinseifer, P. Kleine. In vitro assessment of prosthesis type and pressure recovery characteristics: Doppler echocardiography overestimation of bileaflet mechanical and bioprosthetic aortic valve gradients. J of Thoracic and Cardiovasc Surg. 2012 (144)453–458.

Table 1 (Spatial distribution of the pressure drops in mmHg)

	10	15	20	25	30	35	40	50	60	110	p-value Row	p-value Columns
CROWN 21 Flow												
10L	7.8±0.4	7.9±0.4	7.9±0.4	7.7±0.4	7.4±0.4	7.2±0.5	6.9±0.5	6.2±0.5	5.7±0.4	4.9±0.4	<.01	<.01
15L	15.8±0.5	15.9±0.5	16.1±0.3	15.9±0.2	15.1±0.3	14.6±0.4	14.1±0.5	12.8±0.5	11.7±0.5	9.7±0.3	<.01	<.01
20L	26.3±0.2	26.4±0.4	26.4±0.3	26.1±0.4	24.7±0.4	24.1±0.4	23.2±0.4	20.8±0.4	18.8±0.4	15.4±0.3	<.01	<.01
25L	36.6±0.6	37.3±0.4	37.4±0.4	37.2±0.4	35.2±0.3	34.2±0.3	32.5±0.3	29.5±0.4	26.6±0.4	21.8±0.2	<.01	<.01
MAGNA 19 Flow												
10L	8.4±0.4	8.6±0.4	8.6±0.4	8.5±0.3	8.2±0.3	8.2±0.3	7.8±0.3	7.1±0.3	6.5±0.3	5.9±0.2	<.01	<.01
15L	16.9±0.3	17.1±0.3	17.0±0.3	16.2±0.2	15.7±0.3	15.6±0.3	14.9±0.6	13.3±0.4	12.3±0.4	11.2±0.2	<.01	<.01
20L	26.5±0.6	26.6±0.7	26.6±0.7	25.4±0.6	24.3±0.6	24.4±0.7	23.4±0.7	21.2±0.4	19.3±0.4	16.7±0.5	<.01	<.01
25L	37.1±1.0	37.3±0.9	37.0±1.0	35.1±0.8	34.2±0.7	33.9±0.8	32.4±0.7	29.0±1.0	26.7±0.8	23.2±0.7	<.01	<.01
TRIFECTA 19 Flow												
10L	5.5±0.1	5.9±0.1	5.6±0.2	5.1±0.2	4.8±0.2	4.7±0.1	4.6±0.1	4.4±0.1	4.2±0.1	4.0±0.1	<.01	<.01
15L	10.9±0.3	10.7±0.2	9.8±0.2	8.8±0.3	8.5±0.1	8.4±0.1	8.1±0.1	7.6±0.1	7.2±0.1	7.1±0.2	<.01	<.01
20L	18.2±0.7	17.3±0.6	15.8±0.6	14.4±0.8	13.9±0.5	13.7±0.5	13.2±0.3	12.2±0.2	11.8±0.3	11.2±0.4	<.01	<.01
25L	26.5±0.3	25.3±0.6	23.4±0.4	21.5±0.3	20.6±0.3	20.2±0.3	19.1±0.1	17.5±0.2	17.1±0.2	16.2±0.2	<.01	<.01
CROWN 23 Flow												
10L	5.3±0.1	5.3±0.1	5.3±0.1	5.3±0.1	5.2±0.1	5.1±0.1	5.0±0.1	4.6±0.1	4.2±0.2	3.3±0.2	<.01	<.01
15L	9.7±0.4	9.7±0.4	9.8±0.4	9.7±0.4	9.5±0.3	9.5±0.2	9.1±0.3	8.2±0.2	7.2±0.3	6.2±0.3	<.01	<.01
20L	15.7±0.4	15.5±0.3	15.6±0.4	15.5±0.5	15.1±0.4	14.9±0.5	14.4±0.4	12.8±0.5	11.4±0.4	9.4±0.7	<.01	<.01
25L	22.7±1.1	22.7±1.1	22.8±1.1	22.6±1.1	22.0±1.0	21.9±1.1	21.1±0.9	19.1±0.5	16.8±0.5	13.4±0.8	<.01	<.01
MAGNA 21 Flow												
10L	5.6±0.2	5.6±0.2	5.6±0.2	5.5±0.2	5.3±0.2	5.1±0.2	4.8±0.2	4.2±0.2	3.8±0.2	3.6±0.3	<.01	<.01
15L	11.6±0.4	11.8±0.4	11.7±0.3	11.5±0.3	10.9±0.2	10.6±0.3	10.1±0.2	8.8±0.2	7.9±0.3	7.3±0.3	<.01	<.01
20L	18.9±0.3	18.9±0.4	18.8±0.4	18.5±0.2	17.6±0.3	17.3±0.4	16.4±0.3	14.3±0.3	12.6±0.2	11.4±0.3	<.01	<.01
25L	27.3±0.4	27.4±0.5	27.3±0.5	26.8±0.7	25.3±0.1	25.1±0.5	23.6±0.5	20.8±0.5	18.4±0.2	16.4±0.5	<.01	<.01
TRIFECTA 21 Flow												
10L	3.3±0.1	3.2±0.1	3.2±0.1	3.2±0.1	3.1±0.1	2.9±0.1	2.7±0.1	2.3±0.1	1.9±0.1	1.6±0.2	<.01	<.01
15L	6.5±0.1	6.6±0.2	6.5±0.1	6.3±0.3	5.9±0.3	5.6±0.1	5.2±0.1	4.3±0.2	3.8±0.1	3.2±0.2	<.01	<.01
20L	10.5±0.2	10.3±0.1	10.2±0.1	9.7±0.3	8.9±0.5	8.4±0.4	7.5±0.4	6.5±0.4	5.6±0.2	4.8±0.2	<.01	<.01
25L	14.9±0.1	15.0±0.1	14.1±0.3	11.9±0.3	11.1±0.3	10.3±0.1	9.4±0.1	8.3±0.1	7.7±0.1	6.9±0.2	<.01	<.01

Table 2 Size of the vena contracta and Coefficient of Contraction

Parameters					**p-value**		
Flow rate [l/min]	**10**	**15**	**20**	**25**	**Columns**	**Rows**	**R x C**
EOA doppler (cm^2)							
Crown 21	1.17±0.01	1.27±0.03	1.45±0.03	1.42±0.01	<0.01	<0.01	<0.01
Magna 19	1.11±0.01	1.23±0.01	1.32±0.02	1.38±0.01			
Trifecta 19	1.35±0.04	1.48±0.02	1.58±0.04	1.64±0.06			
Crown 23	1.32±0.01	1.49±0.04	1.57±0.07	1.70±0.06	<0.01	<0.01	<0.01
Magna 21	1.34±0.02	1.38±0.02	1.44±0.02	1.62±0.04			
Trifecta 21	1.56±0.01	1.65±0.04	1.74±0.04	1.96±0.06			
EOA catheter (cm^2)							
Crown 21	1.16±0.04	1.22±0.03	1.28±0.01	1.34±0.01	<0.01	<0.01	<0.01
Magna 19	1.09±0.02	1.17±0.01	1.24±0.02	1.30±0.02			
Trifecta 19	1.33±0.01	1.45±0.02	1.49±0.02	1.57±0.03			
Crown 23	1.39±0.01	1.53±0.02	1.60±0.02	1.71±0.05	<0.01	<0.01	<0.01
Magna 21	1.35±0.03	1.41±0.03	1.47±0.01	1.56±0.03			
Trifecta 21	1.78±0.03	1.88±0.03	1.98±0.02	2.07±0.01			
Cc catheter							
Crown 21	0.51±0.02	0.53±0.01	0.55±0.002	0.58±0.002	<0.01	<0.01	<0.01
Magna 19	0.46±0.01	0.50±0.005	0.47±0.02	0.53±0.01			
Trifecta 19	0.67±0.01	0.74±0.01	0.76±0.01	0.80±0.01			
Crown 23	0.50±0.01	0.55±0.01	0.58±0.01	0.62±0.02	<0.01	<0.01	<0.01
Magna 21	0.46±0.01	0.48±0.01	0.50±0.005	0.53±0.01			
Trifecta 21	0.69±0.01	0.73±0.01	0.77±0.01	0.80±0.003			

Table 3 Fluid dynamics parameters

Parameters						**p-value**	
Flow rate (l/min)	**10**	**15**	**20**	**25**	**Columns**	**Rows**	**R x C**
Velocity doppler (m/s)							
Crown 21	1.43±0.02	1.96±0.03	2.30±0.04	2.94±0.01	<0.01	<0.01	<0.01
Magna 19	1.48±0.03	2.02±0.03	2.52±0.03	3.01±0.03			
Trifecta 19	1.23±0.03	1.68±0.03	2.09±0.08	2.55±0.06			
Crown 23	1.25±0.01	1.66±0.05	2.09±0.09	2.49±0.1	<0.01	<0.01	<0.01
Magna 21	1.24±0.02	1.81±0.03	2.29±0.03	2.59±0.03			
Trifecta 21	1.06±0.01	1.51±0.03	1.90±0.04	2.13±0.06			
ΔP max doppler (mmHg)							
Crown 21	7.4±0.2	13.6±0.5	18.1±0.7	29.7±0.3	<0.01	<0.01	<0.01
Magna 19	8.0±0.3	14.6±0.4	22.3±0.5	31.5±0.6			
Trifecta 19	5.3±0.3	9.5±0.3	14.4±1.3	21.3±1.3			
Crown 23	5.5±0.1	9.3±0.6	14.4±1.5	20.0±1.8	<0.01	<0.01	<0.01
Magna 21	5.3±0.2	11.4±0.5	17.8±0.5	22.0±0.6			
Trifecta 21	3.8±0.01	7.4±0.4	11.4±0.5	13.4±1.1			
ΔP max cath (mmHg)							
Crown 21	7.8±0.4	15.8±0.5	26.2±0.2	36.6±0.6	<0.01	<0.01	<0.01
Magna 19	8.4±0.4	16.9±0.4	24.5±0.6	37.1±1.0			
Trifecta 19	5.9±0.06	10.7±0.25	18.2±0.7	26.5±0.3			
Crown 23	5.3±0.1	9.7±0.4	15.7±0.4	22.7±1.1	<0.01	<0.01	<0.01
Magna 21	5.6±0.2	11.6±0.5	18.9±0.3	27.3±0.5			
Trifecta 21	3.3±0.06	6.5±0.06	10.5±0.21	14.9±0.15			
Net Gradient mmHg							
Crown 21	4.9±0.5	9.1±0.5	15.4±0.3	21.8±0.2	<0.01	<0.01	<0.01
Magna 19	5.9±0.2	11.1±0.1	16.7±0.5	23.1±0.7			
Trifecta 19	4.0±0.1	7.1±0.2	11.2±0.3	16.2±0.2			
Crown 23	3.3±0.2	6.5±0.2	9.4±0.5	13.1±0.6	<0.01	<0.01	<0.01
Magna 21	3.6±0.2	7.1±0.25	11.4±0.4	16.4±0.5			
Trifecta 21	1.6±0.2	3.3±0.2	5.2±0.4	7.3±0.6			
Pr. Recovery (mmHg)							
Crown 21	2.9±0.05	6.1±0.15	10.8±0.2	14.8±0.8	<0.01	<0.01	<0.01
Magna 19	2.5±0.5	5.7±0.1	9.8±0.1	13.8±0.3			
Trifecta 19	1.5±0.01	3.9±0.3	7.0±0.5	10.3±0.1			
Crown 23	2.0±0.2	3.5±0.2	6.3±0.2	9.4±0.6	<0.01	<0.01	<0.01
Magna 21	2.0±0.2	4.3±0.1	7.5±0.03	11±0.4			
Trifecta 21	1.8±0.1	3.2±0.2	5.7±0.5	8.0±0.5			
Pr. Recovery (%)							
Crown 21	37±2	39±2	41±1	40±2	0.6	0.5	0.5
Magna 19	29±5	34±1	37±1	37±1			
Trifecta 19	36±3	35±2	38±2	39±2			
Crown 23	37±4	36±2	40±1	41±2	0.022	<0.01	0.7
Magna 21	36±3	36±1	39±1	39±1			
Trifecta 21	53±4	50±2	55±1	54±1			

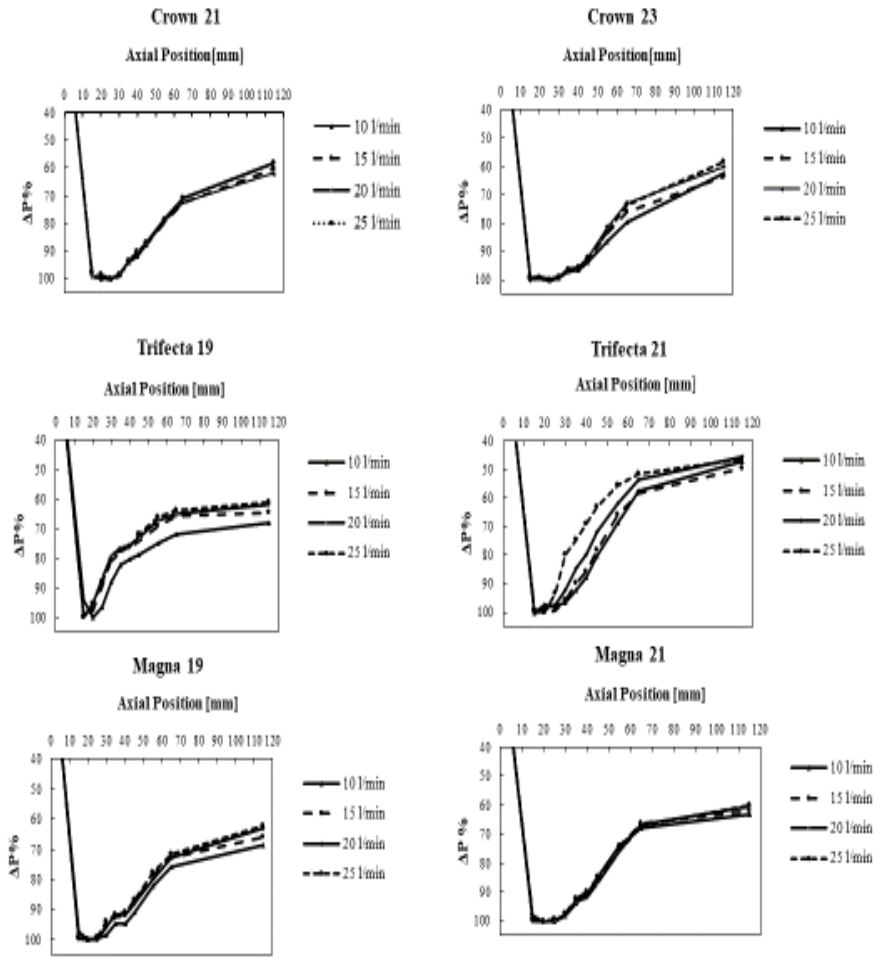

Fig. 3 Pressure recovery for each prosthesis at each flow level.

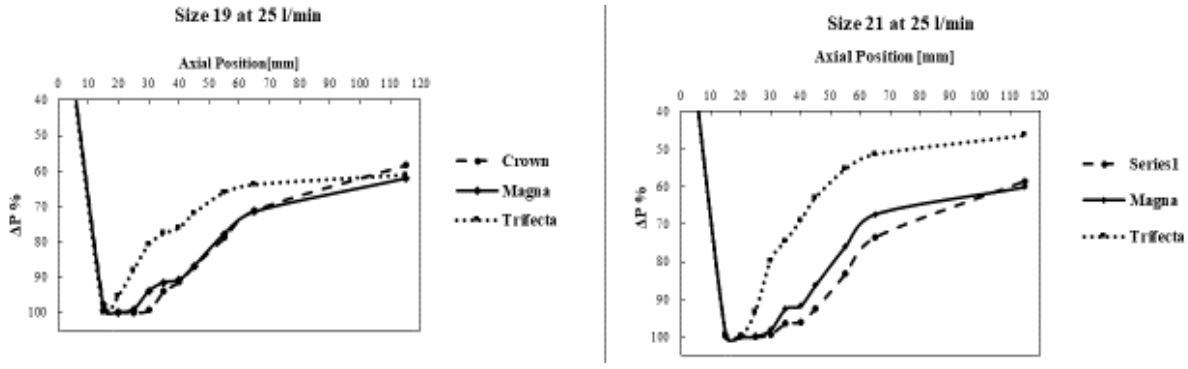

Fig. 4 Pattern of pressure recovery at 25 l/m for each prosthesis

10 L/min **15 L/min** **20 L/min**

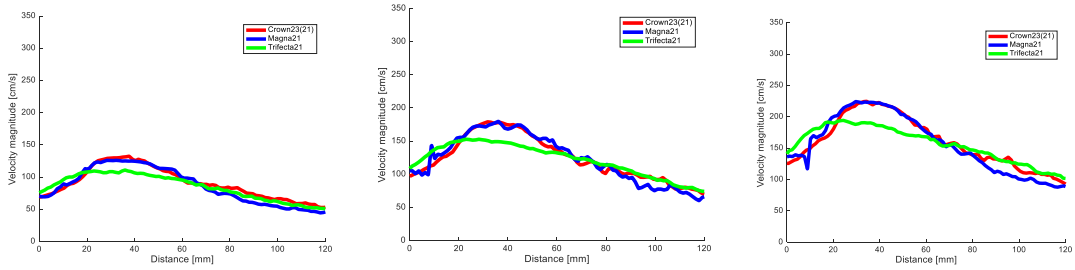

25 L/min

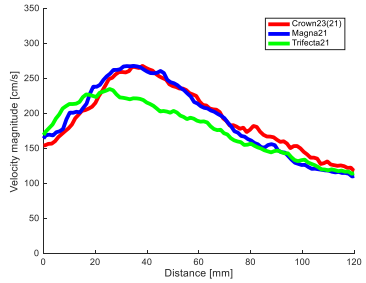

Fig. 6 Velocity profiles at different flow levels for Trifecta 21, Magna 21 and Mitroflow 23.

CHAPTER 4

IMPACT OF AORTIC VALVES PROSTHESIS ON CORONARY FLUID DYNAMIC

These studies have been undertaken in collaboration with the following Institutions:

-Cardiovascular Surgery Depatment, "L. Sacco" Hospital, Università degli Studi di Milano, Milan, Italy.

-ForCardio.lab, Fondazione per la Ricerca in Cardiochirurgia ONLUS, Milan, Italy

-Cardiovascular Department, Cardiac Surgery Unit, Ospedale "A. Manzoni" ASST-Lecco. Lecco, Italy.

This Chapter is based upon the following paper:

-Piola M, Vismara R, Tasca G, Lucherini F, Redaelli P, Soncini M, Romagnoni C, Mangini A, Antona C, Fiore GB. Design of a simple coronary impedance simulator for the in vitro study of the complex coronary hemodynamics. Physiol Meas. 2016 Dec;37(12):2274-2285

Introduction and aims

The need for a mock loop with coronary circulation simulator

Since it is well-known that a bioprosthesis may affect the local fluid dynamics of the aortic root, the coronary blood flow may be disrupted by the implant (1).

A study of the extent of this flow interference, has become necessary due to the number of new devices manufactured. In particular, in the last decade, the spread of transcatheter aortic valve implantation (TAVI) has opened new issues concerning the relation between the device implanted and coronary flow (2,3). Indeed, the issues posed by these new devices, stem not only from their design, but from the fact that the native valve is left in place. This introduces new open issues concerning the interaction of the device with the local biomechanics and hemodynamics.

The very specific geometry of self-expandable TAVI, which are designed to ensure stable deployment and anchoring of the prostheses to the surrounding tissue, is an example of these new design-rules. In addition, implantation strategies and procedures are new and technically challenging for the operators. Often, the safety margin is very limited, and errors in the procedure can have dramatic outcomes (Fig.1).

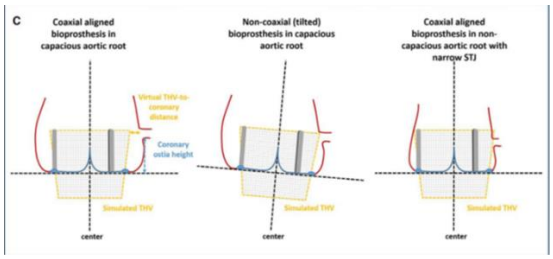

Fig.1. Three different scenarios after implanting a TAVI

One of the critical problems related to the design and deployment of these devices is the interaction with the coronary structure and flow. Potential alteration of the coronary

perfusion due to prosthesis implantation are reported in the literature, particularly in case of peculiar anatomies (4).

The following general specifications drove the designing process of the experimental apparatus: *i*) reliability and consistency with clinical literature of the *in vitro* reproduction of the main determinants of the coronary hemodynamics; *ii*) capability of the coronary impedance simulator (CIS) to directly interface with biological aortic valve to test the delivery/deployment procedure in a realistic scenario, and *iii)* simplicity in the management of the experimental apparatus in the lab, thus making the device suitable also for extensive training procedures.

There are several "*in vitro"* mock loops with a coronary circulation sub-unit reported in literature. These are usually often quite complex and exclusively research-oriented experimental apparatuses with extremely sophisticated (and reliable) control (5-10). Some of these devices are designed to study some specific aspects of the coronary flow and embedding both the coronary in a single hydraulic apparatus, or take into consideration only the left coronary branch, and were not designed to house the entire biological aortic valves.

To our knowledge, a mock loop designed to house a real aortic root harvested from porcine hearts, with a module for the simulation of both left and right coronary circulation, does not exist in the literature.

The experimental device conceives, was dimensioned on the base of a simple lumped parameter model. Then, the time-dependent CIS was realized. The CIS was connected to an existing left-circulation simulator (11), the ForCardioLap Mock Loop, capable of housing a porcine aortic root, and tested simulating physiologic hemodynamics.

In order to test the potentiality of our experimental apparatus in replicating pathological conditions, two scenarios were replicated "*in vitro*".

In the first test was replicated a sudden aortic valve incontinence scenario, which can occur for example in case of acute endocarditis. The sudden drop in cardiac output, due to an acute aortic valve regurgitation, causes a drop in the systemic pressure with a coronary flow reduction characteristically during the diastolic phase.

In the second test, inside the porcine aortic root, were surgically implanting two types of biological prostheses. In this case the presence of a bulky device, such a bioprosthesis, may disrupt the coronary flow in both systolic and diastolic phases.

Materials and Methods

The coronary impedance simulator

In the following paragraphs is reported the dimensioning approach and the manufacturing of the coronary impedance simulator (CIS). Firstly, the design specifications of the CIS were identified and divided in physiological-driven and bioengineering requirements. Secondly, the design of the experimental system was presented, followed by the evaluation of the CIS performances.

1.1 Design specifications: physiology requirements

According to clinical literature, aortic pressure, oscillating between 80 and 120 mmHg, is the main driving force of the coronary circulation, being the left and right coronary branches directly connected to the aorta via coronary ostia which originate from the sinuses of Valsalva and the right atrium (coronary sinus), at atmospheric pressure. Being most of the left coronary vasculature embedded in cardiac muscle tissue, left coronary

blood flow during the phases of muscle contraction (systole) is lower than blood flow during diastole (12) (Figure 1). In these conditions, the left coronary peak flow rate in diastole is 2-3-fold the peak in systolic phase. In the right coronary circulation, these phenomena are less significant due to the epicardial development of the right vasculature. Thus, differences between systole and diastole flows are less pronounced in the right coronary branch. Finally, in physiologic rest conditions, the total mean coronary blood flow is about 250 ml/min. The 70% of this flow rate (175 ml/min) flows in the left coronary, and 30% (75 ml/min) flows in the right compartment (12).

1.2 Design specification: bioengineering requirements

From the technical point of view, three main requirements leaded the design of the CIS. The first requirement was to create a simple-to-use and reproducible circuit, easily connectable with the coronary branches, without damaging the tissues. Secondly, it was necessary to design a compact coronary module which can be easily integrated and connected with an already available mock loop system without interfering with its functioning. Finally, it was necessary to obtain a time-dependent circuit correctly synchronized with the simulated heart systole and diastole in order to have a proper hemodynamic replication in the coronary module.

1.3 Design philosophy of the coronary impedance simulator

The CIS was integrated in an existing mock loop, simulating the left human circulation, and designed to host biologic aortic roots. Briefly, this simulator consisted of a pulsatile piston pump able to mimic the aortic and mitral flow rates at different heart rates, and of a settable systemic input impedance. For a detailed description of this section of the mock

loop refer to Vismara *et al* (11).

Coronary impedance consisted of two independent hydraulic circuits, simulating the left and the right coronary. The inflows were directly connected to the left and right coronary ostia of the biological aortic root. The outflows were connected to a reservoir at atmospheric pressure, thus simulating the coronary venous sinus. Both left and right coronary simulator featured a systolic and a diastolic impedance. A time dependent sub-system switched between the diastolic and systolic impedance, acting synchronously with the piston pump which simulated the systemic flow rate.

A preliminary dimensioning of the coronary impedances was made using a lumped-parameter model. A lumped parameter model of the systemic circulation was forced by imposing a positive sine waveform with a mean systolic flow rate value equal to 6 l/min (and 0 l/min during diastole), in order to determine the reference aortic pressure. The output of the lumped parameter model of the systemic impedance was the aortic pressure, that was used as input for the coronary impedance model. The coronary impedance was modelled as simple time-dependent parallel resistances. The values of the coronary resistance were adjusted to minimize the differences between the modelled coronary flow rate, and reference data obtained from literature (Figure 2).

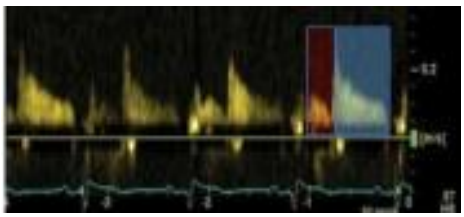

Fig.1. Left coronary doppler pattern. Red. Systolic phase. Blue. Diastolic phase

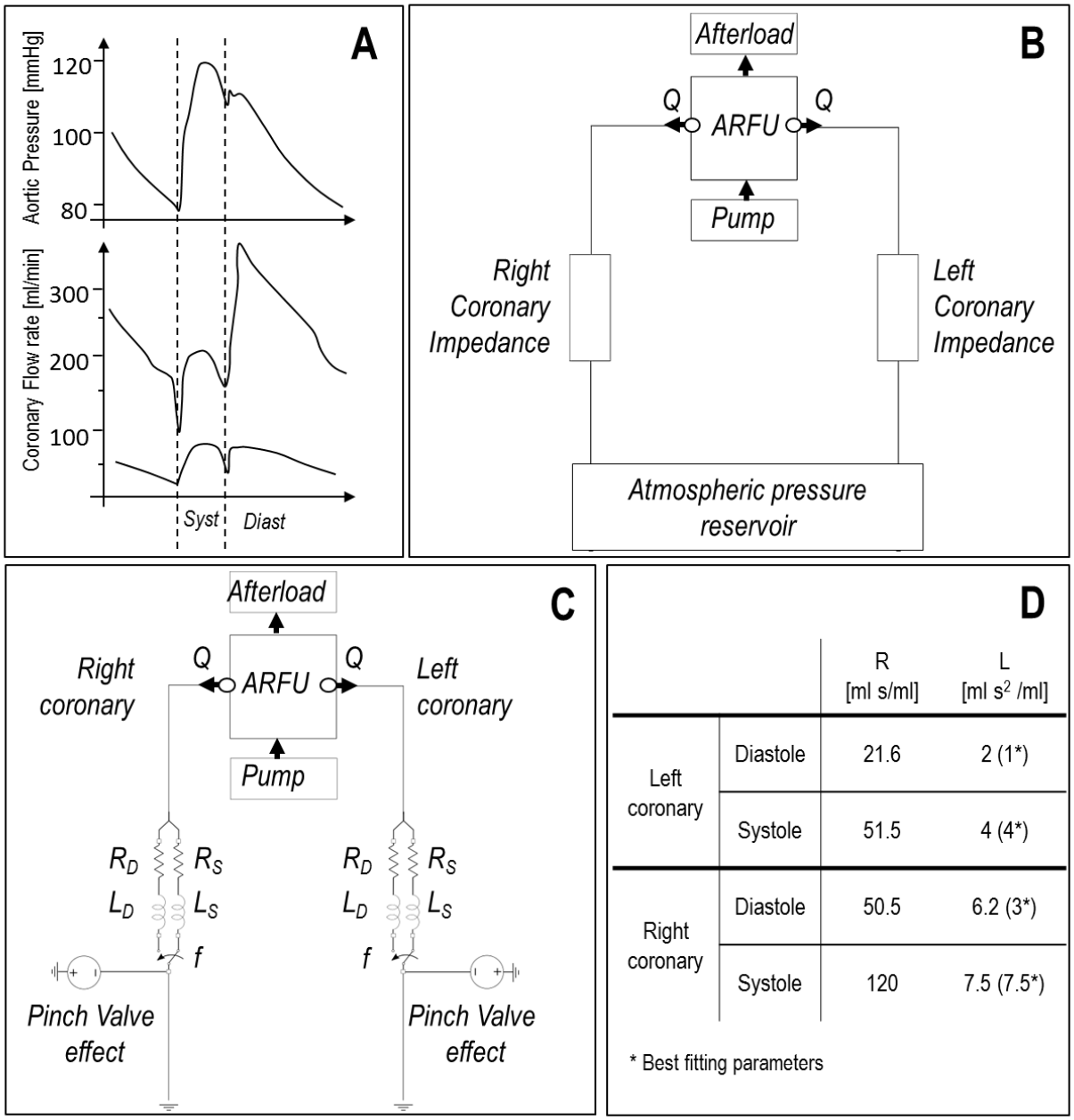

Figure 2. A) Representative aortic pressure and left and right coronary flow rate tracings. B) Schematic of the coronary impedance simulator. C) Lumped parameter model of the coronary impedance simulator. D) Values of the lumped parmater element adopted in the model. AV: aortic root functional unit; Q: flow rate; R_D, R_S: diastolic and systolic hydraulic resistances respectively; L_D, L_S: diastolic and systolic inertance;

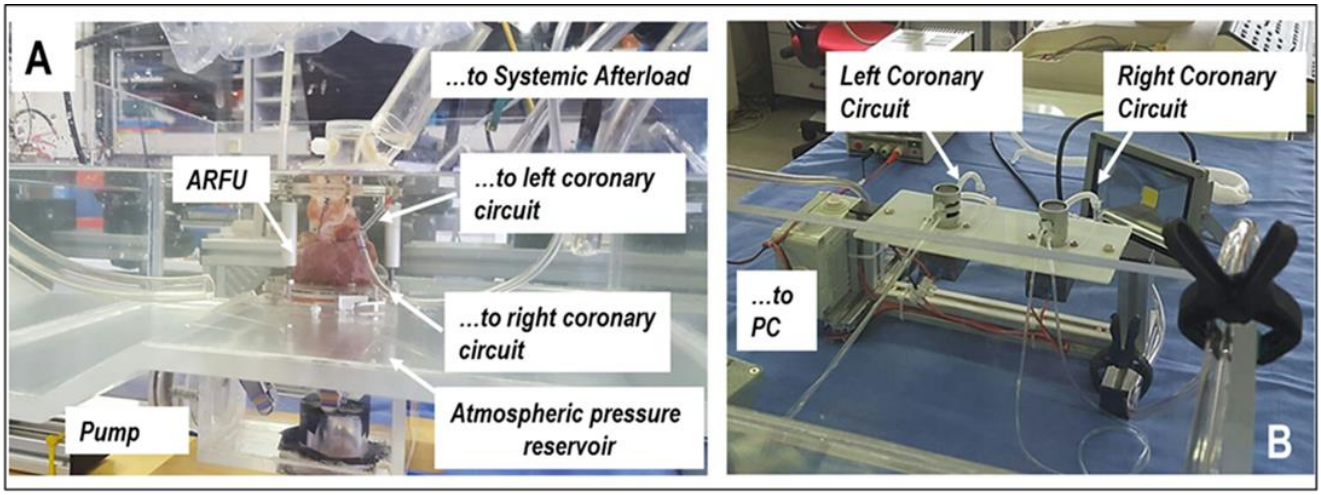

Figure 3. (A) Mock loop with a porcine aortic root sample housed. The picture shows coronary cannulation for connection with the coronary impedance simulator circuits. (B) Picture of the coronary impedance simulator subsystem. Two pinch valves are used to direct the flow either to the systolic or to the diastolic hydraulic circuits.

The coronary circuit was designed on the base of the values of resistances obtained with the lumped parameter model, (Figure 2B). Hydraulic resistances were obtained with PVC tubes. Figure 1B reports a scheme of the circuits. Tubes with an inner diameter of 1.6 mm were used for both the coronary circuits. The length was set at 500 mm, 1000 mm, 1670 mm and 2000 mm for the left-diastolic, left-systolic, right-diastolic and right-systolic circuits, respectively.

Fluid flow switching between the systolic and diastolic branches was provided by two solenoid pinch-valves (S307-06, SIRAI® Elettromeccanica, Italy): one for the left, and one for the right coronary branch. The pinch valves were connected to a PC equipped with a I/O board (USB 6210, National Instruments, Austin TX, USA) and were managed via a in house developed LabView software (National Instruments Corp., TX, USA) that provided the synchronization between the piston pump driver and the valve switching/timing. A voltage signal, generated by the piston pump driver and related to the status of the cardiac cycle, was used to alternate between systolic and diastolic impedance.

In Figure 3, the prototype of the CIS, connected with the left-circulation simulator is

reported. Figure 3A depicts the aortic valve sample hosted into the system and connected with the piston pump, with the coronary circuit simulator, and with the systemic afterload. To keep the sample hydrated, the aortic valve was submerged in a 0.9% NaCl water solution in a open-to-atmospheric reservoir. In figure 3B, the left and right time-dependent hydraulic circuit is shown.

Evaluation of the CIS performances

Preliminary experiments were performed in order to analyze the flow and pressure traces using porcine aortic valve. Briefly, aortic valves were harvested by experienced surgeons from fresh swine hearts obtained from local abattoir. Only samples with physiologic anatomies were considered, and 4 samples were included in this study. Aortic Valves were prepared as previously described (11). In addition, 30 mm of the left and right coronary branches were isolated from the surrounding tissue, and the left circumflex branch was ligated. Samples were housed in the mock loop and the coronary branches were cannulated with connectors consisting of two 3.2 mm-inner diameter PVC tube, secured to the coronary ostia by sutures. The left and right coronary connections were then coupled to the CIS, the mock loop was primed with 0.9% NaCl water solution at room temperature, and the desired working conditions were gradually reached. Transit-time ultrasound flow meters (HT110R, Transonic Systems Inc., Ithaca, NY, USA) equipped with ¼" probes were used for acquiring the coronary flow rate signals, and 1" probe was used to acquire the aortic flow rate. A piezometric pressure transducer (140PC05D, Honeywell Inc., Morristown, NJ, USA) measured the aortic pressure signal. Data were acquired and recorded with a PC equipped with a I/O board (USB 6210,

National Instruments, Austin TX, USA). The aortic and coronary flow rate and the aortic pressure were acquired for about 60 s, at a sample frequency of 200 Hz.

Two set of experiments were conducted. In the first set, the system was tested by setting four different aortic pressure levels (P0, P1, P2 and P3) with mean values comprised in the range of 25 to 130 mmHg, and with a cardiac frequency of 60 bpm. This set of experiment aimed at characterizing the response of the CIS to variations of the mean systemic pressure. In the second set of experiments, the dependency of the CIS response to simulated heart rate variation were analyzed. The aortic pressure was set at P2 (mean value equal 95.1±1.3 mmHg). and the simulated heart rate was set at 60 ad at 80 bpm. The acquired flow rate signals were post-processed for noise filtering using a Butterworth pass band filter with cutoff frequency of 40 Hz, plus an averaging operation on 20 cycles. For the pressure signal a 15-cycle averaging was sufficient. After filtering, the mean left and right coronary flow rate and systemic pressure at P0, P1, P2 and P3 were evaluated in order to obtain the flow rate/pressure relation. Finally, occurring, according to the literature, most of the coronary flow in the diastolic phase, the diastolic aortic pressure represents the main drive factor. Thus, in order to assess the relation between diastolic systemic pressure and coronary flow rate, the slope of the coronary flow rate and systemic pressure waveforms during the diastole were compared.

A lumped parameter model of the CIS (Figure 2C-D) was implemented in order to analyze and interpret the behavior of the CIS. This model enabled us to take into account the contribution of the fluid inertial phenomena and the effects introduced by the dynamics of opening/closing of the pinch valves on the CIS fluid hemodynamics. Tubes were modelled as a series of resistive and inertial elements, while the pinch valve effect

was modelled as an ideal pressure generator (Figure 2 C). Optimal value of the lumped parameters was reported in figure 2 D.

1. Case study: effect of the aortic valve incompetence on the coronary flow rate

The impact of the aortic valve incompetence on the coronary flow rate was studied using porcine aortic valve specimens (*n =4*) housed in the mock loop as previously described. The experiments were organized as follows (Figure 4B). The samples were tested in basal condition (P2, and 60 bmp), and pressure and flow rate were recorded. Following tests in basal condition, in each sample the aortic incompetence was induced by means of two 4 mm diameter holes performed in the left-coronary leaflet, and in the non-coronary leaflet. After the induction of valve incompetence, the samples were tested in the same working condition to verify the reliability of the pathological model. The acute response of the circulation system was replicated in the mock loop, simulating a peripheral vasoconstriction and an increased simulated heart rate (100 bpm), grossly mimicking the physiologic response of the heart/systemic circulation (Figure 4) to this acute pathological condition. Aortic pressure and left and right coronary flow rate were recorded *i*) in basal condition, *ii*) after the induction of pathology, and *iii*) in the post-circulation response scenario. Pressure and flow signals were post-processed as previously described.

2. Case study: effect of aortic valve replacement on the coronary flow rate

A second test was performed by evaluating the coronary flow with the native aortic valve and after 3 surgical implants using bioprostheses of different manufactures.

An aortic root with a native valve annulus of 19 mm was selected and tested to obtain

basal values to compare with those obtained after each valve implant. Then, in the same aortic root were implanted a Trifecta valve (St-Jude. St. Paul. MN) with a labelled size of 19, a Magna-Ease valve (Edwards Lifescience. Irvine. CA) with a labelled size of 19 and finally a Trifecta with a labelled size of 21 mm. In the latter case, was performed a oversizing with the aim to find out to what extent, the bulkiness of the prosthesis, in relation to the size of the aortic root, could disrupt the coronary flow. The valves were implanted by means of a continuous suture. The coronary flows were measured a 3 different imposed flow level such 65 ml, 80 ml and 95 ml.

Results

The designed CIS is able to mimics the main features of the coronary circulation

Figure 4A reports representative coronary flow and aortic pressure *vs*. time traces acquired under physiological condition (P2). The mean aortic pressure was to 95.1±1.3 mmHg. The left coronary flow and pressure waveforms were in counter-phase, with a maximum of flow during the diastole and a minimum during the systole. This evidence was less marked in the right coronary branch. Mean total coronary flow rate was 271.9±13.4 ml/min, representing the 7% of the cardiac output (3.75 ±0.26 l/min). The mean total coronary flow rate flew 68% in the left coronary circuit (184.4±11 ml/min), and 32% (87.5±7.6 ml/min) in the right as reported in literature (12).

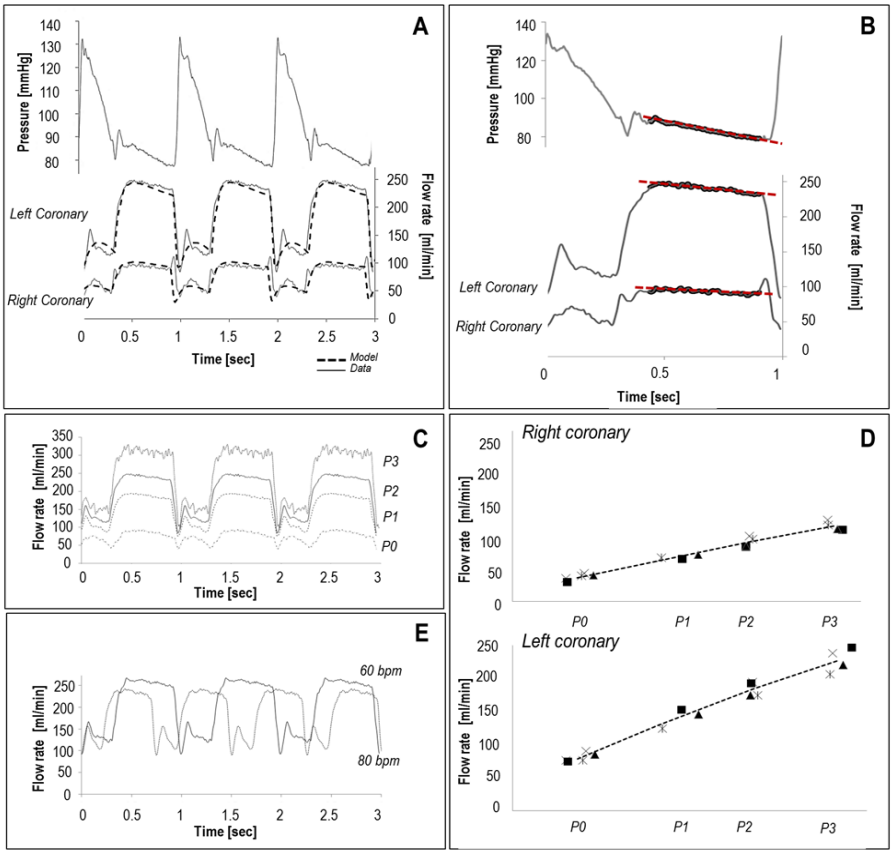

Fig. 4 (A) Representative systemic pressure and left and right coronary flow rate tracings obtained under physiological basal condition (P2). (B) Relation between diastolic pressure slope and coronary flow slope during the diastolic phase (C and E) Right and left coronary flow rate tracings obtained by changing the mean aortic pressure at a fixed beat rate (60 bpm). D Systemic pressure/coronary flow rate relation. Different symbols refer to four distinct experimental sessions.

The left and right coronary flow tracings simulated by the lumped parameter model were obtained by providing the experimental aortic pressure trace as an input in the model (Figure 4A, *dotted line*). Simulated tracings allowed us to estimate the contribution of the inertia and of the pinch valve functioning on the CIS hemodynamics. While the effects caused by inertance are evident during the systolic/diastolic switch (*i.e.*, reluctance of the fluid to respond immediately to rapid aortic pressure change), the pinch valve functioning generated a pressure suction affecting the systolic flow rate.

Figure 4B shows the slopes of the aortic pressure and left and right coronary flow rates during late diastole. In both the coronary branches pressure and flow rate show a *quasi*-linear behavior with comparable slopes (*red dotted line*).This trend is particular marked

in the left coronary circuit with a mean diastolic flow rate/pressure slope ratio equal to 1.2 ml/mmHg min. In the right branch the ratio decrease down to 0.65 ml/mmHg min.

In Figure 4C, the traces of the left coronary flow rate at different aortic pressure are reported. As expected, the left coronary flow rate increased by increasing aortic pressure demonstrating that the aortic pressure was the main driving force of the coronary flow perfusion. Similar results were obtained in the right coronary circuit. Flow/pressure relation is presented in figure 4D. As expected, both circuits demonstrated a linear relation between pressure and flow rate.

Figure 4E depicts a comparison between the behavior of the left coronary circuit in response to two simulated heart rate (60 and 80 bpm). By increasing the simulated heart rate, the diastolic flow rate decreased, being the diastole time shorter in comparison with diastole under basal heart rate condition, while the systolic flow rate remain unchanged. Similar results were obtained in the right coronary circuit.

Effect of the aortic valve regurgitation on the coronary flow rate

Figure 5 reports the results of the *in vitro* simulation of the incontinent aortic valve (5A). Aortic valves regurgitation induced a reduction of the left and right coronary flow rate, due to a severe reduction of the aortic pressure (Figure 5B). Aortic valve regurgitation also affected the diastolic/systolic flow rate ratio in both the left and right branches (Figure 5C). Following the simulation of the pathology, the mean systemic flow rate decreased from 1.87±0.24 l/min (-52% with respect to basal P2 condition), with an associated decrease of the mean systemic pressure from 45.4±3.3 mmHg (-52% with respect to basal P2 condition). The mean left coronary flow rate decreased down to 100.3±19.9 ml/min (-45.6% with respect to basal P2 condition), while in the right branch,

the mean flow rate was 48.4±9.0 ml/min (-44.6% with respect to basal P2 condition) (Figure 5B).

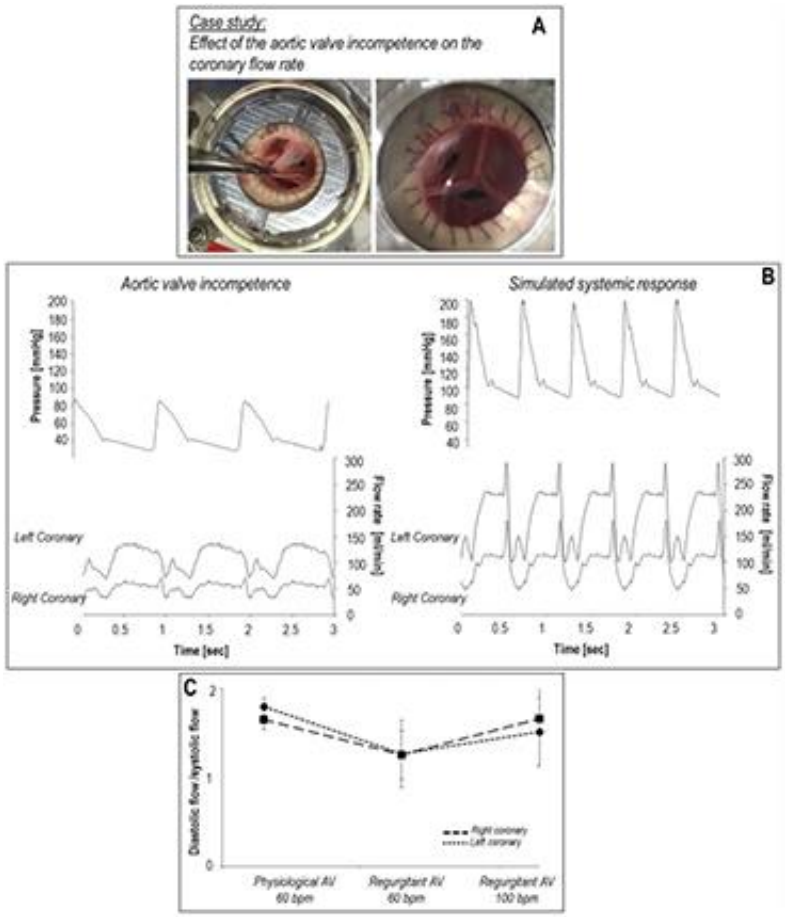

Figure 5. (A) Pathological model: aortic valve regurgitation. Two holes with a mean diameter of 4 mm were pierced in the leaflets to induce valve incontinence. (B) Representative systemic pressure and left and right coronary flow rate tracings obtained with regurgitant aortic valve pre- (left) and post-simulation (right) of the physiological response. (C) Ratio of the diastolic/systolic flow rate during the experiment.

Systemic response to acute aortic valve regurgitation was simulated by increasing both heart rate (up to 100 bpm) and simulated peripheral resistance. Following these maneuvers, the coronary flow rate was restored at basal level obtaining a flow rate of 172.9±31.6 ml/min and 88.7±16.0 ml/min in the left and right coronary circuit, respectively (Figure 5 B and C) with a mean systolic flow rate of 2.51±0.23 l/min and pressure equal to 108.6±6.1 mmHg.

Effect of the aortic valve replacement on the coronary flow rate

The flow of the left coronary artery, after valve implantation, was similar to that of the basal test for all the bioprostheses during both systolic and diastolic phases (Tables 1 and 2, Fig. 6,7 and 8). There was, instead, a systolic flow perturbation on of right coronary flow following the implant of the bioprostheses (Tables 1 and 2 and Fig. 8). While the coronary flow after the implant of the Trifecta 19 was close to the basal value, the mean systolic coronary flow was substantially disrupted after the implant of the Magna-Ease 19 with a value of 12±1 ml/min and after the implant of the Trifecta 21 with a value of 7±1 ml/min.

Table 1 systolic and diastolic flow in both coronaries according to different valve and stroke volumes

						Left coronary flow			Right Coronary flow		
	Stroke Volume set (mL)	Stroke Volume (mL)	Backflow Volume (mL)	Mean aortic pressure (mmHg)	Mean systolic ΔP (mmHg)	systo/diastolic (mL/min)	diastolic (mL/min)	systolic, (mL/min)	Systo/diastolic mL/min	diastolic mL/min	systolic, mL/min
Native Valve	65	50	10	112	0,5	118,0	143,0	83,9	43,7	55,1	29,9
Native Valve	80	60	9	108	0,8	115,0	139,9	81,9	42,2	52,4	30,0
Native Valve	95	72	9	112	1,9	117,6	140,7	85,7	43,2	51,7	31,3
Magna 19	65	39	24	107	8,7	115,6	139,0	83,0	36,4	54,3	11,3
Magna 19	80	51	23	110	12,2	117,5	141,1	84,7	37,3	55,1	12,2
Magna 19	95	63	22	111	16,2	118,6	141,8	86,7	36,9	55,1	11,7
Trifecta 19	65	42	13	108	5,9	118,7	146,0	83,6	42,5	55,8	25,5
Trifecta 19	80	54	14	106	9,4	116,7	142,6	83,4	41,8	55,5	24,9
Trifecta 19	95	66	12	109	13,4	118,9	143,9	85,6	42,6	54,9	26,0
Trifecta 21	65	34	19	109	4,1	120,0	148,2	83,9	34,6	55,1	7,9
Trifecta 21	80	49	17	100	6,2	111,8	136,5	80,2	32,1	51,5	6,5
Trifecta 21	95	61	17	111	8,0	119,6	144,7	85,5	34,6	54,7	6,8

Table 2. Average systolic and diastolic flow in both coronaries in the 4 tested scenarios

	Left coronary flow mean values			Right coronary flow mean values		
	mean systo/diastolic (mL/min)	mean diastolic (mL/min)	mean systolic (mL/min)	mean Systo/diastolic (mL/min)	mean diastolic (mL/min)	mean systolic (mL/min)
Native Valve	**117±2**	**141±2**	**84±2**	**43±1**	**53±2**	**30±1**
Magna 19	**117±2**	**141±2**	**85±2**	**37±1**	**55±1**	**12±1**
Trifecta 19	**118±1**	**144±2**	**84±1**	**42±0,5**	**55±1**	**26±1**
Trifecta 21	**117±5**	**143±6**	**83±3**	**34±1**	**54±2**	**7±1**

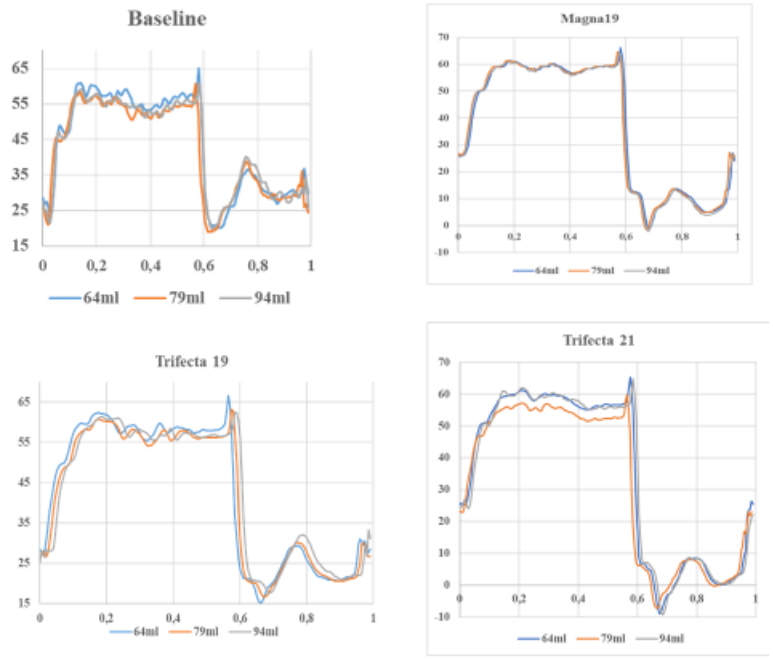

Fig. 6. Comparison of the coronary flow patterns of the right coronary artery at the 3 different stroke volumes for the 4 valves. Basal represent the native valve. The y-axis is the flow in mL/min and the x-axis is time in sec.

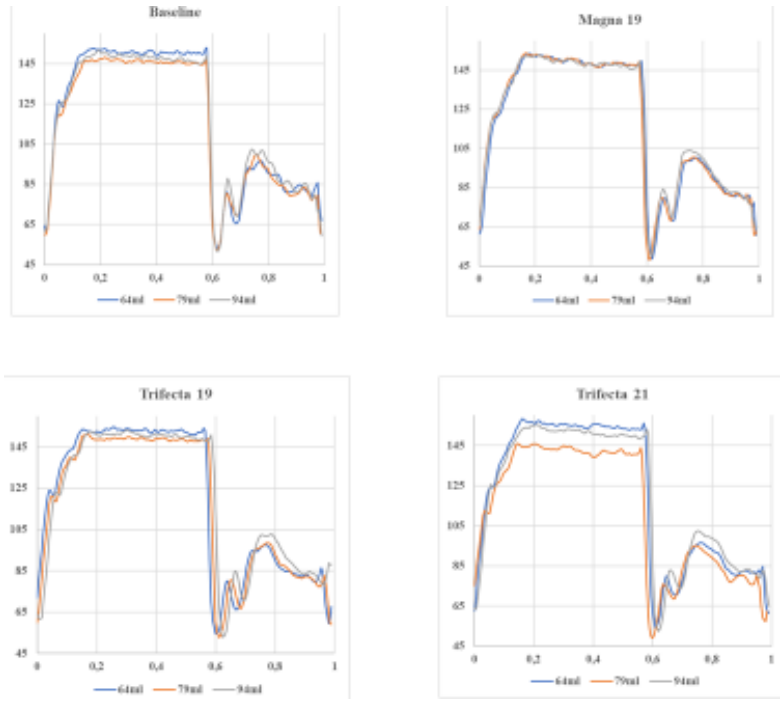

Fig. 7. Comparison of the coronary flow patterns of the left coronary artery at the 3 different stroke volumes for the 4 valves. Basal represent the native valve. The y-axis is the flow in mL/min and the x-axis is time in sec.

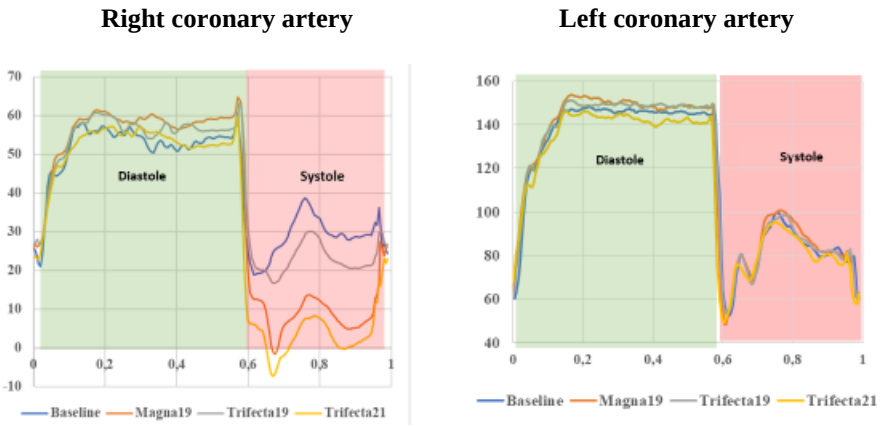

Fig. 8. Comparison of the coronary flow patterns for each coronary artery at a stroke volume of 79 ml for the 4 valves. Basal represent the native valve. The y-axis is the flow in mL/min and the x-axis is time in sec.

Discussion

The results from these experiments support the hypothesis that the novel coronary impedance simulator tested, mimicked the physiological pressure and flow rate patterns of the left and right coronary circulation in different simulated clinical scenarios.

The platform was capable to mimic the complexity of the coronary circulation, being this feature crucial to assess the potential risk of the interaction between the implanted device and the coronary perfusion. In particular, the specification of ease of use of the CIS was satisfied thank to the technical solutions adopted.

The coronary module was easily connected to the porcine left and right coronary branches, and at the same time, it was easily integrated with the available mock loop of the left circulation, without interfering with its functioning. The obtained results demonstrated that the system was able to reproduce *"in vitro"* the main determinants of the coronary circulation, with coronary flow rate correctly synchronized with the aortic pressure and cardiac output. In fact, graphs showed that the measured left and right coronary flow rate are comparable to those reported in literature (3,8,10,12). From a technical point of view, these results suggested that the CIS is a suitable model for studying the impact of novel cardiovascular devices on coronary perfusion, within a controlled and reproducible biomechanical environment.

Compared with other coronary mock loop systems reported in literature, with particular reference to the systems proposed by Geven , Gaillard, and Calderan *et al*. (3,8,10), this CIS was conceived to study the hemodynamic of both the left and right coronary circulation using entire aortic root functional units with intact aortic valve, extracted from

porcine heart. To this purpose, the CIS was equipped with a time-dependent left and right hydraulic circuit and dedicated actuators. The time dependency is controlled by a control hardware/software which automatically switches between systolic and diastolic phase, depending on the state of the cardiac cycle. The use of commercial two-way pinch valves to direct the flow during systole and diastole in the corresponding circuit resulted simple and unsophisticated in comparison with the strategy adopted in the literature.

Functional assessments of the CIS using entire porcine aortic roots under physiological and pathological conditions

Here, we proposed a simple pathological scenario that allowed us to validate our CIS platform. The rationale of our pathological model was that coronary circulation is a time-dependent phenomenon with the most flow occurring during the diastolic phase. Being the diastolic aortic pressure the main driving force, everything that modify this parameter influences the coronary flow.

Aortic stenosis and regurgitation are the most representative determinant of the aortic pressure. While, the impact of aortic valve stenosis on the coronary perfusion was deeply investigated "*in vitro"* by Gaillard and colleagues (10), here we focused on the effects induced by aortic valve regurgitation because regurgitation represents the ideal condition to test the coronary perfusion system. Aortic regurgitation is a clinical condition in which part of the forwarded flow reverses into ventricle through the incontinent aortic valve during the diastolic phase. Aortic valve regurgitation can be both chronic and acute clinical conditions, but the dramatic hemodynamic repercussion are present only in acute phases. This is the case of a sudden rupture of the aortic valve leaflets, owing to infective

endocarditis or traumatic leaflets rupture, with a decrease in cardiac output and in mean systemic pressure consequently with a decrease of the coronary flow. In response to this critical scenario, the self-regulation system aims to preserve vital organ, such the heart by restoring adequate coronary flow and in turn the flow to the nervous system circulation that have to coordinate the regulations put in place. The two immediate and ease mechanisms to restore and maintain the cardiac output are accomplished by increasing the heart rate and the peripheral resistances by a vasoconstriction with an increase of systemic mean pressure as consequence.

Using our model of aortic valve regurgitation, we were able to mimic "*in vitro"* the effect of the aortic back-flow on the left and right coronary circulation, obtaining results similar to those obtained in animal models (13,14) and observed in humans (15).

With the designed CIS, it was also possible to simulate the two main compensative mechanisms by increasing the heart rate (intra cardiac mechanism) and the peripheral vascular resistance (extra cardiac mechanism) to restore basal level of aortic pressure and coronary flow rate.

Functional assessments of the CIS under physiological conditions with surgically implanted bioprostheses.

The coronary impedance system appeared to be capable of detecting subtle differences in coronary flow in the presence of potentially bulky devices such bioprostheses.

When compared with the normal aortic valve the flow in the left coronary artery, in the presence of a bioprosthesis, was similar to that of the basal test for all the bioprostheses during both systolic and diastolic phases and for the 3 different stroke volumes imposed (Fig.6 and 7). There was, instead, a substantial systolic flow perturbation on of the right

coronary flow following the implant of the bioprostheses. While the coronary flow after the implant of the Trifecta 19 was close to that of the basal value, the mean systolic coronary flow was substantially disrupted after both the implant of the Magna-Ease 19 with a value of 12±1 ml/min and after the implant of the Trifecta 21 with a value of 7±1 ml/min. In particular for the Trifecta 21, the degree of flow disruption was the largest and likely caused by the geometric mismatch between the valve size and the size of the aortic root.

Conclusion

The CIS devised in this study, easily integrated with the existing left-circulation simulator, appeared to be a simple and a well-suited system for medical training and cardiovascular research purposes.

The resulting new platform could be used to assess the coronary perfusion after several clinical procedures such as TAVI and conventional aortic valve implantation.

Bibliography

1-Bakhtiary F, Schiemann M, Dzemali O, Dogan S, Schächinger V, Ackermann H, Moritz A, Kleine P. Impact of patient-prosthesis mismatch and aortic valve design on coronary flow reserve after aortic valve replacement. J Am Coll Cardiol. 2007 Feb 20;49(7):790-6.

2-Frisoli, T. M., M. Guerrero,W. W. O'Neill, Mechanical circulatory support with impella to facilitate percutaneous coronary intervention for post-TAVI bilateral coronary obstruction. Catheter Cardiovasc Interv. 2016;88(1):e34:7.

3-Calderan, J., W. Mao, E. Sirois,W. Sun, Development of an In Vitro Model to Characterize the Effects of Transcatheter Aortic Valve on Coronary Artery Flow. Artif Organs. 2016;40(6);612-9.

4-Ribeiro HB1, Nombela-Franco L, Urena M, Mok M, Pasian S, Doyle D, DeLarochellière R, Côté M, Laflamme L, De Larochellière H, Allende R, Dumont E, Rodés-Cabau J. Coronary obstruction following transcatheter aortic valve implantation: a systematic review. JACC Cardiovasc Interv. 2013 May;6(5):452-61.

5-Schampaert, S., K. A. Pennings, M. J. van de Molengraft, N. H. Pijls, F. N. van de Vosse,M. C. Rutten, A mock circulation model for cardiovascular device evaluation. Physiol Meas. 35:687-702, 2014.

6-Schampaert, S., M. van't Veer, F. N. van de Vosse, N. H. Pijls, B. A. de Mol,M. C. Rutten, In vitro comparison of support capabilities of intra-aortic balloon pump and Impella 2.5 left percutaneous. Artif Organs. 35:893-901, 2011.

7-Chodzynski, K. J., K. Z. Boudjeltia, J. Lalmand, A. Aminian, L. Vanhamme, D. R. de Sousa, S. Gremmo, L. Bricteux, C. Renotte, G. Courbebaisse,G. Coussement, An in vitro test bench reproducing coronary blood flow signals. Biomed Eng Online. 14:77, 2015.

8-Geven, M. C., V. N. Bohte, W. H. Aarnoudse, P. M. van den Berg, M. C. Rutten, N. H. Pijls,F. N. van de Vosse, A physiologically representative in vitro model of the coronary circulation. Physiol Meas. 25:891-904, 2004.

9-Moore, B. L.,L. P. Dasi, Coronary Flow Impacts Aortic Leaflet Mechanics and Aortic Sinus Hemodynamics. Ann Biomed Eng. 43:2231-41, 2015.

10-Gaillard, E., D. Garcia, L. Kadem, P. Pibarot,L. G. Durand, In vitro investigation of the impact of aortic valve stenosis severity on left coronary artery flow. J Biomech Eng. 132:044502, 2010.

11-Vismara, R., G. B. Fiore, A. Mangini, M. Contino, M. Lemma, A. Redaelli,C. Antona, A novel approach to the in vitro hydrodynamic study of the aortic valve: mock loop development and test. ASAIO J. 56:279-84, 2010.

12- Guyton, A. C., Textbook of medical physiology. 2d ed.; W. B. Saunders Co.: Philadelphia,, 1961; p 1181 p.

13. Feldman, R. L., W. W. Nichols, C. R. Conti,C. J. Pepine, Influence of acute aortic insufficiency on the hemodynamic importance of a coronary artery narrowing. II. Various magnitudes of aortic insufficiency. J Am Coll Cardiol. 1:1281-9, 1983.

14. Ardehali, A., J. Segal,M. D. Cheitlin, Coronary blood flow reserve in acute aortic regurgitation. J Am Coll Cardiol. 25:1387-92, 1995.

15. Folts, J. D., G. G. Rowe, D. R. Kahn,W. P. Young, Phasic changes in human right coronary blood flow before and after repair of aortic insufficiency. Am Heart J. 97:211-5, 1979.

CHAPTER 5

IMPACT OF THE TYPE OF SURGICAL PROCEDURE ON HYDRODYANAMIC PERFORMANCE OF PERICARDIAL BIOPROSTHESES.

These studies have been undertaken in collaboration with the following Institutions:

-Cardiovascular Surgery Depatment, "L. Sacco" Hospital, Università degli Studi di Milano, Milan, Italy.

-ForCardio.lab, Fondazione per la Ricerca in Cardiochirurgia ONLUS, Milan, Italy

-Cardiovascular Department, Cardiac Surgery Unit, Ospedale "A. Manzoni" ASST-Lecco. Lecco, Italy.

This Chapter is based upon the following papers:

-Tasca G, R. Vismara, G. B. Fiore, C. Romagnoni, A. Redaelli, C. Antona, A. Gamba. "Does the type of suture technique affect the fluidodynamic performance of bioprostheses implanted in small aortic roots? Results from an in vitro study". *J Thorac Cardiovasc Surg*. 2015;149:912-823.

-Tasca G, Vismara R, Mangini A, Romagnoni C, Contino M, Redaelli A, Fiore GB, Antona C. Comparison of the Performance of a Sutureless Bioprosthesis With Two Pericardial Stented Valves on Small Annuli: An In Vitro Study. *Ann Thorac Surg*. 2017 Jan;103(1):139-144.

Introduction and Aims

The *in vivo* fluid dynamic performance of a bioprosthesis, implanted in aortic position, is mainly affected by the size of the area that the valve provides to the flow. This area, in turn, is determinated by the structural characteristics of the prosthesis, such as stent design, type and position of the leaflets. Nevertheless, the valve implantation process, being complex, may compromise the intrinsic fluid dynamic valve properties. Hence, the area provided by the prosthesis depends also upon the manufacturer's sizing strategy (1), the surgeon's attitude and/or experience, and the aortic root characteristics (2,3).

There are patient specific anatomical factors which may further influence the pressure drop, such as the inflow morphology. In particular, the shape and size of left ventricular outflow tract (LVOT) as well the annulus-prosthesis interaction which are influenced by the suture technique (4). Clearly, a prosthesis that possesses an efficient design and an excellent intrinsic fluid-dynamic performance, tends to blunt the effects of a suboptimal valve size implantation and a possible obstructive suture.

The scenario is complex because there are several types of suture to be adopted when an aortic valve replacement is performed, and these are simple interrupted suture, semi-continuous suture and mattress suture with pledgets, in either everting or non-everting fashion.

On the potential fluid dynamic impact sutures, two recent studies (5,6) involving small size bioprostheses, i.e. with labeled sizes of 19 mm and 21 mm, came to completely opposite conclusions. Tabata et al. have reported that the use of a non-everting mattress suture technique with pledgets (MSP), on the ventricular side, compromise the prosthesis

performance resulting in a reduction of effective orifice area (EOA) when compared with the simple suture technique (SIS). Conversely, Ugur et al. did not find any impact, of the type of suture adopted, on bioprosthesis fluid dynamic performance. Nevertheless, these were retrospective and non-randomized clinical studies and, therefore, open to possible bias.

The way in which the suture might negatively impact on valve fluid dynamic performance, should stem from the changes in the LVOT anatomy, the housing of the prosthesis and the attitude of the surgeon in sizing the valve. Hence, even an excellent fluid dynamic performance, derived from an efficient bioprosthesis design, may be ruined when the valve is surgically implanted. This, in particular, may be critical in patients with a small aortic annulus, in whom the risk of developing high gradients (7,8) and patient-prosthesis mismatch (PPM) is higher, with possible negative impact on clinical outcomes (9-13).

A recent technological development has provided a type of bioprosthesis which can be implanted without the need of a surgical suture, offering advantages in terms of procedure simplification, shortening the cross-clamp time, and to eliminate the potential fluid dynamic disruption of the surgical suture. These valves are known as “Sutureless” and offer a promising evolution in the relentless development of biologic artificial heart valves. In particular, the sutureless Perceval valve (PV) (Sorin Group, Saluggia, Italy) was developed by mounting a pericardial “stentless” valve inside a very thin stent (14,16). The use of a stentless valve is a valuable feature because it allows to exploit at best its favourable fluid dynamic characteristics (17).

To address the potential role of the surgical strategy on the fluid dynamics of the

implanted valve, two experimental studies were undertaken. In the first, the fluid-dynamic performance of the valves surgically implanted, with two different surgical techniques, was compared with the aim to ascertain which of the two techniques tested was the most efficient. In the second test, the performance of a type of "sutureless" valve was tested and compared to both standard stented bioprostheses and native aortic valves. Indeed, being the "Sutureless" the ideal valve, from fluid dynamic standpoint, on account of the lack of the suture and the presence of a stentless valve, the results were compared with a native normal valve.

Materials and Methods

FoRcardioLab pulsatile mock loop

Figure 1 shows a scheme of the mock loop used in this experiment (18,19), which consisted of a computer-controlled volumetric pump able to replicate left ventricular flow waveforms, a sample test section designed to house a whole aortic root unit (ARU), and an adjustable hydraulic afterload mimicking the hydraulic input impedance of the systemic circulation. This mock loop was used for both the tests carried out.

In these experimental tests, the mock loop was instrumented with a transit-time flow-meter (HT100R, Transonic System Inc., Ithaca, NY), the 1" probe of which was placed downstream of the ARU sample, and with three pressure transducers (PC140 series, Honeywell Inc., Morristown, NJ): one immediately upstream and one immediately downstream of the sample (P_{ven} and P_{ao}, respectively, in Fig. 1), and the third at the inlet section of the hydraulic afterload. A high-speed digital camera (Phantom Miro2, Visionresearch, Morristown, NJ) was placed downstream of the sample so as to acquire

an aortic view of the working prostheses. In our tests we used saline solution (0.9% w/v NaCl). Data were acquired at 200 Hz via an A/D board (USB 6210, National Instrument, Austin, TX).

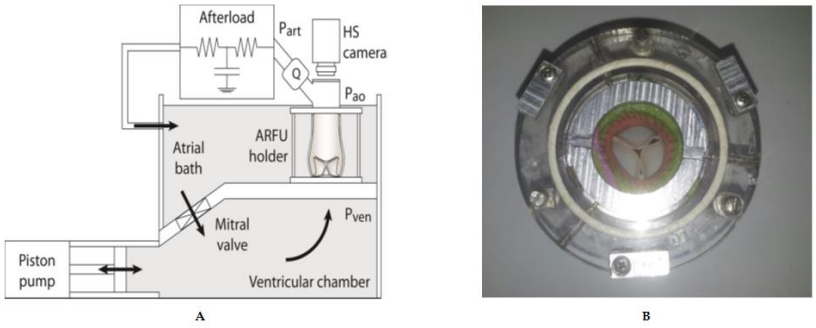

Fig. 1 shows A. the mock loop scheme and B a prosthesis implanted in the ARU housed in the holder.

Sample preparation and prosthesis sizing for the first test (type of suture comparison)

For this test we selected 10 fresh whole swine hearts with native aortic annuli of 19 mm (5 hearts) and 21 mm (5 hearts) measured by a metric probe. To replicate the operating room scenario, we used the probes and the valve replica provided by the manufacture in order to select the prosthesis size that could be comfortably implanted, with only slight forcing at the most. This approach was adopted because the porcine ascending aorta was extremely elastic, a feature that might have introduced a bias into prosthesis size selection. Indeed, oversizing was theoretically possible in the case of all valves, on account of the extreme elasticity of the ARU; in real case scenario, however, the stiffness of the aorta would have made this difficult, if not impossible. The ARU samples were then harvested by two experienced surgeons.

The samples included 1.5 cm of the left ventricular outflow tract, which was rendered cylindrical by closing the mitral valve commissures by means of a running suture to the adjacent muscular septum. The ascending aorta was transected 0.5 cm above the

sinotubular junction and the coronary ostia were ligated to prevent fluid loss. Circular Dacron meshes were sutured to the inflow and outflow of the aortic root sample, in order to fix it into the housing section of the mock loop, as previously described (12-14).

Experimental set-up for the first test (type of suture comparison)

Tests simulating physiologic conditions in patients at rest and under physical activity, were conducted on the mock loop. The stroke volume (SV) imposed by the pulsatile pump was set at 40 ml and increased by steps of 15 ml until an SV of 100 ml was attained. The systolic ejection time was set at ⅓ of the entire cardiac cycle, and the heart rate at 70 bpm, with a mean simulated arterial pressure of 80–104 mmHg.

After being excised and housed in the test section holder of the mock loop, the native leaflets were removed, and the bioprostheses (Trifecta. St.Jude. St. Paul. MN) were implanted by an experienced surgeon and tested in each sample. The size n. 19 prosthesis was implanted in each aortic root with an aortic annulus size of 19 mm; this procedure was performed twice: first with one type of suture technique and then with the other using from 9-10 sutures for the non-everting mattress suture with pledgest (MSP) and 16-17 for simple suture technique (SIS). In exactly the same way, the size n. 21 prosthesis was implanted twice in each aortic root with an aortic annulus size of 21 mm using from 12-14 sutures for MSP and 18-20 for SIS.

The first technique adopted to implant the bioprostheses was by a simple interrupted suture (SIS), whereby all stitches (Ethibond 2/0) were placed radially in the aortic annulus and then in the sewing ring of the prosthesis. The second technique adopted was a non-everting mattress suture (Ethibond 2/0) with pledgets (MSP) on the ventricular side (Fig.2)

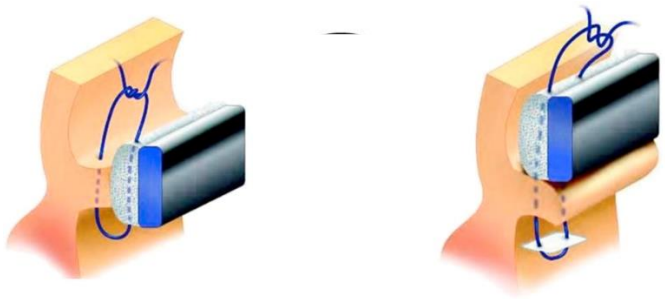

Fig.2 LEFT. Simple Suture technique (SIS). RIGHT. non-everting Mattress Suture with Pledgest (MSP)

The sequence of the type of suture to use, in each aortic root, was randomized.

After implantation, and prior to testing in the mock loop, each prosthesis was visually inspected via the digital video, in order to qualitatively assess its integrity and proper functioning. No prosthesis needed to be discarded during the entire experiment.

For each point, experimental data were evaluated over 5 consecutive simulated heart cycles.

The flow rate, the pressures upstream and downstream of the aortic root, and the pressure in the afterload were acquired via the A/D acquisition board. Post-processing of the raw data was performed to calculate the following quantities:

- The mean systolic pressure drop (Δpm, mmHg) across the ARU, as the difference between pressures measured at p_{ven} and p_{ao} (Fig. 1A) averaged over the systolic interval.
- The maximum systolic pressure drop (ΔpM, mmHg).
- The effective orifice area (EOA) cm2, calculated from the following formula:

$$EOA = \frac{Q_{rms}}{3.1\sqrt{\Delta P_{mean}}}$$

where Qrms (L/min) is the mean square root of the systolic flow rate, Δpm (mmHg) the mean systolic pressure drop across the sample and k a conversion factor (k = 3.1 to yield the EOA in cm^2).

Sample preparation and prosthesis sizing for the second test (with sutureless)

The same mock loop of the above experiment was used in this study as already described in detail.

Sample preparation and prostheses sizing for the second test

Twelve fresh whole swine hearts were selected, 6 samples with a native aortic annulus measuring 21 mm and 6 with an annulus measuring 19 mm. The native aortic annuli were measured with a metric probe.

To replicate the operating theatre setting, the prosthesis sizing was performed using the probes provided by the manufacturer of each prosthesis on the 12 whole porcine hearts, in order to select a prosthesis that fit the ARU according to the standard operating procedure.

The probes that fitted the Magna (Edwards Lifescience. Irvine. CA) valve had the label size of 19 for annuli measuring 19 mm, and 21 for those measuring 21 mm. Corresponding labels for the Crown (Sorin group. Saluggia. Italy) valve were 21 and 23, respectively. For the Perceval valve (Sorin group. Saluggia. Italy), the label sizes were selected according to the manufactures guidelines that corresponded to the “small” (for 19 mm) and “medium” (for 21 mm) aortic annulus diameters.

The ARU samples were harvested by two experienced surgeons and prepared as described previously.

Experimental design for the second test (Sutureless)

Tests were conducted by setting the pump at stroke volumes of 25 ml, 40 ml, 60 ml and 70 ml, 90 ml and 105 ml. The systolic ejection time was set at one third of the entire cardiac cycle, and the heart rate at 70 beats per minute, with a mean simulated arterial pressure ranging from 80 mmHg to 104 mmHg.

After housing each ARU sample in the test-section holder and testing it for basal points, the three bioprostheses were implanted in a randomized sequence and data were acquired. For each experimental point, data were evaluated over 5 consecutive simulated heart cycles.

The CR and MG valves were implanted by means of a continuous suture technique using polypropylene (2/0) (Premilene 2/0 B Braun, Surgical SA, Barcellona, Spain).

After each implantation, and prior to testing in the mock loop, the prostheses were visually inspected via the digital video in working conditions, qualitatively assessing their integrity and correct functioning.

The flow rate, the pressures upstream from and downstream of the aortic root, and the pressure in the afterload, were acquired.

The following measurements were obtained through post-processing the raw data: Mean systolic pressure drop (Δp_m, mmHg) across the ARU, evaluated as the difference between the pressures measured upstream from and downstream of the prosthesis, averaged over the systolic interval.

- Effective orifice area (EOA, cm^2) calculated from the following formula:

$$EOA(cm^2) = \frac{Q_{rms}}{k\sqrt{\Delta p_m}}$$

where Q_{rms} (L/min) is the root mean square systolic flow rate, Δp_m (mmHg) the mean systolic pressure drop across the sample, and k a conversion factor (k = 3.1 to yield the EOA in cm^2).

- Systolic energy loss (mJ): the amount of the energy provided by the pump in the systole that is lost when the fluid passes through the prosthesis.

Statistical analysis

In the first test, the mean and peak pressure drops and EOA were analyzed by means of paired t-test with Bonferroni's correction.

In the second test, the continuous variables were compared using analysis of variance (ANOVA) for repeated measures, with the Bonferroni correction in post-hoc analysis. Values are reported with 95% confidence intervals.

For both tests the continuous variables were expressed as mean values ± standard deviation and the p values < 0.05 were considered significant. The data were analyzed by means of SPSS 17 (SPSS Inc. Chicago, IL).

Results

Results from the first experimental test

In 9 of the 10 aortic roots tested, the MSP technique was associated to a higher gradient and smaller EOA than the SIS technique. The only 1 aortic root tested in which the bioprosthesis implanted with the MSP technique performed better than that implanted with the SIS technique had a 21 mm native aortic annulus and showed a negligible difference in mean pressure drop: -0.77 mmHg, +0.08 mmHg, -0.26 mmHg, -1.17 mmHg and -1.15 mmHg at 40 ml, 55 ml, 70 ml, 85 ml and 100 ml, respectively. As for the EOA, the differences were +0.91 cm^2, -0.11cm^2, +0.02 cm^2, +0.06 cm^2 and +0.01 cm^2 at 40 ml,

55 ml, 70 ml, 85 ml and 100 ml, respectively.

In the whole sample, the mean and peak pressure drops were higher when the MSP technique was used than when SIS was used (see Table 1 and Fig. 3), the differences being statistically significant at each level of SV, except for the peak pressure drop at 70 ml (p=0.10) (Table 1).

The EOA behaved accordingly, being lower at all SV levels in bioprostheses implanted with the MSP technique; the difference was statistically significant at all SV levels except 40 ml (p=0.9) (Table 1).

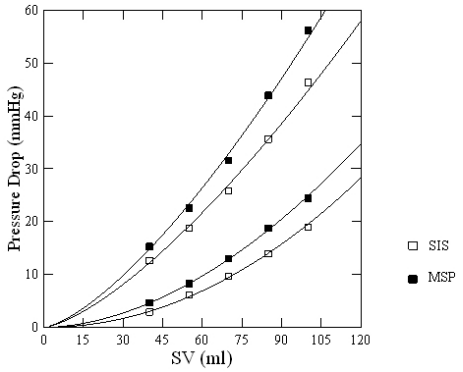

Fig. 3 Mean (lower curves) and Peak (upper curves) pressure drop at each level of stroke volume. (SIS=Simple Interrupted Suture, MSP= non-everting Mattress Suture with Pledgets)

Table 1. Experimental Results

EOA= Effective orifice area

Entire population	Type of Suture	SV 40	SV 55	SV 70	SV 85	SV 100
Mean Pressure Drop (mmHg)	**SIS**	2.93±1.4	6.11±2.8	9.7±4.2	13.9±5.5	19.0±7.1
	MSP	4.60±2.4	8.25±3.9	13.0±5.6	18.8±7.6	24.4±9.3
p-value		p=0.036	p=0.06	p=0.01	p=0.008	p=0.007
Peak Pressure Drop (mmHg)	**SIS**	12.6±2.2	18.8±4.4	25.8±6.2	35.6±9.9	46.3±13.1
	MSP	15.3±3.4	22.6±5.5	31.6±9.8	43.9±14.3	56.2±16.8
p-value		p=0.05	p=0.04	p=0.10	p=0.017	p=0.01
EOA (cm^2)	**SIS**	2.04±0.61	1.95±0.54	1.91±0.39	1.90±0.35	1.88±0.35
	MSP	1.83±0.85	1.68±0.44	1.65±0.38	1.65±0.37	1.65±0.32
p-value		p=0.9	p=0.016	p=0.006	p=0.022	p=0.021
Size 19						
Mean Pressure Drop (mmHg)	**SIS**	4.0±1.0	8.1±2.2	12.9±3.2	17.9±4.6	24.3±5.4
	MSP	6.4±1.3	11.0±3.4	17.1±4.4	24.3±5.8	31.0±6.8
P-value		p=0.007	p=0.48	p=0.17	p=0.05	p=0.028
Peak Pressure Drop (mmHg)	**SIS**	14.5±0.9	23.3±2.7	30.1±3.5	43.0±7.8	56.2±8.6
	MSP	17.5±2.8	26.3±4.5	38.2±8.7	53.8±12.5	67.5±14.4
p-value		p=0.63	p=0.51	p=0.72	p=0.32	p=0.24
EOA (cm^2)	**SIS**	1.59±0.27	1.61±0.17	1.59±0.14	1.64±0.17	1.62±0.13
	MSP	1.28±0.16	1.36±0.16	1.36±0.15	1.38±0.13	1.41±0.15
p-value		p=0.27	p=0.20	p=0.11	p=0.14	p=0.07
Size 21						
Mean Pressure Drop (mmHg)	**SIS**	1.90±0.76	4.13±1.7	6.54±1.9	9.9±2.5	13.8±4.0
	MSP	2.84±1.8	5.47±2.15	8.96±3.2	13.3±4.6	17.8±6.5
p-value		p=0.98	p=0.33	p=0.58	p=0.69	p=0.76
Peak Pressure Drop (mmHg)	**SIS**	10.68±1.0	15.3±2.5	20.7±3.2	28.3±5.3	36.4±8.5
	MSP	13.0±2.3	18.8±3.4	25.0±5.7	34.0±7.6	44.9±10.3
p-value		p=0.64	p=0.21	p=0.44	p=0.21	p=0.54
EOA (cm^2)	**SIS**	2.50±0.5	2.28±0.5	2.22±0.3	2.16±0.3	2.14±0.3
	MSP	2.38±0.9	2.0±0.4	1.94±0.3	1.92±0.3	1.90±0.3
p-value		p=0.99	p=0.63	p=0.43	p=0.80	p=0.75

Analysis of the 2 subgroups, i.e. aortic annulus size of 19 mm and 21 mm, showed a clear trend toward higher mean and peak pressure drops for MSP than SIS in both groups; this difference increased as SV rose (Fig.4). In the 19 mm group, the difference in mean pressure drop was +3.0±1.5 mmHg, +3.0±2.0 mmHg, +4.2±2.0 mmHg, +6.4±2.1 mmHg, and +6.8±1.9 mmHg at SV values of 40 ml, 55 ml, 70 ml, 85 ml and 100 ml, respectively, in valves implanted with the MPS technique in comparison with those implanted with the SIS technique. These differences in mean pressure drop were either statistically significant or close to significance at SV levels of 40 ml, 85 ml and 100 ml (see Table 1). The EOA behaved accordingly, the difference being close to statistical significance (p=0.07) at an SV level of 100 ml.

In the 21 mm group, too, a clear trend toward higher gradients emerged among valves implanted with the MSP technique (see Table 1 and Figure 3). Both mean and peak pressure drops were greater, the difference in mean pressure drop being +0.9±1.3 mmHg, +1.3±0.8 mmHg, +2.5±1.8 mmHg, +3.5±2.8 mmHg, and +3.9±3.5 mmHg at SV levels of 40 ml, 55 ml, 70 ml, 85 ml and 100 ml, respectively. Although appreciable, these differences did not, however, reach statistical significance. Again, the EOA behaved accordingly (Table 1).

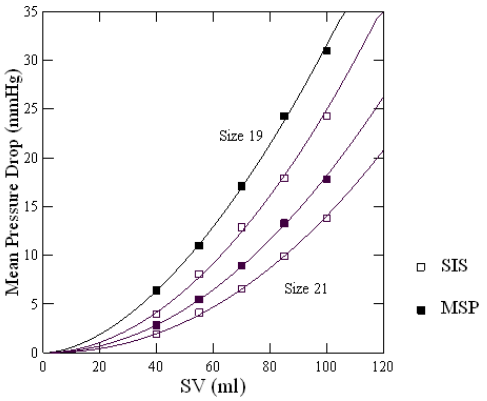

Fig. 4 Mean pressure drops according to prosthesis size (19 and 21) and type of suture adopted. (SIS=Simple Interrupted Suture, MSP= non-everting Mattress Suture with pledgets)

Results from the second experimental test

None of the valves displayed significant structural problems in any of the test sessions and none had to be discarded. Energy loss (Table 2) and mean pressure drop (Figure 5 and 5) increased with stroke volume in all the valves tested.

The PV valve showed lower values compared with the two standard prostheses (Table 2 and Figure 5 and 6). The differences were greater when the data from the subgroup implanted in the 19 mm aortic annulus size were analyzed (Table 2 and Figure 5). The EOA values were stable across the stroke volume interval and were in accordance with the pressure drop. The PV valve showed the greatest value for EOA (Table 2 and Figure 5 and 6). The two standard bioprostheses showed similar fluid dynamics, with the CR valve exhibiting a slightly lower pressure drop and larger EOA, but without statistical significance (Table 2, Fig. 5 and 6).

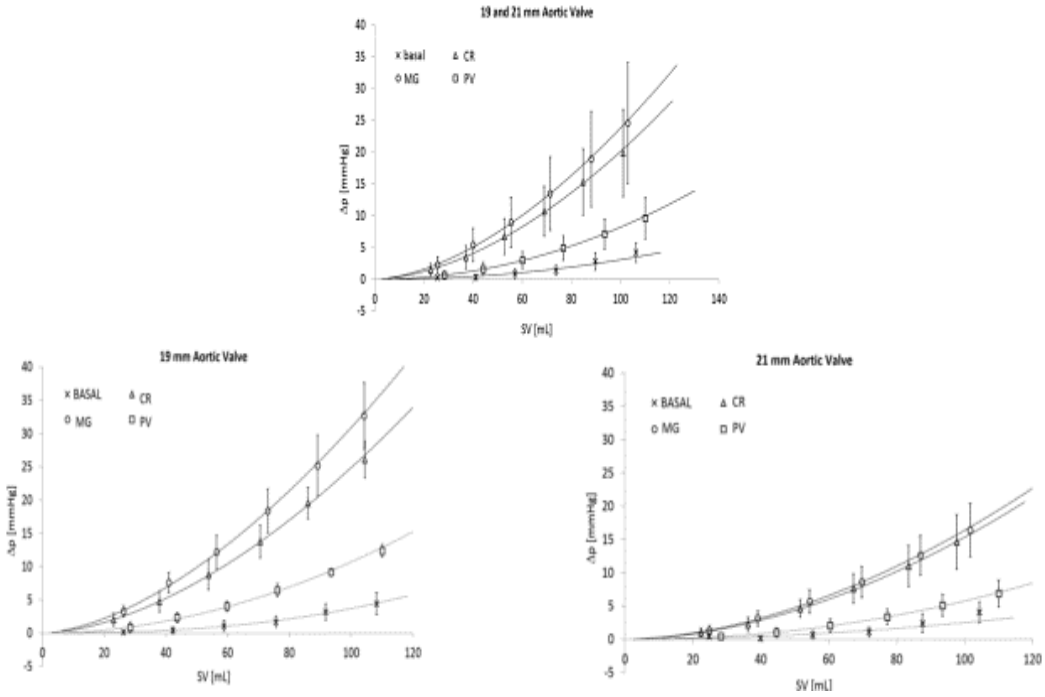

Fig. 5 Mean pressure drops for 19 mm and for 21 mm aortic valves. CR=Crown valve; MG=Magna valve; PV=Perceval valve.

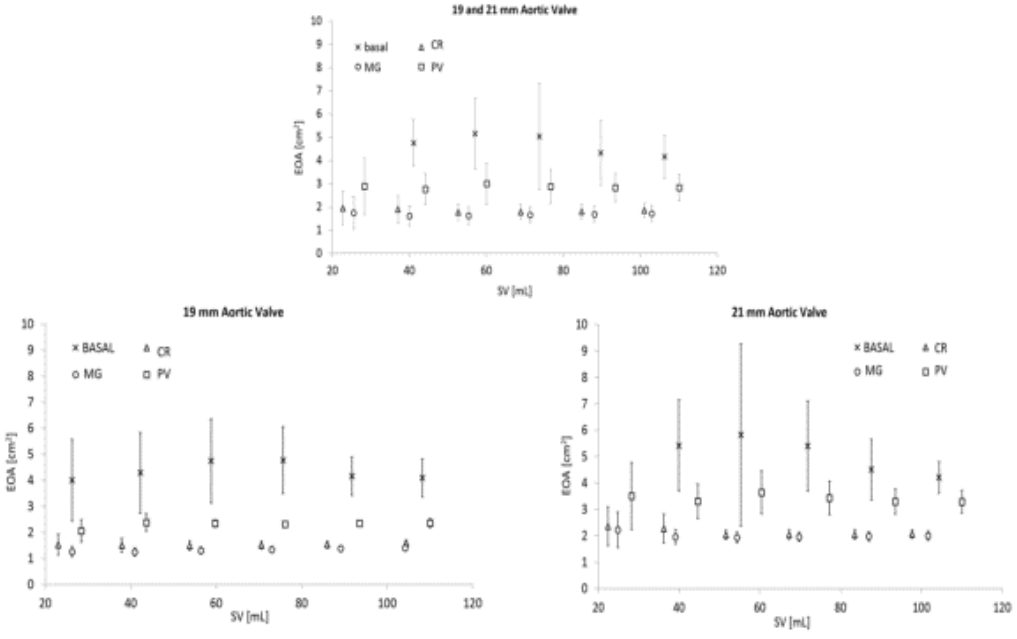

Figure 6. Mean effective orifice area for 19 mm and for 21 mm aortic valves. CR=Crown valve; MG=Magna valve; PV=Perceval valve.

Table 2. Hydrodynamic results according to annulus size

Stroke volumes						Effect	p-value
25 ml	**40 ml**	**60 ml**	**70 ml**	**90 ml**	**105 ml**		
2.0±0.95	4.7±1.5	8.8±2.3	13.8±2.5	19.5±2.3	26.1±2.7	Valve	<0.001
3.3±0.82	7.6±1.5	12.2±2.5	18.4±3.3	25.2±4.6	32.7±5.0	Time (SV)	<0.001
0.86±0.8	2.3±0.8	4.0±0.7	6.4±0.96	9.1±0.5	12.4±0.94	Interaction	<0.001
8±4	31±11	83±26	173±37	295±46	481±51	Valve	<0.001
15±2	54±9	123±27	237±44	396±79	601±98	Time (SV)	<0.001
5±4	18±6	43±8	87±13	152±13	237±14	Interaction	<0.001
1.52±0.4	1.50±0.27	1.49±0.19	1.51±0.15	1.53±0.14	1.59±0.12	Valve	<0.001
1.26±0.20	1.25±0.15	1.30±0.13	1.33±0.12	1.38±0.12	1.40±0.13	Time (SV)	<0.001
2.05±0.43	2.38±0.34	2.34±0.14	2.32±0.11	2.35±0.10	2.36±0.17	Interaction	<0.001
1.0±0.64	2.2±1.1	4.6±1.3	7.6±2.2	11.0±3.1	14.6±4.1	Valve	<0.001
1.3±0.75	3.2±1.1	5.7±1.7	8.6±2.3	12.6±3.0	16.4±4.0	Time (SV)	<0.001
0.41±0.38	1.01±0.70	2.03±1.02	3.36±1.16	5.1±1.64	6.87±2.01	Interaction	<0.001
4±3	14±7	43±14	92±32	168±62	261±91	Valve	<0.001
6±2	23±8	57±20	103±36	195±53	298±82	Time (SV)	<0.001
2±3	8±6	22±11	48±19	83±29	130±43	Interaction	<0.001
2.36±0.74	2.28±0.54	2.04±0.17	2.05±0.18	2.05±0.18	2.07±0.16	Valve	<0.001
2.23±0.67	1.96±0.28	1.94±0.20	1.96±0.17	1.96±0.18	2.00±0.17	Time (SV)	<0.001
3.50±1.27	3.31±0.65	3.65±0.81	3.43±0.63	3.30±0.47	3.29±0.43	Interaction	<0.001

EOA= effective orifice area. CR= Crown Valve, MG= Magna Valve, PV= Perceval Valve.

Discussion

Fluid dynamic performance of an aortic bioprosthesis depends mainly upon the size of the geometric area provided to the flow, albeit only a portion of this area is used by the flow as effective orifice area. This geometric area is, in turn, related to the internal diameter of the prosthesis and to the leaflet aperture according to the nature and position of the leaflets as well as the design of the stent. Nevertheless, as showed by the results of this experiment, the surgical technique used for the implant can undermine the valve performance. In particular, the adoption of the MSP technique may yield a higher pressure drops than the SIS technique when the valves are implanted in small annuli. Nevertheless, adopting a surgical strategy whereby the valve is implanted without the need of a surgical suture, i.e. by implanting a "sutureless" valve, the fluid dynamic result is not only better compared with that of a standard valve implantation, but it may be close to the native aortic valve performance. This is of utmost importance in patients with small aortic annuli, who are at risk of high residual gradients.

Interpretation of the results of the first experimental test

In 9 out of 10 experimental comparisons, we observed a greater pressure drop and a smaller EOA in the MSP group than in the SIS group, in a range of SV values from 40 ml to 100 ml (Table 1). The EOA behaved accordingly, being smaller for the MSP technique at each SV level; these differences were statistically significant, except at the SV of 40 ml.

Doppler gradient across the prosthesis is mainly dependent on both SV and EOA, while left ventricular ejection time plays a minor role, at least at physiologic heart rate (17). The

EOA is related to the geometric orifice area, which is in turn, is related to the internal diameter of the prosthesis and the area provided the leaflets when the valve is full opened. Thus, for a given size of prosthesis, a high gradient is present when there is a mismatch between EOA and SV. This mismatch is typically present either when the SV increases, such as during physical activity, or at rest when the SV is too high for the implant size, i.e. as in PPM. However, as expected, the differences we found between the two groups were small, at least at those SV values that corresponded either to the rest condition or were consistent with mild PPM, i.e. ≤ 70 ml, for the sizes used in this experiment. Thus, it is likely that, in the clinical scenario, the difference would be negligible in most cases. Indeed, a clinical effect, such on hypertrophy regression, may be seen when the difference in mean gradient is at least 4 mmHg (13,20). Nevertheless, when the SV increases, as during physical activity or in the case of moderate PPM, the difference might be clinically relevant.

Difference between annulus sizes

The results suggested that the type of suture technique may be relevant in annuli ≤21 mm. Indeed, as can be seen in Table 1, in the 19 mm group the mean pressure drop was markedly greater in the MSP group technique than in those in the SIS technique: +3.0±1.5 mmHg, +3.0±2.0 mmHg, +4.2±2.0 mmHg, +6.4±2.1 mmHg, and +6.8±1.9 mmHg at SV levels of 40 ml, 55 ml, 70 ml, 85 ml and 100 ml, respectively. However, when the aortic annulus size was 21 mm, the difference in pressure drop was smaller and not statistically significant. Nevertheless, there was still a clear trend toward greater pressure drop among valves implanted with the MSP technique: +0.9±1.3 mmHg, +1.3±0.8 mmHg, +2.5±1.8 mmHg, +3.5±2.8 mmHg, and +3.9±3.5 mmHg at SV levels of 40 ml, 55 ml, 70 ml, 85 ml

and 100 ml, respectively. It is reasonable to assume that the encumbrance, due to the pledgets and the tissue gathered underneath the valve, is the same whatever the internal diameter of the prosthesis is. Therefore, the smaller the internal diameter, the greater the percent reduction in the geometric orifice area due to the pledgeted tissue protruding into the area available for the flow, leading to a more significant effects on pressure drops in smaller annuli. This suggests that, in the case of small annuli, the safety margin on which the surgeon can rely to avoid performing a potentially obstructive suture is reduced. Hence, it can be hypothesized that, *in vivo* as well, in small annuli the simple suture may help to optimize the hemodynamics of a bioprosthesis, thereby reducing the incidence, or the degree of PPM.

Potential mechanisms of flow obstruction in the MSP technique

When a non-everting mattress suture with pledgets is used, the main mechanism involved in reducing prosthesis performance appears to be that of LVOT shrinkage as tissue is gathered underneath the prosthesis (Fig. 7).

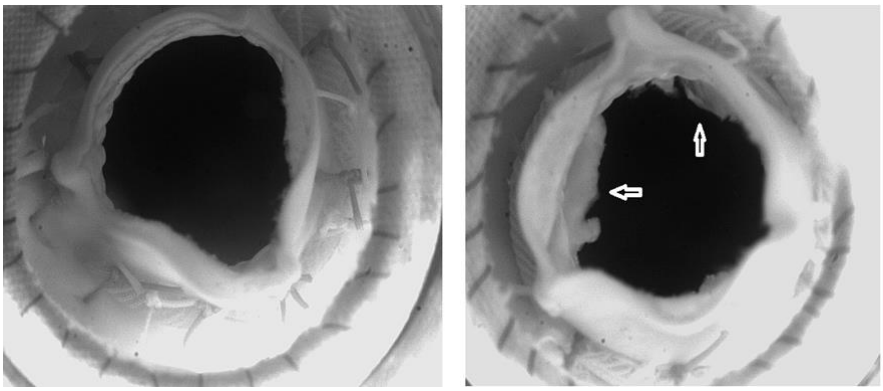

Fig. 7 Left. A 21-size prosthesis implanted with SIS. Right: the same prosthesis implanted with MSP suture. Arrows point to the tissue gathered underneath the valve.

However, flow may also be obstructed when the bioprosthesis is implanted in a tilted position, still due to the reduction in the LVOT diameter. Another, but less apparent, mechanism concerns the size chosen by the surgeon (i.e. ineffective sizing) because, being aware of the annulus shrinkage due to the suture, the surgeon may be prompted to select a smaller size to house the prosthesis inside the aortic root more safely and without tilting it. This mechanism may partly explain the results of the retrospective study by Tabata et al., in which the MSP group displayed a smaller EOA and a higher incidence of PPM. Indeed, the MSP group in that study had a larger aortic annulus and a lower prosthesis-annulus size ratio, revealing the propensity of the surgeon to implant a larger valve when using a simple interrupted suture than when using the non-everting mattress suture with pledgets. With a lower prosthesis-annulus size ratio, it is possible that more tissue may be gathered underneath the prosthesis, obstructing the LVOT flow. That issue was avoided in the current experiment because the same prosthesis was implanted by both suture techniques, in the same aortic root anatomy. Moreover, several variables were kept constant: the surgeon and the amount of SV increment. These conditions are almost impossible to obtain in clinical studies, especially in non-randomized ones, thus making it very difficult to investigate the effect of the suture technique on bioprosthesis performance. This may explain why Ugur et al. (6) found neither a significant difference nor a difference in trend in their study on using the same prostheses used in this experiment. Besides, we do not know anything about the sizing.

The study by Ugur et al. was conducted on echocardiographic data collected after 1 year. It is possible that the initial tissue gathered underneath the valve might has remodeled over time and that the initial obstruction might has decreased. In this regard, the data from

Tabata et al. showed a trend supporting this assumption (5).

The results of this experimental test support the hypothesis that the simple interrupted suture is an effective technique that contributes to optimizing hemodynamic results. Besides, these data corroborate a clinical study on patients with small aortic annuli (average native aortic annulus of 21 mm), in whom the Trifecta bioprosthesis was implanted by means of with the SIS technique. In that randomized study, a very low mean gradient of 5.5 mmHg and a PPM incidence of only 15% were found on discharge (21). These hemodynamic results were similar to those obtained using a stentless bioprosthesis.

Interpretation of the results of the second experimental test

The results of this experimental study suggest that the sutureless PV valve has overcome some of the typical limitations of stented valves such the need of the surgical suture. This has brought about an excellent fluid dynamic performance even for the smallest annulus diameter with mean pressure drops ranging from 2 mmHg to 4 mmHg at physiologic stroke volumes for a 1.9 cm native aortic annulus (i.e. 40 ml and 60 ml, respectively). The presence of the very thin stent, in which the pericardial leaflets are not strictly bonded, allowed the valve to function as a stentless. Moreover, being an expandable prosthesis, it can adapt the size of its internal diameter, to a certain extent, to that of the ventricular-arterial junction, with potentially a benefit in terms of fluid-dynamics. In contrast, a standard stented valve has a fixed internal diameter, specific for each type and size of valve. Besides, the inflow shape and prosthesis/annulus interaction in the PV valve avoids any abrupt geometrical discontinuity between the LVOT/native annulus and the prosthesis ring, guiding the flow from the LVOT into the valve, with less flow disturbance and reduced loss of mechanical energy compared with a classic stented prosthesis.

On account of its structural characteristics and the standardized sizing strategy, the sutureless valve provides a more reproducible and thus less surgeon-dependent fluid-dynamic performance, as illustrated by the narrow confidence intervals shown in Figures 5 and 6.

The PV valve is an interesting evolution in the field of bioprostheses and possesses the fluid-dynamic characteristics of a stentless valve, because the leaflets are not firmly bounded to a stiff, bulky stent. Instead, the stent is thin, leaving the leaflets to move freely, resulting in pressure drop as low as the transcatheter aortic valves (15) and consequently a lower incidence of patient-prosthesis mismatch, even in small aortic annuli, avoiding its potential negative clinical consequences (10-13).

The CR valve has structural characteristics that are similar to its predecessor (i.e. the Mitroflow). Aware of the conservative sizing strategy reported for the Mitroflow (22) valve and the misleading effect of the labeled size on valve comparison and selection, in the study the bioprostheses were compared according to their corresponding aortic annulus size. In the 19 mm aortic root, both CR 21 (External Diameter=24 mm) and Magna 19 (External Diameter=24 mm) fit the aortic annulus size and were then implanted and compared. Thus, it was not tested a CR valve with a labeled size of 19, which fits a native annulus with a diameter of < 19 mm. CR 19 should be used only in rare cases (i.e. in <1 % of patients) with an annulus size of ≤ 18 mm (2,23).

These experimental findings showed that the CR valve performed slightly better than the MG valve, with a greater difference with the 19 mm annulus size. Even though, the internal diameter of the CR valve is smaller than that of the MG valve, its lower gradient may be explained by the presence of the pericardium outside the stent posts, which allows

optimal exploitation of the internal diameter area. The MG bioprosthesis represents a point of reference in the bioprosthesis field, because it is the evolution of a valve that has shown excellent durability. In this study, as expected, it provided a good fluid-dynamic performance.

Comment on the results of both studies

The results of these two in-vitro studies, outlines the detrimental fluid-dynamic effects of the type of suture adopted for bioprosthesis implantation especially in small annuli ≤ 21 mm. Thus, to optimize the prosthesis performance in small annulus and reduce the incidence of patient-prosthesis mismatch, the role of the suture technique should not be neglected. One of the valid options to decrease drastically the fluid dynamic perturbation owing to the suture, is to implant a sutureless bioprosthesis. This type of valve provides the lowest pressure drop and somewhat close to the performance of a native aortic valve. Thus, the approach with the use of a "sutureless" valve represents an interesting evolution in the bioprostheses field.

Study limitations

The internal diameter of the sutureless valve used in this study adapts to the size of the native annulus. Because we implanted this valve in an isolated aortic root without the surrounding tissues that are present in a whole heart, the internal diameter may have been larger than that in the true heart, producing a lower pressure drop than expected.

Bibliography

1-Doenst T, Amorim PA, Al-Alam N, Lehmann S, Mukherjee C, Faerber G. Where is the common sense in aortic valve replacement? A review of hemodynamics and sizing of stented tissue valves. J Thorac Cardiovasc Surg 2011;142:1180-7.

2-Ruzicka DJ, Hettich I, Hutter A, et al. The complete supraannular concept: in vivo hemodynamics of bovine and porcine aortic bioprostheses. Circulation. 2009;120(11 Suppl):S139-45.

2- Von Oppell UO, Segadal L, Busund R, et al. Aortic annulus diameter and valve design each determine the valve size implanted. J Heart Valve Dis. 2012;21(5):591

4-Sievers HH. Prosthetic aortic valve replacement. J Thorac Cardiovasc Surg. 2005;129: 961-965.

5- Tabata M, Shibayama K, Watanabe H, Sato Y, Fukui T, Takanashi S. Simple interrupted su-turing increases valve performance after aortic valve replacement with a small supra-annular bi-oprosthesis. J Thorac Cardiovasc Surg. 2014;147:321-325.

6- Ugur M, Byrne JG, Bavaria JE, Cheung A, Petracek M, Groh MA, Suri RM, Borger MA, Schaff HV. Suture technique does not affect hemodynamic performance of Trifecta biopros-thesis. J Thorac Cardiovasc Surg. 2014;12:1-5.

7- Suri RM, Zehr KJ, Sundt III TM, Dearani JA, Daly RC, Oh JK, Schaff HV. Left Ventricular Mass Regression After Porcine Versus Bovine Aortic Valve Replacement: A Randomized Comparison, Ann Thorac Surg 2009;88:1232–7.

8- Tasca G, Brunelli F, Cirillo M, Dalla Tomba M, Magna Z, Troie G, Quaini E. Mass regression in aortic stenosis after valve replacement with small size pericardial bioprosthesis. Ann of Thorac Surg 2003;76,4:1107-1113.

9- Blais C, Dumesnil JG, Baillot R, Simard S, Doyle D, Pibarot P. Impact of prosthesis-patient mismatch on short-term mortality after aortic valve replacement. Circulation. 2003;108:983–988.

10- Tasca G, Mhagna Z, Perotti S, Berra Centurini P, Sabatini T, Amaducci A, Brunelli F, Cirillo M, Dalla Tomba M, Quiani E, Troise G, Pibarot P. Impact of Prosthesis-Patient Mismatch on Cardiac Events and Midterm Mortality After Aortic Valve Replacement in Patients With Pure Aortic Stenosis. Circulation. 2006;113:570-576.

11- Ruel M, Rubens FD, Masters RG, Pipe AL, Bedard P, Hendry PJ, Lam BK, Burwash IG, Goldstein WG, Brais MP, Keon WJ, Mesana TG. Late incidence and predictors of persistent or recurrent heart failure in patients with aortic prosthetic valves. J Thorac Cardiovasc Surg. 2004;127: 149–159.

12- Mohty D, Dumesnil JG, Echahidi N, Mathieu P, Dagenais P, Voisine P, Pibarot P. Impact of Prosthesis-Patient Mismatch on Long-Term Survival After Aortic Valve Replacement: Influence of Age, Obesity, and Left Ventricular Dysfunction. J Am Coll of Cardiol. 2009; 53: 39-47.

13-Tasca G, Brunelli F, Cirillo M, et al. Impact of Valve Prosthesis-Patient Mismatch on Left Ventricular Mass Regression Following Aortic Valve Replacement. Ann Thorac Surg. 2005;79(2):505-510.

14- Santarpino G, Pfeiffer S, Concistrè G, Fischlein T. Perceval sutureless aortic valve prosthesis: easy, fast, and safe. Innovations (Phila). 2011;6(6):378-381.

15- D'Onofrio A, Messina A, Lorusso R, et al. Sutureless aortic valve replacement as an alternative treatment for patients belonging to the 'gray zone' between transcatheter aortic valve implantation and conventional surgery: a propensity-matched, multicenter analysis. J Thorac Cardiovasc Surg. 2012;144(5):1010-1016.

16-Santarpino G, Pfeiffer S, Schmidt J, Concistrè G, Fischlein T. Sutureless aortic valve replacement: First-year single-center experience. Annals of Thoracic Surgery. 2012:504-509.

17- Cheng D, Pepper J, Martin J, Stanbridge R, Ferdinand FD., Jamieson, WRE, Stelzer P, Berg G, Sani G. Stentless Versus Stented Bioprosthetic Aortic Valves: A Systematic Review and Meta-Analysis of Controlled Trials. Innovations: Technology & Techniques in Cardiothoracic & Vascular Surgery. 2009;4(2):61-73.

18- Vismara R, Leopaldi AM, Mangini A, Romagnoni C, Contino M, Antona C, Fiore GB. In vitro study of the aortic interleaflet triangle reshaping. J Biomech. 2014;47(2):329–333.

19- Vismara R, Mangini A, Romagnoni C, Contino M, Redaelli A, Fiore GB, Antona C. In vitro study of a quadricuspid aortic valve J Heart Valve Dis. 2014;23(1):122-6.

20- Kendler K, Moller CH, Hassager C, Olsen PS, Lilleor N, Steinbruchel DA. Patient-Prosthesis Mismatch and reduction in left ventricular mass after aortic valve replacement. Ann Thorac Surg. 2013;96(1):66-71.

21-20- Tasca G, Martino AS, Giannico F, Lobiati E, Riva B, Galanti A, Triggiani M, Gamba A. Early hemodynamic evaluation of Trifecta and Freestyle bioprostheses in patients with a small aortic root. Preliminary results from a prospective randomized study. J Heart Valve Dis. 2015.

22-Diab M, Faerber G, Botheh W, et al. Sizing strategy is a major determinant of postoperative pressure gradients in commonly implanted stented tissue valves. Eur J Cardio-thoracic Surg. 2013;44.

23- von Oppell UO, Segadal L, Busund R, et al. Aortic annulus diameter and valve design each determine the valve size implanted. J Heart Valve Dis. 2012;21(5):591-598.

CHAPTER 6

Conclusive Considerations

In the present research project, the bioengineering approach has allowed to describe what the biomechanics of an implanted heart valve is constituted of. It is evident that, besides the macroscopic structural characteristics of a device, many other aspects are to be considered when the impact of its performance on patients is to be assessed. Thus, an in-depth knowledge of the devices themselves as well as of their impact on the surrounding biological structures are of paramount importance for their best use. The acquisition of this knowledge, may bring about to a change in the clinical perspective, allowing the physicians to fulfil the medical deeds with more discernment.

Cardiac surgery is no longer in its pioneering era and the aortic valve replacement has become to a such standardized procedure that the current operative mortality is ≤ 1% in patients with age <70 years. Concomitant technological improvement of the devices and refinement of the technical skills of surgeons are at the base of such an achievement. Concerning the technological advancement, in the recent years, there has been a considerable acceleration in the technological evolution in the cardiovascular field, yielding a sheer number of new devices and therapeutic approaches. In particular, the advent of the transcatheter approach (transcatheter aortic valve implantation or TAVI), has imposed a change of paradigm, making the cardiac surgery obsolete for some patients. Unfortunately, the technological evolution has been so relentless and overwhelming that the sophisticated devices created have features which are not well understood and

exploited by the physicians. On account of the complex nature of the technology involved, too many physicians have turned their attention and efforts in developing only their technical skills, becoming mere executors with the ultimate consequence of losing the therapeutic role of the medical deed. In this regard, the formula “in scientia et coscientia” which recitation is performed on the day of the graduation of any medical doctor, allude to the relationship between science and consciousness in the decision-making process and implies professional credibility and responsibility. To hold the meaning of the formula nowadays, in this time of relentless technological advancement, it is required a change in the attitude on the physician part. Thus, for specialists of any disciplines and for those in the cardiovascular field in particular, it should be required, in addition to the acquisition of the technical skills, a knowledge of the principles that lay at the foundation of the new technologies as well as their impact upon the physiological context, i.e. the patient, where are these devices are inserted. That means that, in the context of the cardiovascular field, it is important to know and understand the structural characteristics of a device (design and materials), its functional performance (fluid dynamics and biomechanics) and the identification of the effect of the specific patient context on the performance of the prosthesis itself as well as the perturbation on the local physiology caused by the device itself. For this to happen, it is necessary a cultural shift in the “cursus studiorum” of physicians avoiding exposing them only to strictly medical disciplines.

In this perspective, considering that the transcatheter approach as well as any new devices, are spreading with a dramatic speed, physicians should either be exposed much more to bioengineering discipline, during the courses of Medicine and Surgery, or during the

residency programs envisioning novel classes in which medicine and bioengineering are merged.

The variable considered as crucial to improve patient survival, in the context of the treatment of aortic valve pathology, is the fluid dynamic performance of the implanted device. Unfortunately, the fluid dynamic result of an implanted valve depends upon many factors, such as prosthesis design and materials (Chapter 1), anatomical and physiological context in which it is implanted (Chapter 2), as well as the surgical strategy adopted for the implant (Chapter 4). Albeit the structural features of bioprostheses, from different manufactures, are often substantial (i.e. valve design and material adopted), the biomechanical differences are sometime subtle. However, an in-depth knowledge of each device characteristics should allow them to be exploited at best in order to provide a more patient tailored approach.

A potential negative impact on patient quality of life and survival, but as yet neglected, is the local coronary fluid dynamic interference due to the presence of an artificial device implanted in aortic root (Chapter 3). As mentioned, this aspect has been examined, in the presence research, by devising a specific experimental system that allowed to preliminary investigate the potential impact on the local fluid dynamics of a bioprothesis surgically implanted. Yet, the test revealed that the type and the size of the bioprosthesis played an important role. If the experimental system was capable to recognize differences among surgically implanted bioprostheses, it should be fit for the study of the transcatheter aortic valve (TAVI) or devices of any kind that require to be inserted in the aortic root. In particular for the TAVI, which have been conceived to be implanted without removing

the native pathological leaflets, the perturbation on the local fluid dynamics and on the coronary flow is expected to be even larger.

One of the aspects of the bioprostheses that has not been considered in the current project, is the structural valve deterioration which affects the valve after a certain time after the implantation. This stem from the mechanical characteristics of the material used to make up the bioprosthesis other than the “environment”, i.e. the patient, in which are implanted. Valve durability is an important matter because when the valve fails usually it require a reoperation, which brings risks in term of operative mortality. Some Authors have found a relation between fluid dynamics and the rate of structural valve deterioration highlighting that those bioprostheses which are fluid dynamically less efficient may develop a faster structural deterioration compared with valves with a better fluid dynamics. This link between fluid dynamics and structural deterioration is an intriguing and it is worth studying in deep.

Manuscripts written and published during the 4 years of the PhD course

Studies performed to understand the fluid dynamics of the valves.

"In Vitro" Studies

1-**Tasca G**, R. Vismara, G. B. Fiore, C. Romagnoni, A. Redaelli, C. Antona, A. Gamba. "Does the type of suture technique affect the fluidodynamic performance of bioprostheses implanted in small aortic roots? Results from an in vitro study". *J Thorac Cardiovasc Surg*. 2015;149:912-823.

2-**Tasca G**, R. Vismara, GB Fiore, A. Mangini, C. Romagnoni, S. Pelenghi, C. Antona, A. Redaelli, A. "Fluid dynamic results of "in-vitro" comparison of 4 pericardial bioprostheses implanted in small porcine aortic roots. *Eur J Cardiothorac Surg*. 2015;47:e62-7.

3-**Tasca G**, Vismara R, Fiore GB, Mangini A, Romagnoni C, Redaelli A, Gamba A, Antona A. A comprehensive fluid dynamic and geometric study from an "in-vitro" comparison of 4 pericardial stented valves surgically implanted. The complex scenario of an implanted bioprosthesis. *J Heart Valve Dis* 2015 ;24(5):596-603.

4-**Tasca G**, Vismara R, Mangini A, Romagnoni C, Contino M, Redaelli A, Fiore GB, Antona C. Comparison of the Performance of a Sutureless Bioprosthesis With Two Pericardial Stented Valves on Small Annuli: An In Vitro Study. *Ann Thorac Surg*. 2017;103(1):139-144.

5-**Tasca G**, Fiore GB, Redaelli P, Romagnoni C, Redaelli A, Gamba A, Antona C, Vismara R. Hydrodynamic and Geometric Behavior of Two Pericardial Prostheses Implanted in Small Aortic Roots. *ASAIO J*. 2018;64(1):86-90.

"In vivo" Studies

1-**Tasca G**, P. Redaelli, B. Riva, CC De Carlini, E. Lobiati, A. Gamba. Hemodynamic comparison between Trifecta and Freestyle aortic valve during exercise in patients with small aortic root. *J Card Surg.* 2015;30:400–404.

2-**Tasca G**, Martino AS, Giannico F, Riva B, Redaelli P, Lobiati E, Triggiani M, Galanti A, Gamba A. Hemodynamic comparison between Trifecta and Freestyle valves implanted in small aortic roots. One-year echocardiographic results from a prospective randomized study. *J Heart Valve Dis*. 2015; 24:360-367.

3-**Tasca G**, AS Martino, F. Giannico, E. Lobiati, B. Riva, A. Galanti, M. Triggiani, A. Gamba. "Early hemodynamic evaluation of Trifecta and Freestyle bioprostheses in patients with a small aortic root. Preliminary results from a prospective randomized study". *J Heart Valve Dis*. 2014;23:633-641.

4-**Tasca G**, Trinca F, Riva B, Skouse D, Lobiati E, et al. Mass Regression after Aortic Valve Replacement in Aortic Stenosis: A Comparison between "Appropriate" and "Inappropriate" Left Ventricular Hypertrophy. Int J Clin Cardiol 2018;5:110. doi.org/10.23937/2378-2951/1410110

Studies performed to understand the leaflets kinematics of the valves.

"In vitro" studies

1-**Tasca G**, Fiore GB, Mangini A, Romagnoni C, Gamba A, Redaelli A, Antona C, Vismara R. Opening-closing pattern of four pericardial prostheses: results from an in vitro study of leaflets kinematics *J Artif Organs*. 2016;19(4):350-356.

2-**Tasca G**, Selmi M, Votta E, Redaelli P, Sturla F, Redaelli A, Gamba A. Aortic Root Biomechanics After Sleeve and David Sparing Techniques: A Finite Element Analysis. *Ann Thorac Surg*. 2017;103(5):1451-1459.

"In vivo" studies

11-**Tasca G**, Vismara R, Trinca F, Riva B, Gamba A, Lobiati E. Opening/closing pattern of Trifecta and Freestyle vs native aortic valve. Are stentless valves more physiologic that a stented valve? *J Card Surg.* 2017;32(11):680-685.

Study of a new coronary impedance simulator

1-Piola M, Vismara R, **Tasca G**, Lucherini F, Redaelli P, Soncini M, Romagnoni C, Mangini A, Antona C, Fiore GB. Design of a simple coronary impedance simulator for the in vitro study of the complex coronary hemodynamics. *Physiol Meas*. 2016 Dec;37(12):2274-2285.